# Contribution à la modélisation analytique des couches limites turbulentes et dispersion de particules en suspension

Rafik Absi

# Université de Cergy-Pontoise

# Habilitation à Diriger des Recherches

Mécanique des Fluides

présentée par


## Rafik ABSI

Enseignant-chercheur à l'EBI Cergy-Pontoise


# Contribution à la Modélisation analytique des Couches limites turbulentes et Dispersion de particules en suspension

Soutenue le vendredi 16 Septembre 2011

En Amphithéâtre « Colloque » - au site de Saint Martin

Devant le Jury composé de :

| | | |
|---|---|---|
| Rapporteurs/examinateurs : | | |
| M. Mohammed EL GANAOUI | Professeur | Université Nancy 1 |
| M. Willi H. HAGER | Professeur | ETH Zürich |
| M. Christophe MENEZO | Professeur | Chaire EDF / INSA de Lyon |
| Examinateurs : | | |
| M. Rachid BENNACER | Professeur | ENS Cachan |
| M. François DUNLOP | Professeur | Université de Cergy-Pontoise |
| Mme Béatrice LEDESERT | Professeur | Université de Cergy-Pontoise |

## Remerciements

Je tiens à exprimer ma gratitude à Monsieur le Professeur M. EL GANAOUI, à Monsieur le Professeur W. H. HAGER et à Monsieur le Professeur C. MENEZO pour avoir accepté d'examiner cette étude et d'en avoir été les rapporteurs.

Je tiens à remercier Monsieur le Professeur R. BENNACER, Monsieur le Professeur F. DUNLOP et Madame le Professeur B. LEDESERT pour l'intérêt qu'ils ont porté à ce travail et pour l'honneur qu'ils m'ont fait de faire partie du jury.

Mes remerciements se tournent également à Madame F. DUFOUR, Directeur Général de l'Ecole de Biologie Industrielle pour m'avoir encouragé à présenter ce travail ainsi que les instances de l'Université de Cergy-Pontoise.

Je tiens aussi à remercier vivement tous mes amis et collaborateurs qui ont contribué par leurs conseils précieux et leur soutien moral à l'accomplissement de ce travail.

## Dédicace

Je dédie ce travail à mes parents, mon père Tahar ABSI et ma mère Fadila DAKHIA ABSI.

# Table des matières

Chapitre 1

# Introduction Générale

Ce dossier d'HDR donne un aperçu de mon expérience dans l'enseignement, l'animation de la recherche et mon implication dans la vie de l'établissement qui paraissent suffisantes pour solliciter une habilitation à diriger les recherches (HDR). Pour plus de précision, j'inclus une présentation succincte de mes activités dans les domaines de l'enseignement et de la recherche.

Dans la première partie, après une présentation de mon curriculum vitae, j'exposerai mes activités pédagogiques, administratives et d'encadrement. Dans la deuxième partie, une description synthétique de mes activités de recherche [1] au niveau du thème principal qui concerne la modélisation analytique des couches limites turbulentes et de la dispersion de particules sera présentée. J'ai commencé ce travail de recherche en thèse de doctorat qui a porté une analyse de la turbulence en couches limites oscillantes ainsi que la modélisation des concentrations de sédiments en suspension. L'application concernait l'effet des écoulements oscillants que produit la houle au voisinage du fond marin sur le transport sédimentaire. Cette thématique a continué à susciter mon intérêt compte-tenu des différentes applications industrielles et environnementales. Je présenterai dans la troisième partie[2], une méthode innovante qui m'a facilité l'enseignement de la mécanique des fluides et d'autres activités de recherche et d'expertise.

Le thème de recherche principal a été structuré autour de deux axes :

**Modélisation analytique des couches limites turbulentes**

Nous avons commencé par travailler à l'amélioration de la prévision des vitesses en couches limites turbulentes, ce qui nécessite une bonne description de la turbulence pariétale. En modélisation statistique de la turbulence les profils de vitesses calculés dépendent de la viscosité turbulente qui dépend à son tour de l'énergie cinétique turbulente (ECT) $k$ (modèles au premier ordre). L'obtention de l'ECT passe par la résolution numérique d'une équation aux dérivées partielles (EDP), l'équation de transport modélisée pour $k$. Notre travail a porté sur la résolution analytique de cette équation. La solution semi-analytique de Nezu et Nakagawa [80] pour les écoulements à surface libre a été révisée. Nous montrerons que cette première solution est valable uniquement au delà d'une certaine distance par rapport à une paroi. Une seconde solution est proposée au voisinage immédiat de la paroi [3]. Cette solution a été d'une part validée par des données de simulation numérique

1. En anglais, afin que cela soit accessible à un rapporteur non francophone

directe (DNS) obtenues pour des écoulements en canal turbulent, d'autre part elle a été évaluée par ma doctorante au niveau du code commercialisé Fluent [36] [34] [37]. Ces relations algébriques permettent dans certains cas (écoulements en canal plan, écoulements à surface libre, couche limite atmosphérique, ...) d'éviter la résolution numérique de l'EDP pour $k$. Ces lois peuvent représenter donc pour l'ingénieur un outil accessible et facile à utiliser. En effet, les ingénieurs ont souvent besoin d'outils à la fois pratique et précis. Ces lois peuvent aussi trouver une utilité chez les expérimentateurs. Ces solutions analytiques nous ont permis de proposer, d'une part, une relation analytique pour la longueur de mélange basée sur la première solution pour $k$ et l'hypothèse de similitude de von Karman [113] [2]. Cette relation analytique pour la longueur de mélange a été évaluée au niveau d'un code d'écoulements à surface libre, ce travail a été mené avec un doctorant [23] (thèse de Doctorat soutenue en 2008). D'autre part, l'utilisation combinée de la seconde solution pour $k$ avec la longueur de mélange de van Driest [110], a permis une bonne description des vitesses au voisinage immédiat d'une paroi [5]. L'étude des écoulements à surface libre dans des canaux étroits (rapport d'aspect $< 5$) montre des profils de vitesses avec un maximum au-dessous de la surface libre. A partir d'une analyse des équations de Navier-Stokes moyennées au sens de Reynolds (RANS), nous avons obtenu une équation différentielle ordinaire (EDO) pour les vitesses ainsi que sa solution semi-analytique. Les profils de vitesses calculées ont été validés par des données de mesures [4] [7].

**Modélisation de la concentration de particules solides en suspension**

Une bonne prévision des concentrations de particules en suspension passe par une bonne estimation du nombre de Schmidt turbulent $Sc_t$. Le modèle cinétique [30] [119] [44] a permis d'obtenir une relation analytique pour $Sc_t$ qui l'exprime comme fonction du nombre de Stokes et donc des caractéristiques des particules solides et de l'écoulement turbulent [8] [12]. Le calcul des concentrations de particules de sable en suspension sous l'effet d'un écoulement oscillant sur un fond de rides est un exemple intéressant qui a attiré notre attention [1]. En effet, ce test permet de voir clairement l'importance d'une estimation adéquate de $Sc_t$. Il permet aussi de distinguer l'effet de sédimentation du phénomène de détachement tourbillonnaire [6]. Le modèle analytique de viscosité turbulente sera généralisé aux écoulements oscillants et validé par le modèle à deux équations $k$-$\omega$.

En conclusion, cette présentation succincte de mon expérience pédagogique et des efforts consentis dans le domaine de la recherche sera complétée par les perspectives à court et à moyen terme. Les annexes en fin de rapport donnent des indications plus précises sur différents aspects mentionnés dans l'exposé. Les publications dans des revues internationales permettent d'avoir de plus amples informations sur les différents sujets traités.

# Première partie

# Bilan de mes Activités

Chapitre 2

# Curriculum Vitae

## 2.1 Renseignements Personnels


— NOM et Prénom : ABSI Rafik
— Date et lieu de naissance : $18-01-1972$ à Alger (Algérie)
— Adresse personnelle : 15, Rue Jean Dollfus 75018 Paris
— Poste actuel : Enseignant-chercheur à l'EBI - Ecole d'Ingénieurs
— Adresse professionnelle : EBI, 32 Boulevard du Port, 95094 Cergy-Pontoise
— Tél. : 01 30 75 62 42
— Fax. : 01 30 75 62 51
— Courriel : r.absi@ebi-edu.com ; rafik.absi@yahoo.fr

— Situation familiale : Marié, un enfant

## 2.2 Titres Universitaires

— Doctorat de l'Université de Caen Basse-Normandie en Mécanique des milieux fluides, 2001
Titre de la thèse : Modélisation de la turbulence pariétale et du transport sédimentaire dans des couches limites oscillantes,
Inscrit sur les listes de qualification aux fonctions de maître de conférences :
- 60e section du CNU (Mécanique, génie mécanique, génie civil) en 2002 et 2006
- 37e section du CNU (Météorologie, océanographie physique et physique de l'environnement) en 2006

— Diplôme d'Etudes Approfondies (D.E.A) d'Energétique et Aérothermochimie (actuellement Master "Energie, Fluides, Environnement"), Université et INSA de Rouen CORIA, 1996

— Diplôme d'Ingénieur de l'École Nationale Polytechnique (Algérie), Promotion 1994

— Baccalauréat, 1989

## 2.3 Expérience professionnelle

— Visiting professor à Tohoku University, Japan (financement de la JSPS 'Japan Society for the Promotion of Science', JSPS Invitation Fellowship Program for Research in Japan 2010-2011), du 12 décembre 2010 au 07 février 2011

— Visiting researcher, St-Anthony Falls Laboratory, University of Minnesota, Minneapolis, USA (séjour financé par SAFL), du 19 janvier au 15 février 2009

— Depuis le 12 avril 2007, Membre nommé au comité d'experts spécialisés CES "Evaluation des risques liés aux eaux et aux agents biologiques"' placé auprès de l'AFSSET - Agence française de sécurité sanitaire de l'environnement et du travail, (Actuellement ANSES Agence nationale de sécurité sanitaire de l'alimentation, de l'environnement et du travail)

— Depuis septembre 2002. Enseignant-chercheur à l'EBI - Ecole de Biologie Industrielle (Ecole d'Ingénieurs habilitée par la CTI, membre de la Conférence des Grandes Ecoles), Institut Polytechnique Saint-Louis, Cergy-Pontoise

— 2001-2002. Ingénieur au sein du bureau d'étude d'une PME en région parisienne

— 1999-2000. Attaché Temporaire d'Enseignement et de Recherche. Université de Caen, Ecole d'Ingénieurs de Cherbourg (actuellement ESIX Normandie)

— 1997-1999. Enseignant vacataire à l'Université de Caen, IUT de Caen, IUT de Cherbourg à Sait-Lô, UVSQ, ESITC

Chapitre 3

# Publications et Reconnaissance Scientifique

## 3.1 Revues internationales avec comité de lecture

### 3.1.1 En préparation, soumis et en révision

R22. **Absi R.**, Tanaka H., Analytical eddy viscosity for oscillatory turbulent boundary layers : Calibration by a two equation $k$-$\omega$ model, in preparation.

R21. Bernard C., Broyart B., **Absi R.**, Granda P., Relkin P., Vasseur J., Prediction of Thermo-hydric-history of whey protein concentrate droplets during spray, *Drying Technology*, submitted.

R20. **Absi R.**, Analytical modeling of eddy viscosity and velocity profiles in turbulent channel flows, *Journal of Fluids Engineering*, ASME, submitted.

### 3.1.2 Publiés et sous presse

R19. El Gharbi N., **Absi R.**, Benzaoui A., Numerical investigation toward improving heat transfer predictions in a turbulent channel flow, ***International Journal of Thermal Science***, Elsevier, In Press, Corrected Proof.

R18. El Gharbi N., **Absi R.**, Benzaoui A., Effect of different near-wall treatments on indoor airflow simulations, ***Journal of Applied Fluid Mechanics***, accepted, in press.

R17. **Absi R.** (2011) Discussion of 'Vertical mixing in the fully developed turbulent layer of sediment-laden open-channel flow', ***Journal of Hydraulic Engineering, ASCE***, American Society of Civil Engineers, **137**(9), 1094-1095.

R16. **Absi R.**, Nalpas C., Dufour F., Huet D., Bennacer R., Absi T., (2011) Teaching fluid mechanics for undergraduate students in applied industrial biology : from theory to atypical experiments, ***International Journal of Engineering Education*** (IJEE), **27**(3), 550-558.

R15. **Absi R.**, Tanaka H. (2011) Toward improving prediction of sediment transport over wave-induced ripples, ***Tohoku Journal of Natural Disaster Science***, Japan, Vol. **47**, pp 213-218.

R14. **Absi R.** (2011) An ordinary differential equation for velocity distribution and dip phenomenon in open-channel flows, ***Journal of Hydraulic Research***, IAHR, Taylor & Francis, **49**(1), 82-89.

R13. El Gharbi N., **Absi R.**, Benzaoui A., Bennacer R. (2011) An improved near wall treatment for turbulent channel flows, ***International Journal of Computational Fluid Dynamics***, Taylor & Francis, **25**(1), 41-46.

R12. **Absi R.**, Marchandon S., Lavarde M. (2011) Turbulent diffusion of suspended particles : analysis of the turbulent Schmidt number, ***Defect and Diffusion Forum***, Trans Tech Publications, Vols. **312-315**, pp 794-799.

R11. El Gharbi N., **Absi R.**, Benzaoui A. (2011) Numerical simulations of heat transfer in plane channel flow, ***Defect and Diffusion Forum***, Trans Tech Publications, Vols. **312-315**, pp 671-675.

R10. **Absi R.** (2010) Concentration profiles for fine and coarse sediments suspended by waves over ripples : An analytical study with the 1-DV gradient diffusion model, ***Advances in Water Resources***, Elsevier, **33**(4), 411-418.

R9. Lagriffoul A., Boudenne J.L., **Absi R.**, Ballet J.J., Berjeaud J.M., Chevalier S., Creppy E.E., Gilli E., Gadonna J.P., Gadonna-Widehem P., Morris C.E., Zini S. (2010) Bacterial-based additives for the production of artificial snow : What are the risks to human health ?, ***Science of the Total Environment***, Elsevier, **408**(7), 1659-1666.

R8. **Absi R.** (2009) A simple eddy viscosity formulation for turbulent boundary layers near smooth walls, ***Comptes Rendus Mecanique***, Académie des Sciences, Elsevier, **337**, 158-165.

R7. **Absi R.** (2008) Analytical solutions for the modeled k-equation, ***Journal of Applied Mechanics, Transactions of the ASME***, American Society of Mechanical Engineers, **75**(4), 044501.

R6. **Absi R.** (2008) Comments on 'Turbulent velocity profile in fully-developed open channel flows', ***Environmental Fluid Mechanics***, Springer, **8**(4), 389-394.

R5. Cherif E.-A., **Absi R.**, Ouahsine A., Sergent P. (2008) Modélisation numérique des processus de transport des sédiments et de l'évolution des fonds, ***European Journal of Environmental and Civil Engineering***, Lavoisier/Hermès, **12**(1-2), 87-104.

R4. **Absi R.** (2006) One-dimensional wave bottom boundary layer model comparison : specific eddy viscosity and turbulence closure models : Discussion, ***Journal of Waterway, Port, Coastal and Ocean Engineering, ASCE***, American Society of Civil Engineers, **132**(2), 139-141.

R3. **Absi R.** (2006) A roughness and time dependent mixing length equation, ***Journal of the Japan Society of Civil Engineers***, Division B : Doboku Gakkai Ronbunshuu B, **62**(4), 437-446.

R2. **Absi R.** (2005) Comment on 'Turbulent diffusion of momentum and suspended particles : A finite-mixing-length-theory', ***Physics of Fluids***, American Institute of Physics, **17**(7), 079101.

R1. **Absi R.** (2000) Calibration of Businger-Arya type of eddy viscosity model's parameters, ***Journal of Waterway, Port, Coastal and Ocean Engineering, ASCE***, American Society of Civil Engineers, **126**(2), 108-109.

TABLE 3.1 – Journals Impact factors.

| Journal | Impact factor |
|---|---|
| Science of the Total Environment, Elsevier | 2,579 |
| Advances in Water Resources, Elsevier | 2,354 |
| Physics of Fluids, AIP | 1,78 |
| International Journal of Thermal Sciences | 1,770 |
| Journal of Hydraulic Engineering, ASCE | 1,272 |
| Journal of Applied Mechanics, ASME | 1,065 |
| Journal of Hydraulic Research, IAHR, Taylor & Francis | 1,005 |
| Environmental Fluid Mechanics, Springer | 1 |
| Journal of Waterway Port Coast Oc Eng, ASCE | 0,864 |
| Compte Rendu Mecanique, Elsevier | 0,538 |
| International Journal of Computational Fluid Dynamics | 0,571 |
| International Journal of Engineering Education | 0,552 |

## 3.2 Conférences internationales avec comité de lecture

### 3.2.1 Actes/Proceedings

C23. **Absi R.**, Tanaka H., Specific eddy viscosity and turbulence closure models for sediment transport in wave boundary layers, *7th IAHR Symposium on River, coastal and estuarine morphodynamics*, 6-8 September, Beijing, China, *accepted*.

C22. El Gharbi N., **Absi R.**, Guerri O., Benzaoui A., Simulation of forced convection in plane channel flow with a low Reynolds number $k$-$\varepsilon$ turbulence model, *7th International Conférence on Computational Heat Transfer*, 18-22 July 2011, Istanbul, Turkey, *accepted*.

C21. **Absi R.** (2011) Engineering modelling of wave-related suspended sediment transport over ripples, *Coastal Sediments '11, seventh international Symposium on Coastal Engineering and Science of Coastal Sediment Processes*, held May 2-6, 2011, in Miami, Florida, USA., edited by Julie D Rosati, Ping Wang and Tiffany M Roberts, World Scientific Publishing, pp. 1096 1108. (oral)

C17. El Gharbi N., **Absi R.**, Benzaoui A., Amara E.-H. (2009) Effect of near-wall treatments on airflow simulations, *International Conference on Computational Methods for Energy Engineering and Environment*, 20-22 November 2009, Sousse, Tunisia, pp 185-189. (BEST POSTER AWARD)

C16. **Absi R.** , Porté-Agel F. (2009) Large-eddy simulation of particle-laden flows with a scale-dependent dynamic subgrid-scale model, *Turbulence, Heat and Mass Transfer 6*, K. Hanjalic, Y. Nagano and S. Jakirlic (editors), Begell House Inc., ISBN 978-1-56700-262-1, pp. 733-736.

C15. **Absi R.** (2009) Analytical methods for velocity distribution and dip-phenomenon in narrow open-channel flows, *Environmental Hydraulics : Theoretical, experimental and computational solutions*, Editors P.A. Lopez-

Jimenez *et al.*, Valencia, Spain, accepted for oral presentation, CRC Press / Balkema, Taylor & Francis Group, pp. 127-129.

C14. **Absi R.** (2007) On the effect of sand grain size on turbulent mixing, In : Coastal Engineering 2006, *30th International Conference on Coastal Engineering*, ASCE, Jane McKee Smith (editor), World Scientific Publishing, ISBN 978-981-270-636-2, pp 3019-3029. (oral)

C12. **Absi R.** and Bennacer R. (2006) A new wall function for turbulent kinetic energy $k$, In *Turbulence, Heat and Mass Transfer 5*, K. Hanjalic, Y. Nagano and S. Jakirlic (editors), Begell House Inc., ISBN 1-56700-229-3, pp. 389-392.

C11. **Absi R.** (2006) Modeling turbulent mixing and sand distribution in the bottom boundary layer, In *Coastal Dynamics 2005* - State of the Practice, by Agustin Sanchez-Arcilla, (editor) Reston, VA : ASCE / Copri, ISBN 0-7844-0855-6. (oral)

C6. **Absi R.** (2003) Wave boundary layer instability near flow reversal, In : Coastal Engineering 2002, Proc. *28th International Conference on Coastal Engineering*, ASCE, Jane McKee Smith (Ed.), World Scientific Publishing, ISBN 981-238-238-0, vol. 1, pp. 532-544. (oral)

C4. **Absi R.** (2001) Time-dependent eddy viscosity models for wave boundary layers, In : Coastal Engineering 2000, Proc. *27th International Conference on Coastal Engineering*, Billy L. Edge (Ed.), ASCE Press, ISBN 0-7844-0549-2, vol. 2, pp. 1268-1281. (oral)

C2. **Absi R.** (1999) Sediment concentration due to wave action, In Proc. *I.A.H.R. Symposium on River, Coastal and Estuarine Morphodynamics*, Genova, Italy, vol. 1, pp. 457-466. (oral)

C1. **Absi R.**, Abdelgader A., Belorgey M. (1997) Bottom boundary layer study for the sediment transport modeling, In Proc. *3rd International Conference on Mediterranean Coastal Environment*, Malta, E. Özhan (ed.), Medcoast Publications, pp. 1275-1285.

### 3.2.2 Résumés/Abstracts

C20. **Absi R.**, Tanaka H. (2011) Toward improving prediction of sediment transport over wave-induced ripples, *Tohoku Conference on Natural Disaster Science*, 8-9 January 2011, Koriyama, Fukushima Prefecture, Japan. (oral)

C19. **Absi R.**[1] , Marchandon S., Lavarde M. Turbulent diffusion of suspended particles : analysis of the turbulent Schmidt number, In Book of Abstracts of *6th International Conference on Diffusion in Solids and liquids*, 5-7 July 2010, Paris, (oral).

C18. El Gharbi N., **Absi R.**, Benzaoui A. Numerical simulations of heat transfer in plane channel flow, In Book of Abstracts of *6th International Conference on Diffusion in Solids and liquids*, 5-7 July 2010, Paris, (poster).

C13. **Absi R.** (2006) On the effect of sand grain size on turbulent mixing, In Book of Abstracts of ICCE 2006, San Diego, Ca., USA, September 2-8, Paper

1. Nom souligné : auteur ayant présenté la communication.

No 135. (oral)

C10. **Absi R.** (2005) Modeling turbulent mixing in the sea wave bottom boundary layer, In Book of Abstracts of the 5th International Conference on Coastal Dynamics, LIM/UPC, Barcelona, Spain, 4-8 April 2005, pp. 112-113. (oral)

C9. **Absi R.** (2003) A Simple mixing length equation from an extension of von Kármán's similarity hypothesis, In Book of Abstracts of *5th EUROMECH Fluid Mechanics Conference*, Toulouse, 24-28 August 2003, page 307. (oral and poster)

C8. **Absi R.** (2003) On accurate modeling of intra-wave suspended sediment concentration, In Book of Abstracts : *Coastal Sediments'03*, American Society of Civil Engineers, May 18-23, 2003, Clearwater Beach, Florida, USA, pp. 276-277.

C7. **Absi R.** (2003) Simple tools for turbulence calculations in the sea wave bottom boundary layers, In Sea wave bottom boundary layer. Foti, E. & Fredsoe, J. (Ed.), Book of abstracts *Euromech colloquium n° 451*, 26-29 October 2003 Taormina, Italy.

C5. **Absi R.** (2002) Vertical momentum exchange around flow reversal beneath large waves, In Book of Abstracts of *ICCE 2002*, Cardiff, Wales, UK, July 07-12, Paper No 292. (oral)

C3. **Absi R.** (2000) Turbulence model for wave boundary layers, In Book of Abstracts of *ICCE 2000*, Sydney, Australia, July 16-21, Paper No 17, ISBN 085825 722 X. (oral)

## 3.3 Conférences nationales avec comité de lecture

CN9. El Gharbi N., **Absi R.**, Benzaoui A., (2011) Amélioration de la prévision du transfert thermique près d'une paroi, *Congrès SFT 2011, Energie Solaire et Thermique*, Société Française de Thermique, Perpignan 24 - 27 mai 2011.

CN8. **Absi R.**[2], Le Gall C., Marchandon S. Hammad P.-A. (2008) Interprétation des profils de concentration pour des particules de sable en suspension de différentes tailles, Actes des *Xèmes Journées Nationales 'Génie côtier - Génie civil'*, Sophia Antipolis, ISBN 2-9505787-9-9, pp. 9-18. (orale)

CN7. Coumert C., **Absi R.** et Grémare A. (2007) Mise en oeuvre d'un système d'imagerie des profils de sédiments, Actes des *IXièmes Journées d'Ecologie Fonctionnelle*, INRA-CNRS, 19-22 mars 2007, Biarritz, page 88. (orale)

CN6. Cherif E.-A., **Absi R.**, Ouahsine A., Sergent P. (2006) Simulations numériques de l'évolution des fonds et effet du mélange turbulent sur le transport sédimentaire. Application au remplissage d'une fosse d'extraction, Actes des *IXèmes Journées Nationales 'Génie côtier - Génie civil'*, Brest, 12-14 septembre, Editions Paralia, pp. 167-177. (orale)

CN5. **Absi R.** et Marchandon S. (2004) Longueur de mélange et diffusion tur-

2. Nom souligné : auteur ayant présenté la communication.

bulente des sédiments, Actes des *VIIIème Journées Nationales 'Génie côtier - Génie civil'*, Compiègne, 7-9 septembre 2004, pp. 279-287. (orale)

CN4. **Absi R.**, Yaici S., Absi A. (2004) Sur la turbulence en écoulement intra artériel. In *L'eau et le monde vivant*, 28èmes Journées de l'Hydraulique, Paris 12-13 octobre 2004, Publications de la SHF, ISBN : 2-906831-59-X, pp. 177-184. (orale)

CN3. **Absi R.** (2003) Expression analytique instationnaire pour la longueur de mélange basée sur une extension de l'hypothèse de von Kármán, *16ème Congrès Français de Mécanique*, Nice, 1-5 Septembre 2003 ; 6 pages. (poster)

CN2. **Absi R.** et Belorgey M. (1999) Sédiments en suspension dans des couches limites turbulentes oscillantes, *14ème Congrès Français de Mécanique*, Toulouse, 6 pages. (orale)

CN1. **Absi R.** et Belorgey M. (1998) Modélisation de la couche limite de fond générée par un écoulement de houle, Actes des *Vème Journées Nationales 'Génie côtier - Génie civil'*, Toulon, Editions Paralia, pp. 11-18. (orale)

## 3.4 Rayonnement national et international

### 3.4.1 Reviewer d'articles pour des revues internationales

— Journal of Hydraulic Engineering, ASCE, American Society of Civil Engineers (see *Journal of Hydraulic Engineering* (2009) volume **135** No 12 page 1117 and (2010) volume **136** No 12 page 1093)
— Journal of Hydraulic Research, IAHR, Taylor & Francis (see List of reviewers in *Journal of Hydraulic Research* (2011) volume **49** Issue 1, pages 140 - 141)
— Advances in Water Resources, Elsevier
— Journal of Fluids Engineering, Transactions of ASME, American Society of Mechanical Engineers
— Journal of Hydrologic Engineering, ASCE, American Society of Civil Engineers
— International Journal of Thermal Science, Elsevier

### 3.4.2 Reviewer de livre pour éditeur

— Wiley, New Book Proposal, volume devoted to fluid mixing on the microscale

### 3.4.3 Membre de comités scientifiques de conférences

— CONFERE, Colloque des sciences de la conception et de l'innovation :

CONFERE 2010, 17ème Colloque des sciences de la conception et de l'innovation, Sousse, Tunisie, 1er et 2 juillet 2010, http ://etudes.ebi-edu.com/confere/
- Membre du comité scientifique
- Membre du comité de lecture : évaluation des résumés soumis

- Président du thème 2 : Ergonomie au service de la santé
- Participation à l'organisation

CONFERE 2011, 18ème Colloque des Sciences de la Conception et de l'Innovation, 30 Juin et 1er Juillet 2011, Montbéliard, http ://web.utbm.fr/confere2011/
- Membre du comité scientifique
- Membre du comité de lecture : évaluation des résumés soumis

### 3.4.4 Membre du comité éditorial de revue

— International Journal of Environmental Protection (IJEP), http ://www.ij-ep.org/ , http ://www.ij-ep.org/editorialBoard.aspx
— Online journal : Algerian Journal of Applied Fluid Mechanics, ISSN 1718-5130 www.ajafm.com

### 3.4.5 Mise en place et organisation de journées scientifiques

— 1ère journée de modélisation des procédés, en partenariat avec Comsol France (FEMLAB), Cergy-pontoise le 9 octobre 2003
— 2ème Journée de modélisation, avec la participation des sociétés Fluent, Pro-Sim et DynaSys et l'Université de Cergy-Pontoise, Cergy-pontoise le 19 novembre 2004
— Journée de Contrôle-commande des procédés, en partenariat avec la société INFORS-HT, Cergy-pontoise le 17 novembre 2008

### 3.4.6 Activité d'expertise à l'Agence française de sécurité sanitaire de l'environnement et du travail (AFSSET)

**Actuellement ANSES (Agence nationale de sécurité sanitaire de l'alimentation, de l'environnement et du travail)**

— Membre nommé au comité d'experts spécialisés "CES" "Evaluation des risques liés aux eaux et aux agents biologiques"

— Membre nommé au groupe de travail "Évaluation du risque sanitaire pour l'homme lié à la présence de virus Influenza pandémique dans l'air des bâtiments et à sa propagation éventuelle par les dispositifs de ventilation" en tant qu'expert, du 29 mai 2007 à Mai 2009. Saisine n°2006/003

— Membre nommé au groupe de travail "Evaluation des risques sanitaires liés à l'utilisation d'adjuvants pour la fabrication de la neige de culture" en tant qu'expert, du 19 juillet 2007 à juillet 2008. Saisine n° 2005/SA/007. Ce travail d'expertise a été publié dans la revue 'Science of the Total Environment' [66].

Chapitre 4

# Activités Pédagogiques, Administratives et d'Encadrement

---

## 4.1 Activités Pédagogiques

### 4.1.1 Activité d'enseignement

**A l'Ecole de Biologie Industrielle :** (depuis septembre 2002)
*Cycle préparatoire :*
- Mécanique des fluides (Cours et TD, 2ème année cycle préparatoire, 120 élèves ingénieurs)
*Cycle Ingénieur, Tronc-commun :*
- Opérations unitaires fondamentales (Cours et TD, 2ème année cycle ingénieur, 120 élèves ingénieurs)
*Cycle Ingénieur, Majeure : Ingénierie des Procédés Industriels et Production :*
- Extrapolation et modélisation des procédés (Cours, TD et TP, 5ème année EBI, 3ème année cycle ingénieur)
- Contrôle-commande des procédés (Cours, TD et TP, 5ème année EBI, 3ème année cycle ingénieur)
- Opérations unitaires mécaniques (Cours, TD et TP, 4ème année EBI, 2ème année cycle ingénieur)
Cycle Ingénieur, Optionnel : Ingénierie des Procédés Industriels et Production :
- Techniques de simulation avancées (Cours, TD et TP, 5ème année EBI, 3ème année cycle ingénieur)
Création de nouveaux cours (Modélisation-simulation et contrôle-commande) et mise en place de travaux pratiques en mécanique des fluides (pertes de charge, pompes, fluidisation) et automatique (régulation de niveau).

**Autres :**

*Attaché Temporaire d'Enseignement et de Recherche à plein temps (1999/2000) :*
Enseignements effectués à l'Ecole d'Ingénieurs de Cherbourg (actuellement ESIX Normandie) et à l'Université de Caen : Mécanique Analytique (TD, 1ère année cycle ingénieur) ; Résistance des Matériaux (TP, 3ème année) ; Méthode des Eléments Finis (TD, 2ème année cycle ingénieur) ; Construction Mécanique et CAO/DAO avec DMT (TP, 2ème année cycle ingénieur) ; Mécanique Générale (TD, DEUG 2ème année cycle préparatoire).

*Autres interventions :*
- Université de Cergy-Pontoise (2004/2005) : DESS Techniques de modélisation et de simulation : Cours et TP (6 heures)
- IUT de Cherbourg - Manche à Saint-Lô, (1998/1999) : DUT Génie Thermique et Energie 1ère année : TP de Mécanique des Fluides, Thermique et Thermodynamique (58 heures).
- IUT de Caen (1998/1999) : DUT Mesure Physique 1ère année : TP de Mécanique (27 heures).
- Université de Caen (1998/1999) : Maîtrise : Méthodes Numériques : TP (15 heures) ; DEUG 1ère année : Mathématiques : Cour et TD (30 heures).
- Université de Versailles (UVSQ) (1998/1999) : DEUG MIAS, 2ème année : TP de Méthodes Numériques et Algèbre Linéaire avec Maple (96 heures).
- ESTACA - Ecole Supérieur des Techniques Aéronautiques et de Construction Automobile à Levallois-Perret (2001/2002) : Cours (100 élèves x 2) et TD de Mécanique des Fluides (72 heures).
- ESITC - Ecole Supérieure des Ingénieurs des Travaux de la Construction Caen : Matériaux - Génie Civil : TP, 1ère année (44 heures).

### 4.1.2 Proposition de solutions pédagogiques

— Membre de la commission 'Pédagogie par compétences' à l'EBI. But : Proposer et mettre en oeuvre des solutions pédagogiques

— Mise en oeuvre de solutions pédagogiques innovantes pour faciliter l'enseignement de la mécanique des fluides : Utilisation d'expériences atypiques et analyse des fiches d'évaluations (voir chapitre "8" et article **Absi R.**, Nalpas C., Dufour F., *et al.*, Teaching fluid mechanics for undergraduate students in applied industrial biology : from theory to atypical experiments, ***International Journal of Engineering Education*** (IJEE), **27**(1), in press).

## 4.2 Activités Administratives

A l'Ecole de Biologie Industrielle :
— Coordinateur Recherche à l'EBI pendant 4 ans (de janvier 2005 à décembre 2008)
- Réalisation du dossier 'Recherche' annuel pour le Conseil d'Orientation Scientifique
- Organisations des réunions 'Recherche'
- Préparation du dossier 'Recherche' pour l'audit du 21 décembre 2007 dans le cadre de la candidature à la Conférence des Grandes Ecoles (CGE). L'EBI est membre de la CGE depuis le 9 décembre 2008
- Participation à la préparation du dossier 'Recherche' pour le renouvelle-

ment de l'habilitation CTI Commission des titres d'Ingénieurs (septembre 2006)
- Participation à la préparation du dossier pour l'Agence Universitaire de la Francophonie AUF (2008)
- Participation à la préparation du dossier pour l'agrément au Crédit Impôt Recherche
- Participation à la préparation de la Semaine de la Recherche et de l'Innovation en Val d'Oise
- Participation aux Réunions PRES Recherche du Pôle de recherche et d'enseignement supérieur (PRES) Cergy University
- Participation aux Réunions d'organisation de la Semaine de la Recherche et de l'innovation en Val d'Oise, Interviewé sur le développement durable en tant qu'enseignant-chercheur à l'EBI et expert à l'AFSSET (interview publiée dans la plaquette de la 4ème édition de la Semaine de la Recherche et de l'innovation en Val d'Oise, du 21 au 25 mai 2007.

— Responsable de l'activité de recherche n° 9 du Laboratoire EBInnov (laboratoire de R&D de l'EBI) : Modélisation d'Ecoulements Environnementaux, Biologiques et Industriels M2EBI

— Suivi pédagogique, étudiants à l'université de Cranfield (Royaume Uni)
- Master of Science Environmental water management
- Master of Water and Wastewater Engineering

— Membre du comité pédagogique de l'EBI (en tant que membre titulaire depuis 2003)
— Participation aux différentes réunions de l'Ecole (séminaires pédagogiques, conseil d'orientation scientifique, conseils de promotions ; réunions recherche ; comités d'admission) aux journées portes ouvertes et salons (salon de l'éducation ...) (depuis 2002)

## 4.3 Activités d'Encadrement

### 4.3.1 Co-encadrement de thèses de Doctorat

— Codirection de la thèse de doctorat de Mlle Najla EL GHARBI, actuellement Attachée de Recherche au Centre de Développement des Énergies Renouvelables (Algérie) ; Thème : Contribution à la modélisation de l'aéraulique en canal turbulent avec transfert de chaleur : Application aux chaudières de récupération des centrales solaires ; Directeur de thèse A. Benzaoui, Faculté de Physique, USTHB Alger (Algérie). Soutenance prévue 2011-2012 (voir liste des publications), taux d'encadrement : 75 %

— Participation au co-encadrement de la thèse de doctorat de Mr El-Amine

CHERIF. Thèse soutenue le 27 Mars 2008 à l'Université des Sciences et Technologies d'Oran (Algérie) ; Thème : Modélisation des écoulements transitoires liquide-solide à surface libre pendant les crues ; Directeur de thèse M. Errih (voir liste des publications), taux d'encadrement : 20 %

— Codirection de la thèse de doctorat de Mr Karim MOUSSA, Thème : Modélisation de l'encrassement par le lait en régime turbulent dans un échangeur de chaleur à plaques ; Directeur de thèse A. Mouheb, Faculté de Génie Mécanique et Génie des Procédés, USTHB Alger (Algérie), en cours

### 4.3.2 Suivi de stages Ingénieurs à l'EBI

Suivi de stages Ingénieurs dans les domaines de l'environnement, les procédés et la production. Président de jury de soutenances de stages de fin d'études à l'EBI et participation aux soutenances à l'Université de Cranfield (UK).

Deuxième partie

# Analytical Modeling of Turbulent Boundary Layers and Diffusion of Suspended Particles

# Introduction

The development of theoretical and semi-theoretical analytical methods for turbulent flows is of great importance in both practical engineering applications and basic turbulence research. Turbulent flows are significantly affected by the presence of walls. Successful predictions of turbulence models used for wall-bounded turbulent flows depend on accurate description of the flow in the near-wall region. The fully developed plane channel flow (fig. 4.1) is considered to be the simplest and most idealized boundary layer flow. Figure (4.1.a) represents the flow between two infinitely large plates where the channel half width is $\delta$. In figure (4.1.b), the flow is driven by a pressure gradient in the streamwise direction.

Fully developed plane channel flow has been investigated by many experimental and computational studies. Experiments in the range of $190 < Re_\tau < 1900$ were performed to investigate the effects of the Reynolds number very near the wall [116] (hereafter, $Re_\tau$ denotes the friction Reynolds number defined based on $u_\tau$, the kinematic viscosity $\nu$ and the channel half-width $\delta$). There are several direct numerical simulation (DNS) studies of plane channel flows which have allowed to improve the knowledge of the boundary layer dynamics. The DNS was performed at $Re_\tau = 180$ [62], up to $Re_\tau = 590$ [77], up to $Re_\tau = 642$ [60] (2002), up to $Re_\tau = 950$ [29], and recently at $Re_\tau = 2003$ [58]. Experiments and DNS show that the near-wall or inner region can be subdivided into three layers. A viscous sublayer (for a distance from the wall $y^+ < 5$), where the mean velocity $U^+$ is approximated by $U^+ = y^+$ and the turbulent kinetic energy (TKE) $k^+$ by a quadratic variation $k^+ \approx y^{+2}$ [52] [68] [87] (variables with the superscript of $+$ are those nondimensionalized by the wall friction velocity $u_\tau$ and the kinematic viscosity $\nu$). A fully-turbulent or log-law layer (for $30 < y^+ < 0.2\, Re_\tau$), where $U^+$ is approximated by the logarithmic profile [104] and $k^+$ by some analytical and semi-analytical solytions in the equilibrium region (for $y^+ > 50$) [80] [72] [3]. Between these two layers, a buffer layer where there is no analytical description of TKE. In the outer region, the log-law deviates from experimental and DNS data.

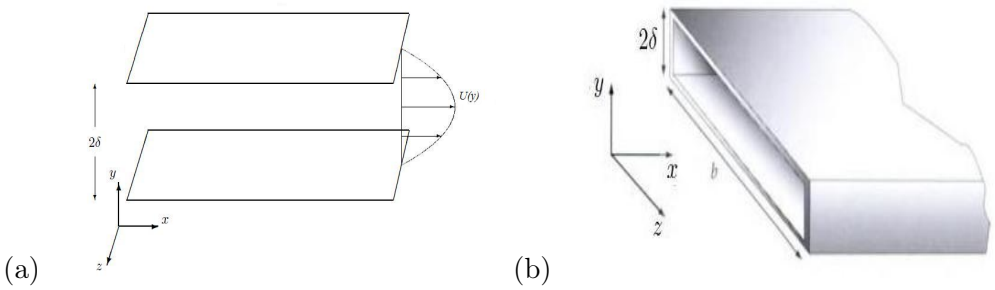


(a) (b)

FIGURE 4.1 – Sketch of plane channel flow ; (a) flow geometry, (b) apparatus (Adapted from [87])

In order to allow a suitable description of $U^+$, the log-law was corrected by adding the Coles' wake function [25] [55].

The aim of our study is to improve the description of :
— turbulent kinetic energy (TKE) and velocity profiles in turbulent channel flows
— concentration profiles of suspended particles in turbulent boundary layers

The next chapter presents analytical solutions of turbulent kinetic energy $k = 0.5(\overline{u^2} + \overline{v^2} + \overline{w^2})$ (where $u$, $v$, $w$ denote the velocity fluctuations in the streamwize, wall-normal and spanwise directions). The profile of Nezu and Nakagawa [80] for TKE in open-channel flows will be first revisited. With adequate approximations and assumptions, we will present a more general solution, which improves the description of TKE in the buffer layer. This solution will be validated and calibrated by DNS data of turbulent channel flows. A User Defined Function (UDF) based on our near-wall analytical profile for TKE is developed and implemented in Fluent (part of my student's Ph.D. thesis). The aim of the chapter 6 is to improve the prediction of velocity profiles by using analytical mixing length and eddy viscosity formulations based on our TKE profiles. Chapter 7 provides analytical formulations for the turbulent Schmidt number $Sc_t$ for mass transfer of suspended particles. Two formulations of $Sc_t$ are presented based on a kinetic model for turbulent two-phase flows [30] [119] [44] [8] and a finite-mixing-length theory [85]. The kinetic model provides $Sc_t$ which depends on particle Stokes number $St$ and therefore on TKE, eddy viscosity and particles settling velocity. The second approach provides a simple profile useful for our analytical study of concentration profiles for fine and coarse sediments suspended by waves over ripples.

**Notation**

$A_r$ = open-channel aspect ratio ($= b/h$)
$a_m$ = wave orbital amplitude or near-bed flow semi-excursion
$b$ = open-channel width
$c$ = concentration
$c_0$ = concentration at reference level $y_0$
$F$ = Froude number ($= U/(gh)^{1/2}$)
$f_s$ = dimensionless settling velocity
$g$ = gravitational acceleration
$h$ = free-surface flow depth or the distance from the wall to the axis of symmetry or free surface
$G$ = production of turbulent kinetic energy
$k$ = turbulent kinetic energy (TKE)
$k_0$ = turbulent kinetic energy at $y_0$ ($= k(y_0)$)
$k_s$ = equivalent roughness
$l$ = turbulent legth scale
$l_m$ = mixing length
$N_i$ = non-linearity parameter for an oscillatory flow ($= U_c/u_\tau$)
$Re$ = Reynolds number
$Re_\tau$ = friction Reynolds number ($= \delta\, U_\tau/\nu$ or $h\, U_\tau/\nu$)
$Ri$ = Richardson number
$S$ = channel slope ($= sin\theta$)
$Sc_t$ = turbulent Schmidt number
$St$ = Stokes number
$U$, $V$, $W$ = mean velocity components respectively in the $x$, $y$ and $z$ directions
$U_a$ = dimensionless streamwise mean velocity
$U_{a,max}$ = maximal value of $U_a$ at dip position $U_a(\xi = \xi_{dip})$
$U_c$ = velocity at wave crest for an oscillatory flow
$\hat{u}$ = total velocity amplitude for an oscillatory flow
$u_\tau$ = wall friction velocity
$u$, $v$, $w$ = velocity fluctuations in respectively the streamwise, wall normal and spanwise directions
$u'$ = the root-mean-square of turbulent velocity fluctuation $u$
$u_m$ = mixing velocity
$x$, $y$, $z$ = coordinates in respectively the streamwise, vertical and lateral directions
$y$ = vertical distance from bed
$Z = z/(b/2) = (2\,z)/b$ = dimensionless lateral distance from side wall
$y_0$ = hydrodynamic roughness
$\alpha$ = parameter related to $Ar$, $Z$ and $\xi_{dip}$
$\beta$ = inverse of turbulent Schmidt number
$\beta_b$ = $\beta$ close to a bed
$\delta$ = channel half-width or boundary layer thikness
$\varepsilon$ = dissipation of turbulent kinetic energy
$\varepsilon_s$ = turbulent diffusion of suspended particles

$\kappa$ = Kármán constant ($\approx 0.4$)
$\nu$ = kinematic viscosity
$\nu_t$ = eddy viscosity
$\eta_r$ = ripple height
$\lambda_r$ = ripple wavelength
$\Pi$ = Coles parameter
$\rho = \rho_f$ = density of fluid
$\rho_s$ = density of particles
$\tau$ = shear stress
$\tau_w$ = wall shear stress ($= \rho\, u_\tau^2$)
$\theta$ = angle of channel bed to horizontal axis
$\omega$ = specific dissipation rate of turbulent kinetic energy
$\omega_s$ = settling velocity of particles
$\omega_{st}$ = terminal settling velocity in an infinite fluid
$\xi$ = dimensionless distance from bed ($= y/h$)
$\xi_0$ = relative roughness ($= y_0/h$)
$\xi_{dip}$ = dip distance of maximum velocity
All variables with the superscript of + are those nondimensionalized by $u_\tau$ and $\nu$

**Abreviations**
CFD = Computational fluid dynamics
DNS = Direct numerical simulation
sDMLW-law = simple dip-modified-log-wake law
fDMLW-law = full dip-modified-log-wake law
ODE = ordinary differential equation
RANS = Reynolds-averaged Navier-Stokes
TKE = Turbulent kinetic energy
UDF = User Defined Function of Fluent

Chapitre 5

# Analytical solutions for turbulent kinetic energy

*p@@p@12*



## 5.1 Introduction

Most of existing analytical solutions for turbulent kinetic energy (TKE) are based on local equilibrium assumption. For steady open-channel flows in local equilibrium, where the energy production $G$ is balanced by the dissipation $\varepsilon$, Nezu and Nakagawa [80] suggested a semi-analytical solution for TKE given by

$$\frac{k}{u_\tau^2} = D_1 \, e^{(-2\,C_k\,\xi)} \tag{5.1}$$

where $\xi = y/h$, $y$ is the distance from the bed, $h$ the scale of the flow (the flow depth or the boundary layer thickness), $u_\tau$ the friction velocity, $D_1$ and $C_k$ are coefficients ($C_k$ was estimated empirically equal to 1 [80]). Eq. (5.1) is valid from a certain distance from the bed, where the flow is in local equilibrium [3]. However, it is not adapted in the vicinity of a wall. In this region, from expanding the fluctuating velocity components in Taylor series about the normal distance $y$ from the wall, the near-wall asymptotic behavior is described by [52] [68] [87]

$$k^+ = a y^{+2} + b y^{+3} \tag{5.2}$$

where $y^+ = y\,u_\tau/\nu$ is the dimensionless wall distance, $k^+ = k/u_\tau^2$ and $a$ and $b$ two coefficients given by $0.025 < a < 0.05$ [86] and $b = -a/8$ [90]. Often, this equation is simplified to the first term in the right-hand side as $k^+ \approx a y^{+2}$. However, this quadratic variation of $k$ is valid only inside the viscous sublayer, $y^+ < 5$. In order to provide a unique solution for TKE in the entire boundary layer, L'vov *et al.* [72] proposed a more complete analytical solution based on the same assumption of local equilibrium. However, this solution fails to improve TKE profiles in viscous and buffer layers.

In this chapter, the derivation of Nezu and Nakagawa for Eq. (5.1) will be first revisited. Based on our derivation and with an estimation of $G - \varepsilon$, we will present a more general solution for the modeled $k$-equation, which improves the description of TKE in the vicinity of a wall. This solution will be validated and calibrated by direct numerical simulation (DNS) data of turbulent channel flows. Finally, a User Defined Function (UDF), based on our analytical profile for TKE, is developed and implemented in Fluent (part of my student's Ph.D. thesis, El Gharbi *et al.* [36] [37]). Turbulent kinetic energy profiles are validated by DNS data.

## 5.2 Nezu and Nakagawa's profile revisited

The modeled $k$-equation is given by [80]

$$\frac{\partial\, k}{\partial\, t} = G + \frac{\partial}{\partial\, y}\left(\nu_t \frac{\partial\, k}{\partial\, y}\right) - \varepsilon \tag{5.3}$$

where $G$ is the energy production, $\varepsilon$ the dissipation and $\nu_t$ the eddy viscosity. For steady open-channel flows, equation (5.3) becomes

$$\frac{\partial}{\partial\, y}\left(\nu_t \frac{\partial\, k}{\partial\, y}\right) = -(G - \varepsilon) \tag{5.4}$$

### 5.2.1 Nezu and Nakagawa's derivation

In local equilibrium, where the energy production is balanced by the dissipation ($G = \varepsilon$), It is possible to write (5.4) as

$$\nu_t \frac{d\, k}{d\, \xi} = const \equiv -\,2\, C_k \tag{5.5}$$

Nezu and Nakagawa [80] wrote an approximation for the eddy viscosity $\nu_t$ as

$$\nu_t \approx \frac{k^2}{\varepsilon} \approx \frac{l}{k}\left(\frac{k}{u'}\right)^3 \approx \left(\frac{u_\tau^2}{k}\right)(u_\tau\, h) \approx \frac{1}{k} \tag{5.6}$$

where $l$ is a turbulent length scale, $u'$ the root-mean-square of turbulent velocity fluctuation $u$. Inserting (5.6) into (5.5) and by integrating, they obtained Eq. (5.1) [80].

### 5.2.2 proposed derivation

From (5.6), we write

$$\nu_t = C'_{\nu_t} \frac{1}{k} \tag{5.7}$$

where $C'_{\nu_t}$ is a constant. Inserting (5.7) into (5.5) and by integrating, we obtain

$$\frac{k}{u_\tau^2} = D_1 \, e^{(-2\, C_{k1}\, \xi)} \tag{5.8}$$

where $C_{k1} = C_k / C'_{\nu_t}$, or

$$\sqrt{k} = \sqrt{k_0} \, e^{[-C_{k1}(\xi - \xi_0)]} \tag{5.9}$$

where $k_0 = k(y_0)$, $\xi_0 = y_0/h$ is the relative roughness, with $y_0$ is the hydrodynamic roughness, and $D_1 = (k_0 \, e^{2\, C_{k1}\, \xi_0})/u_\tau^2$.

The approximation $\nu_t \approx 1/k$ is not completely realistic. It is possible to write a more appropriate approximation by assuming a shape given by a dimensionless function $f(\xi)$, as

$$\frac{k}{u_\tau^2} = D_1 \, f^2(\xi) \tag{5.10}$$

and

$$\frac{u'}{u_\tau} = D_u \, f(\xi) \tag{5.11}$$

a more rigorous approximation for $\nu_t$ is [1]

$$\nu_t \approx \frac{k^2}{\varepsilon} \approx \frac{l}{k} \left( \frac{k}{u'} \right)^3 \approx \frac{l(\xi)}{k} \, u_\tau^3 \, f(\xi)^3 \approx \frac{g}{k} \tag{5.12}$$

where

$$g(\xi) = l(\xi) \, u_\tau^3 \, f(\xi)^3 \tag{5.13}$$

With $g$, (5.12) is dimensionally valid and with a dimensionless constant $C_{\nu_t}$, we write $\nu_t$ as

$$\nu_t = C_{\nu_t} \frac{g}{k} \tag{5.14}$$

From (5.7) and (5.14), we have $C'_{\nu_t} = C_{\nu_t} \, g$. Inserting (5.14) into (5.5), we obtain

$$\frac{g(\xi)}{k}\,\frac{d\,k}{d\,\xi} = -2\,C_n \tag{5.15}$$

where $C_n = C_k/C_{\nu_t}$. Equation (5.15) can be expressed as

$$\left(\frac{g(\xi)}{\sqrt{k}}\right)\,\frac{d\sqrt{k}}{d\xi} = -C_n \tag{5.16}$$

By integrating (5.16) between $\xi_0$ and $\xi$, we obtain [1]

$$\sqrt{k} = \sqrt{k_0}\,e^{-C_n\,\int_{\xi_0}^{\xi}\frac{d\xi}{g(\xi)}} \tag{5.17}$$

From this equation, we find equation (5.9) only in the case where

$$g = const, \tag{5.18}$$

since $C_{k1} = C_k/C'_{\nu_t} = C_k/(C_{\nu_t}\,g) = C_n/g$. Condition (5.18) allows therefore to obtain for steady open-channel flows in local equilibrium an analytical solution for the modeled $k$-equation.

We can notice finally that in the Nezu and Nakagawa's derivation

$$g \approx u_\tau^3\,h = const \tag{5.19}$$

### 5.2.3 Interest and limits

We write equation (5.8) in wall units as

$$k^+ = D_1\,e^{\left(-\frac{y^+}{A_1^+}\right)} \tag{5.20}$$

where $y^+ = y\,u_\tau/\nu$, $A_1^+ = A_1\,u_\tau/\nu$ and $A_1 = h/(2\,C_{k1})$. Fig. 5.1 presents a comparison between the profile of Eq. (5.20) and direct numerical simulation (DNS) of turbulent channel flow of Iwamoto *et al.* [59] [60] for $Re_\tau = 642$. With $D_1 = 4.2$ and $A_1^+ = 360$ this solution represents well DNS data. However, Eq. (5.20) is not appropriated near the wall. In fact, for $y^+ < 20$, $k^+$ decreases to 0 and equation (5.20) is not able to predict TKE in this region (Fig. 5.1).

The analysis of $A_1^+$ by DNS data shows that $A_1^+$ is $Re_\tau$-dependent and is given by a linear relation (Fig. 5.2) as [12]

$$A_1^+(Re_\tau) = C_{A1}\,Re_\tau - C_{A2} \tag{5.21}$$

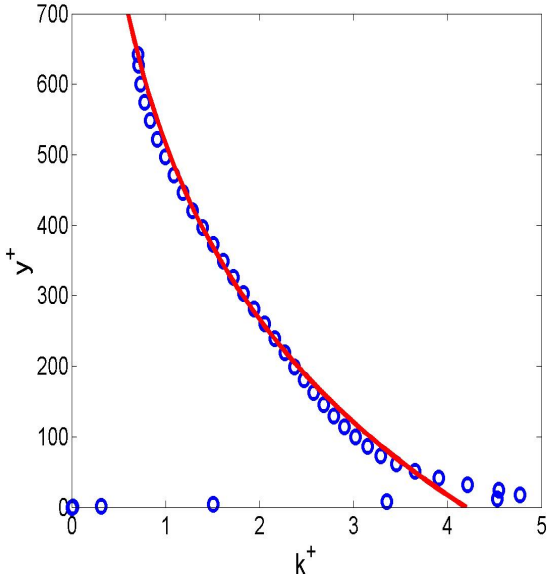


FIGURE 5.1 – Turbulent kinetic energy. o, DNS data [60] for $Re_\tau = 642$ ; Curve, Eq. (5.20) with $A_1^+ = 360$ and $D_1 = 4.2$.

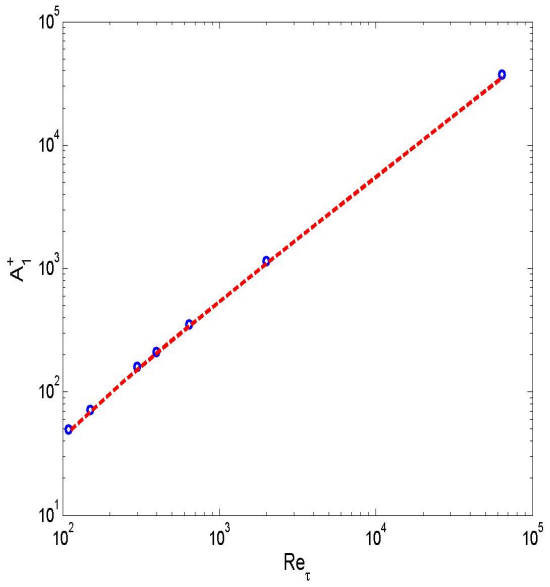


FIGURE 5.2 – Calibration of $A_1^+$ by DNS data. o, DNS data ; Curve, Eq. (5.21).

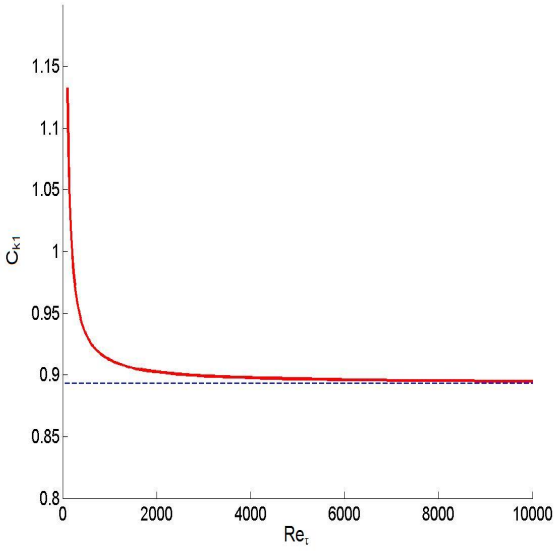


FIGURE 5.3 – Variation of coefficient $C_{k1}$, Eq. (5.22).

The calibration by DNS data provides values $C_{A1} = 0.58$ and $C_{A2} = 17$ (Fig. 5.2).

From Eqs. (5.20) and (5.8), we have $2C_{k1}\xi = y^+/A_1^+$ and since $\xi = y/h = y^+/Re_\tau$, it is possible to obtain a relation between $C_{k1}$ and $A_1^+$ as $C_{k1} = 0.5Re_\tau/A_1^+$. Eq. (5.21) provides therefore the following equation for $C_{k1}$ [9]

$$C_{k1}(Re_\tau) = \frac{0.5\, Re_\tau}{C_{A1}\, Re_\tau - C_{A2}} \tag{5.22}$$

For high $Re_\tau$ numbers (Fig. 5.3), $C_{k1}$ becomes equal to $C_{k1} \approx 0.5/C_{A1}$ (since $C_{A1}\, Re_\tau >> C_{A2}$). For $C_{A1} = 0.58 \Rightarrow C_{k1} \approx 0.86$ which is close to the empirical value $C_{k1} = 1$ proposed by Nezu and Nakagawa [80]. Instead of this empirical $Re_\tau$-independent value, our Eq. (5.22) is $Re_\tau$-dependent and provide a more acurate value for TKE profiles. Figure (5.4) presents a comparison of TKE profiles obtained by Eq. (5.8) with $C_{k1} = 1$ (dashed lines) and $C_{k1} = 0.86$ (solide lines) and experimental data [101] (symbols). This figure shows that our value for $C_{k1}$ is able to improve the accuracy of TKE.

Eq. (5.20) is valid only in the equilibrium region and therefore is not appropriate near the wall (Fig. 5.1). In order to provide a more accurate solution, we need an estimation of $G$ and $\varepsilon$. We will first suggest an approximation for $G - \varepsilon$ and then we will present a more general solution. This solution will allow to improve the TKE profile the buffer layer.

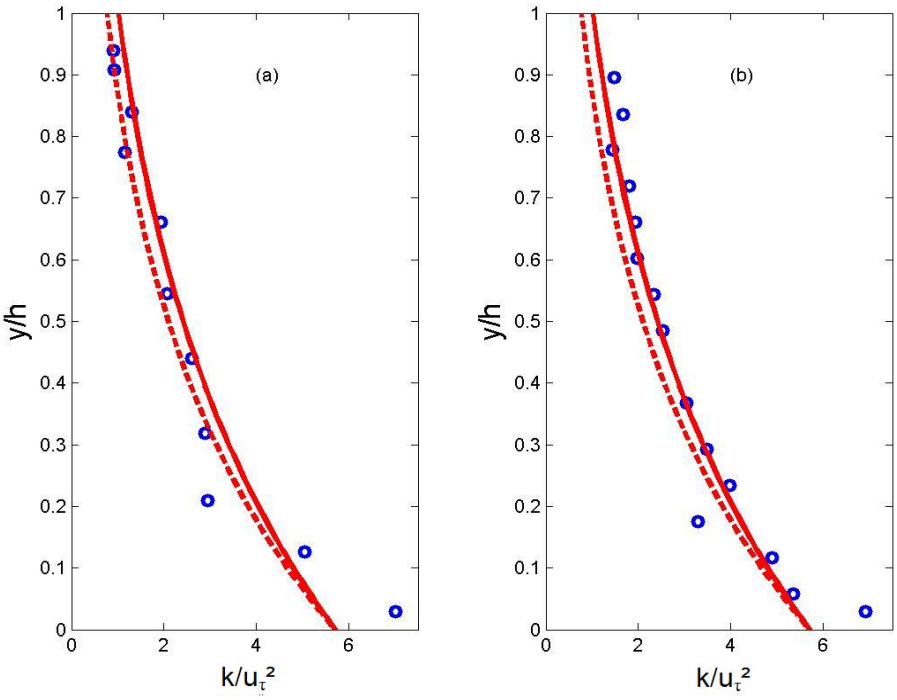


FIGURE 5.4 – Comparison of TKE profiles from Eq. (5.8) with : dashed lines, $C_{k1} = 1$ ; solide lines, $C_{k1} = 0.86$ and o, experimental data of Sukhodolov *et al.* [101].

## 5.3 Generalized analytical solution for TKE

### 5.3.1 Used approximations and assumptions

#### 5.3.1.1 Case of rough surface

From measurements of Sukhodolov *et al.* [101], we noticed that from a certain distance from the bed the approximation $\frac{G\,h}{u_\tau^3} = \frac{C_G}{(y/h)^2}$ (where $C_G$ is a dimensionless constant), which can be expressed as follows [3]

$$G = C_G\,\frac{u_\tau^3\,h}{y^2} \tag{5.23}$$

represents well, with $C_G = 1$, experimental data. An appropriate fit for $G$ gives $C_G = 0.6$. Equation (5.19) shows that Eq. (5.23) is in the form of $G \approx \frac{g}{y^2}$.

We noticed from these experimental data [101] that $\varepsilon$ has a shape similar to $G$, we wrote therefore

$$\varepsilon = C_\varepsilon\,\frac{u_\tau^3\,h}{y^2} \tag{5.24}$$

where $C_\varepsilon$ is a constant. As for $G$, this equation is in the form $\varepsilon \approx \frac{g}{y^2}$. With $C_\varepsilon = 1$, (5.24) represents the shape of experimental data [101]. An appropriate fit for $\varepsilon$ gives $C_\varepsilon = 0.5$.

This shape for $G$ and $\varepsilon$ is confirmed by wind tunnel experiments of Krogstad and Antonia [64] over rough walls.

From equations (5.23), (5.24) and (5.19), we are able to write $G - \varepsilon \approx \frac{g}{y^2}$. Therefore, $G - \varepsilon$ can be approximated by [3]

$$G - \varepsilon = C_d\,\frac{g}{y^2} \tag{5.25}$$

where $C_d$ is a dimensionless coefficient ($C_d = C_G - C_\varepsilon$). With (5.14) and (5.25), we write equation (5.4) as

$$\frac{d}{d\xi}\left(C_{\nu_t}\,\frac{g}{k}\,\frac{dk}{d\xi}\right) = -C_d\,\frac{g}{\xi^2} \tag{5.26}$$

#### 5.3.1.2 Case of smooth surface

The assumption $\frac{d}{dy}\left(\nu_t\,\frac{dk}{dy}\right) \approx \frac{1}{y^2}$ of Eq. (5.26), which is valid for rough surface, seems to be valid even for smooth surface, since even if $G$ decreases very close to a wall, the term of molecular viscosity in the $k$-equation increases there.

Indeed, very close to a wall the modeled $k$-equation is given by

$$\frac{\partial}{\partial\,y}\left(\nu_t\frac{\partial\,k}{\partial\,y}\right) = -\left(G + \frac{\partial}{\partial\,y}\left(\nu\frac{\partial\,k}{\partial\,y}\right) - \varepsilon\right) \tag{5.27}$$

The approximation (for the right-hand side of Eq. 5.27)

$$G + \frac{\partial}{\partial y}\left(\nu \frac{\partial k}{\partial y}\right) - \varepsilon \approx \frac{1}{y^2}, \tag{5.28}$$

allows to obtain the same Eq. (5.26).

We are able to integrate equation (5.26), and therefore to find an analytical solution, only in the case where $g = const$. We will assume, as for the first solution in local equilibrium, that $g = const$.

By integrating (5.26) with the assumption of condition (5.18), we obtain

$$\frac{g}{k}\frac{dk}{d\xi} = \frac{C_d}{C_{\nu_t}}\, g\, \left(\frac{1}{\xi} + const\right) \tag{5.29}$$

### 5.3.2 Proposed analytical solution

We write equation (5.29) as

$$\frac{1}{\sqrt{k}}\frac{d\sqrt{k}}{d\xi} = \left(\frac{C}{\xi} - C_2\right) \tag{5.30}$$

where $C = \dfrac{C_d}{2\, C_{\nu_t}}$ and $C_2 = -const\, C$. By integrating equation (5.30), we obtain [3]

$$\frac{k}{k_0} = \left(\frac{\xi}{\xi_0}\right)^{2\,C}\, e^{[-2\,C_2\ (\xi - \xi_0)]} \tag{5.31}$$

which can be expressed as

$$\frac{k}{u_\tau^2} = D\, \left(\frac{y}{y_0}\right)^{2\,C}\, e^{\left(-\dfrac{y}{A}\right)} \tag{5.32}$$

where $D = (k_0\, e^{2\,C_2\,\xi_0})/u_\tau^2$ and $A = h/(2\,C_2)$.

With the dimensionless wall distance $y^+ = u_\tau y/\nu$ (wall unit), we write equation (5.32) as

$$k^+ = B\, (y^+)^{2\,C}\, e^{(-y^+/A_k^+)} \tag{5.33}$$

where $A_k^+ = A\, u_\tau/\nu$, $k^+ = k/u_\tau^2$, $B = D/(y_0^+)^{2\,C}$ and $y_0^+ = y_0\, u_\tau/\nu$.

We notice that we find equation (5.20) from our solution (5.33) for $C = 0$. This confirms that equation (5.20) is a particular case of our solution (5.33), when $G = \varepsilon$. Indeed, coefficient $C$ is related to $C_d$ and therefore to $G - \varepsilon$.

### 5.3.3 An analytical profile for TKE for $y^+ \leq 20$

The examination of Eq. (5.33) by DNS data of channel flows shows that for $y^+ \leq 20$, $C = 1$, $A_k^+ = 8$ and $B$ is $Re_\tau$-dependent (Fig. 5.5). The coefficient $C$ is therefore equal to 1 for $y^+ \leq 20$, where $k^+$ is given by [3]

$$k^+ = B\ (y^+)^2\ e^{(-y^+/A_k^+)} \tag{5.34}$$

In order to verify the universality of this function (5.34), we validate the proposed equation with different DNS data. Fig. (5.5) presents a comparison between our proposed solution (5.34) and DNS data [60] for different values of $Re_\tau$. These figures confirm the ability of Eq. (5.34) to represent $k^+$, with $C = 1$ and $A^+ = 8$. However, $B$ is depend on $Re_\tau$.

Table 5.1 presents values of $B(Re_\tau)$ obtained from Eq. (5.34) and DNS data [58], [60]. We propose the following function (Eq. 5.35) for the coefficient $B$ [5]

$$B(Re_\tau) = C_{B1}\ \ln(Re_\tau) + C_{B2} \tag{5.35}$$

where $C_{B1}$ and $C_{B2}$ are constants. The calibration (Fig. 5.6) gives $C_{B1} = 0.0164$ and $C_{B2} = 0.0334$ [5].

TABLE 5.1 – Values of coefficient $B(Re_\tau)$ obtained from Eq. (5.34) and DNS data.

| $Re_\tau$ | 109 | 150 | 298 | 395 | 642 | 2003 |
|---|---|---|---|---|---|---|
| $B$ | 0.11 | 0.116 | 0.127 | 0.132 | 0.14 | 0.158 |

We notice that the series expansion of the exponential in Eq. (5.34) at the first order gives $k^+ = By^{+2} - (B/A_k^+)y^{+3}$. This equation is similar to the approximation $k^+ = ay^{+2} + by^{+3}$ (Eq. 5.2) [52] [68]. We can deduce that $a = B$, $b = -B/A_k^+$ and therefore $b = -a/A_k^+$. Our value $A_k^+ = 8$, obtained from DNS data gives therefore $b = -a/8$ and confirms the value of Rahman and Siikonen [90]. Eq. (5.34) is a more general and more accurate solution.

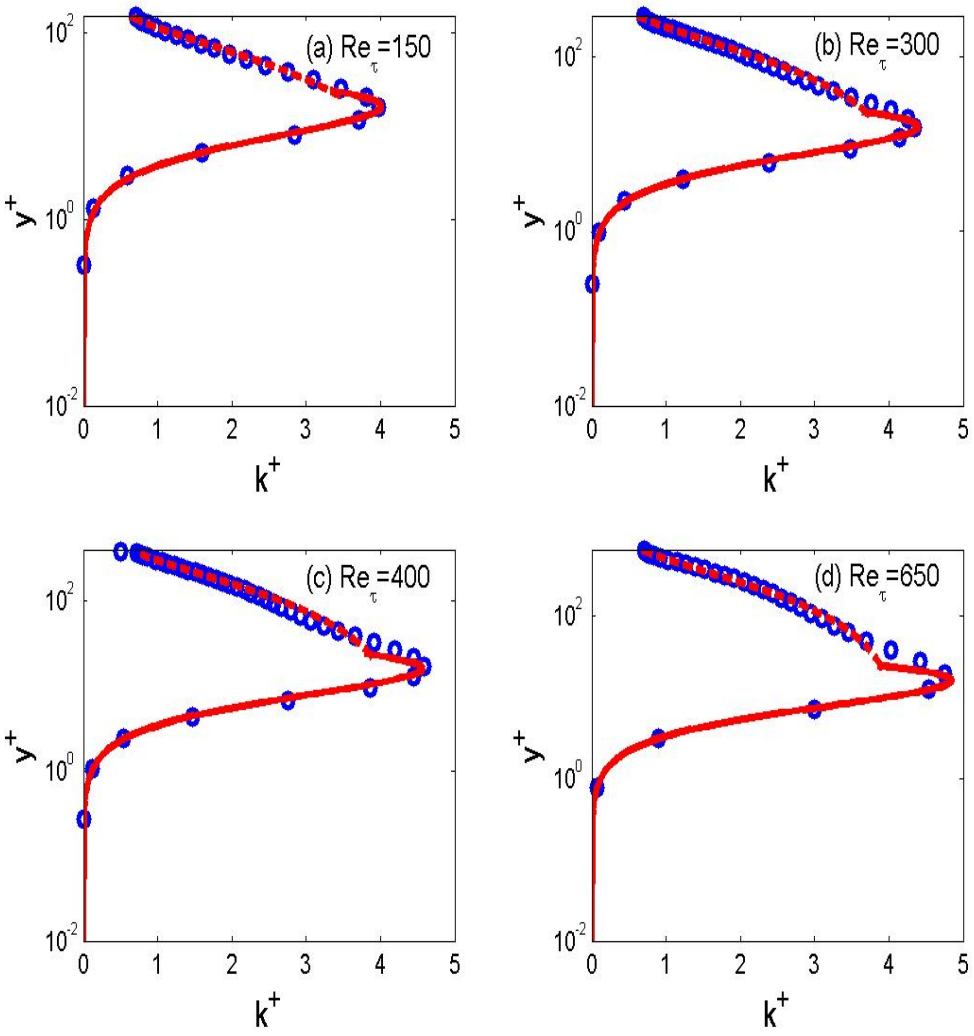


FIGURE 5.5 – TKE profiles for different Reynolds numbers $Re_\tau$. Dashed lines : Eq. (5.20), solid lines : Eq. (5.34).

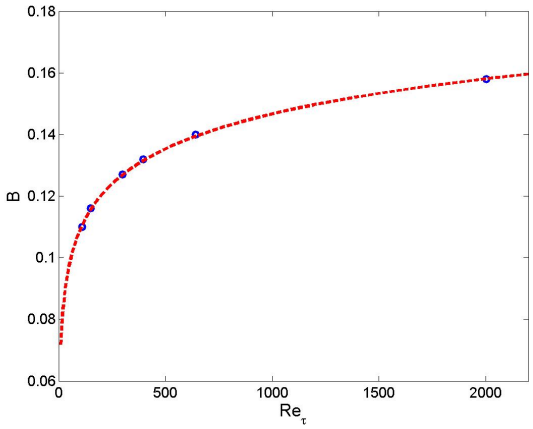


FIGURE 5.6 – Dependency of the coefficient $B$ on the Reynolds number $Re_\tau$. o, values obtained from DNS data ; Curve, proposed function (5.35).

## 5.4 Evaluation in a CFD code

This section, which is a part of my student's Ph.D. thesis (El Gharbi *et al.* [36] [37]), presents a comparative study between different near wall treatments and presents an improved method. Simulations were performed with the aid of the commercial CFD code Fluent [43]. Near wall treatments available in Fluent were tested : Standard Wall Functions, Non Equilibrium Wall Function and Enhanced Wall Treatment. A User Defined Function (UDF), based on the analytical profile for TKE (Eq. 5.34), is developed and implemented. Predicted turbulent kinetic energy profiles are presented and validated by DNS data.

### 5.4.1 Assessment of different near wall treatments available in Fluent

Different near wall treatments available in Fluent were tested : Standard Wall Functions "SWF", Non Equilibrium Wall Function "EWF" and Enhanced Wall Treatment "EWT". A coarse mesh ($500 \times 19$) was used for the standard wall function and the non equilibrium wall function, the wall $y^+$ value is equal to 31.05, while for the enhanced wall treatment a finer mesh was used in the viscous sublayer ($500 \times 57$), for which the wall $y^+$ value is equal to 0.34 [36] [37]. The results obtained for the turbulent kinetic energy $k^+$ profiles are presented in Figure (5.7).

In Fig. (5.7) TKE profiles obtained by Standard Wall Functions, Non Equilibrium Wall Function and Enhanced Wall Treatment are presented with DNS data of Moser *et al.* [77] for $Re_\tau = 590$. The standard and non equilibrium wall functions are not able to provide details about TKE in the viscous and buffer layers. For enhanced wall treatment the TKE is underestimated (dashed line).

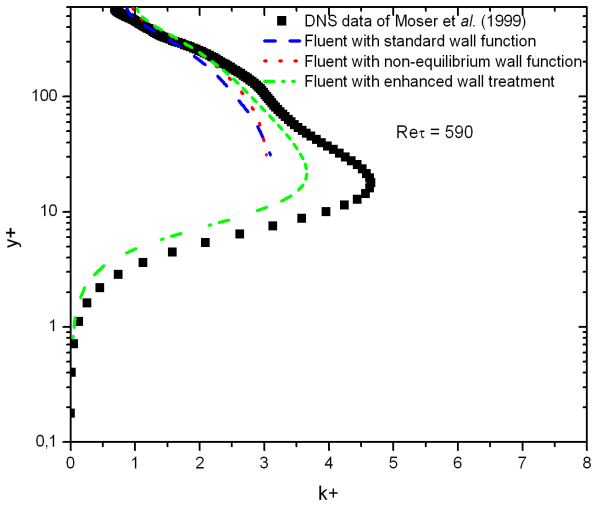


FIGURE 5.7 – Comparison between predicted profiles of turbulent kinetic energy using standard $k-\varepsilon$ model with different wall treatments : Standard Wall Functions, Non Equilibrium Wall Function and Enhanced Wall Treatment and DNS data.

### 5.4.2 Evaluation in Fluent through a UDF

The User Defined Functions (UDF) tool is used to implement Eq. (5.34) in Fluent in order to improve TKE profiles. The UDF was created using the C programming language and added to the solution setup through the Define macros provided by Fluent [36] [37].

Figure (5.8) presents a comparison between TKE profiles obtained by Fluent with Enhanced Wall Treatment (dashed line) and from the UDF which implements our near-wall analytical solution Eq. (5.34) (solid line). This figure shows that result of UDF is closer to DNS data than the TKE profile obtained by enhanced wall treatment without UDF. The approach introduced so far can be readily extended to study more specific flows in confined environments (e.g. Buffone *et al.* 2004 [18]) and may potentially be an efficient approach to characterize these flows near the wall region and/or in a mixed convection problem (Ben Hamed and Bennacer 2008 [15]).

## 5.5 Conclusions

This chapter presented analytical solutions for TKE. The profile of Nezu and Nakagawa [80] for TKE in open-channel flows was revisited. With adequate approximations and assumptions, we presented a general solution, which improves the description of TKE in the near-wall region. This near-wall solution was validated and calibrated by DNS data of turbulent channel flows. A User Defined Function

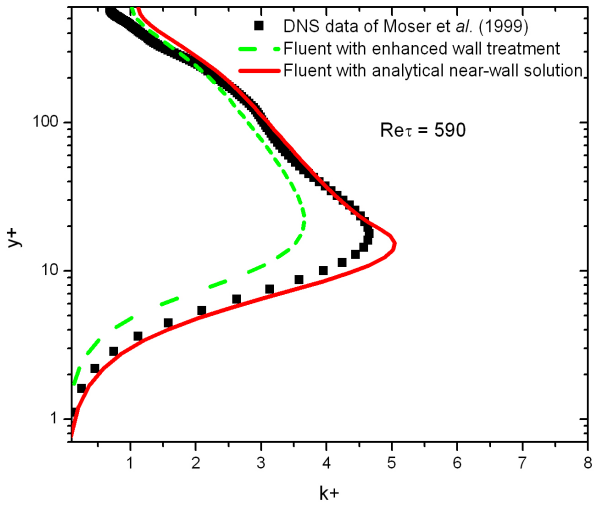


FIGURE 5.8 – Comparison between predicted TKE profiles and DNS data ; dashed line : Fluent with Enhanced Wall Treatment, solid line : Fluent with User Defined Functions (UDF) which implement our near-wall analytical solution.

(UDF) based on our near-wall analytical profile for TKE was developed and implemented in Fluent (part of my student's Ph.D. thesis). The UDF was applied for simulation of TKE, mean velocity and mean temperature profiles in a turbulent channel flow with heat transfer. Comparisons with DNS data show that the UDF improves significantly the prediction of temperature profiles [35].

Chapitre 6

# Eddy viscosity formulations and mean streamwise velocity profiles

*p@@p@12*



## 6.1 Introduction

For turbulent channel flow the mean momentum equation is given by [87] [97] [65]

$$-\overline{uv}^{+} + \frac{dU^{+}}{dy^{+}} = 1 - \left(\frac{y^{+}}{Re_{\tau}}\right) \tag{6.1}$$

By integrating Eq. (6.1), we obtain [5]

$$\frac{dU^{+}}{dy^{+}} = \frac{1}{1+\nu_{t}^{+}}\left(1 - \frac{y^{+}}{Re_{\tau}}\right) \tag{6.2}$$

where $\nu_{t}^{+} = \nu_{t}/\nu$. Resolution of Eq. (6.2) needs the dimensionless eddy viscosity $\nu_{t}^{+}$.

The logarithmic profile provides accurate description of mean streamwise velocity $U^+(y^+)$ in the log-law layer ($30 < y^+ < 0.2Re_\tau$). However, it fails on the one hand in viscous and buffer layers and on the other hand in the outer layer. This chapter aims to improve predicted velocity profiles by using analytical eddy viscosity formulations based on TKE profiles presented in the last chapter.

The well known mixing length equation of van Driest [110] is given by

$$l_m = \kappa\, y\, \left(1 - e^{-y^+/A_l^+}\right) \tag{6.3}$$

where $l_m$ is the mixing length, $\kappa$ the Kármán constant ($\approx 0.41$) and $A_l^+ = 26$. Eq. (6.3) is used in viscous and buffer layers. For $y^+ >> A_l^+$, it reverts to the classical linear mixing length equation

$$l_m = \kappa\, y \tag{6.4}$$

Among the most used eddy viscosity equations, the parabolic profile given by [117] [45] [80]

$$\nu_t = \kappa\, u_\tau\, y\, \left(1 - \frac{y}{h}\right) \tag{6.5}$$

where $h$ represents the flow depth. This profile is a very useful tool in hydraulic engineering. It is also extensively used in the analysis of experimental data of open-channel and free-surface flows (e.g. Rivers) [118] [101].

Nezu and Rodi [81] improved this profile by the log-wake modified eddy viscosity distribution given by

$$\frac{\nu_t}{u_\tau\, h} = \kappa\, \left(1 - \frac{y}{h}\right)\, \left[\frac{h}{y} + \pi\, \Pi\, sin\left(\frac{\pi\, y}{h}\right)\right]^{-1} \tag{6.6}$$

where $\Pi$ is the Coles parameter expressing the strength of the wake function. Another interesting analytical eddy viscosity model is expressed as

$$\nu_t = \alpha_1\, \kappa\, u_\tau\, y\, e^{-C_1\, \frac{y}{\delta}} \tag{6.7}$$

where $\delta$ is the boundary layer thickness and $\alpha_1$ and $C_1$ two parameters. Eq. (6.7), which was proposed for the planetary boundary layer [19], was based on experimental data. It presents the interest that the vertical profile is similar to the time-averaged eddy viscosity from a two-equation $k$-$\varepsilon$ model [56].

From TKE and mixing length, the eddy viscosity reads as $\nu_t = C_P\, l_m\, \sqrt{k}$ [97]. Eqs. (6.5) and (6.4) allow therefore to write TKE as $\sqrt{k} = (1/C_P)\, u_\tau\, (1 - y/h)$. However, this equation is inconsistant with experiments and DNS (see previous chapter and [2]). In the equilibrium region, TKE profile of Eq. (5.8) is in agreement with eddy viscosity of Eq. (6.7) and log-law profile. Since for local equilibrium $dU/dy = C_P\, (\sqrt{k}/l_m)$, with TKE given by $\sqrt{k} = (1/C_P)\, u_\tau\, f(y)$, the mixing length should therefore reads as $l_m = \kappa\, y\, f(y)$ in the log-law layer ($dU/dy = u_\tau/(\kappa\, y)$).

## 6.2 Eddy viscosity and velocity profiles in viscous and buffer layers

The eddy viscosity (Eq. 6.8) obtained from van Driest's [110] mixing length equation (6.3) as

$$\nu_t = \kappa\, y\, u_\tau \left(1 - e^{-y^+/A_l^+}\right), \tag{6.8}$$

fails to provide an accurate velocity profile in viscous and buffer layers. In order to improve the description of $U^+$, we will use in this section our TKE profile given by Eq. (5.34).

### 6.2.1 An eddy viscosity formulation

We write the dimensionless eddy viscosity in viscous and buffer layers as

$$\nu_t^+ = C_\nu \sqrt{k^+}\, l_m^+ \tag{6.9}$$

where $l_m^+ = l_m\, u_\tau/\nu$ is the dimensionless mixing length and $C_\nu$ a coefficient. In Eq. (6.9), we use $k^+$ given by Eq. (5.34) [3] and $l_m^+$ of van Driest (Eq. 6.3) [110]. The dimensionless eddy viscosity is therefore given by [5]

$$\nu_t^+ = C_\nu\, \kappa\, B^{0.5}\, y^{+2}\, e^{-y^+/(2A_k^+)} \left(1 - e^{-y^+/A_l^+}\right) \tag{6.10}$$

### 6.2.2 Results and discussion

Predicted mean streamwise velocity $U^+(y^+)$ profiles are obtained from Eq. (6.2) and Eq. (6.10). Figure (6.1) shows predicted $U^+(y^+)$ profile for $Re_\tau = 642$ and DNS data [60]. The predicted $U^+(y^+)$ profile (solid line) shows good agreement with DNS data. Values of $A_k^+ = 8$ and $B = 0.14$ are those of the $k^+$ profile [3].

In order to verify the dependency of the coefficient $C_\nu$ on the Reynolds number $Re_\tau$, we present predicted $U^+(y^+)$ profiles for different $Re_\tau$ (Fig 6.2). Profiles of figure (6.2) for $Re_\tau = 395$, $Re_\tau = 642$ and $Re_\tau = 2003$ were obtained with $C_\nu = 0.3$ and values of $A_k^+ = 8$ and $B$ from the $k^+$ profiles [5]. It seems that $C_\nu$ is independent of the Reynolds number for $Re_\tau \geq 395$ and is equal to 0.3. The values of $B(Re_\tau)$ obtained from the $k^+$ profiles are suitable for computation of $U^+(y^+)$ profiles. However, for $Re_\tau = 150$ and $Re_\tau = 109$ (Fig 6.3) the required values of $C_\nu$ are respectively 0.25 and 0.2. Therefore, $C_\nu$ seems to be $Re_\tau$-dependent for $Re_\tau$ less than 395. This dependency seems to be associated to low-Reynolds-number effects. Indeed, Moser *et al.* [77] showed that low-Reynolds-number effects are absent for $Re_\tau > 390$. We notice that for $y^+ < 20$, the required $C_\nu$ is different from $C_\mu^{1/4}$ (with $C_\mu$ is the empirical constant in the $k$-$\varepsilon$ model, equal to 0.09). For $Re_\tau \geq 395$, $C_\nu = C_\mu^{1/2}$.

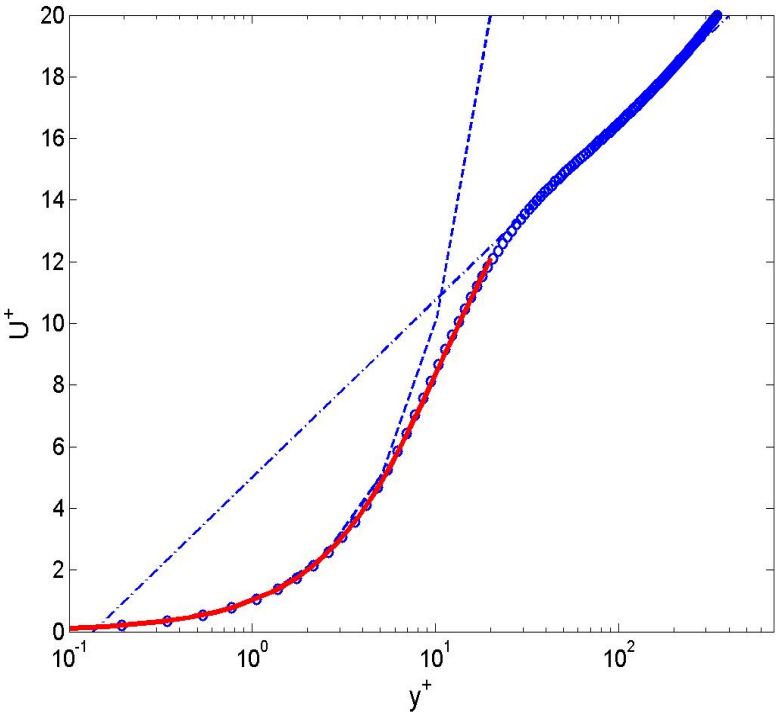


FIGURE 6.1 – Mean streamwise velocity profile $U^+(y^+)$ for $Re_\tau = 642$. o, DNS data [60]. Curves : bold red solid line, solution of Eq. (6.2) with Eq. (6.10) ($C_\nu = 0.3$, $A_l^+ = 26$, $A_k^+ = 8$ and $B = 0.14$) ; dashed line, $U^+ = y^+$ ; dash-dotted line, $U^+ = 2.5\, ln(y^+) + 5.0$.

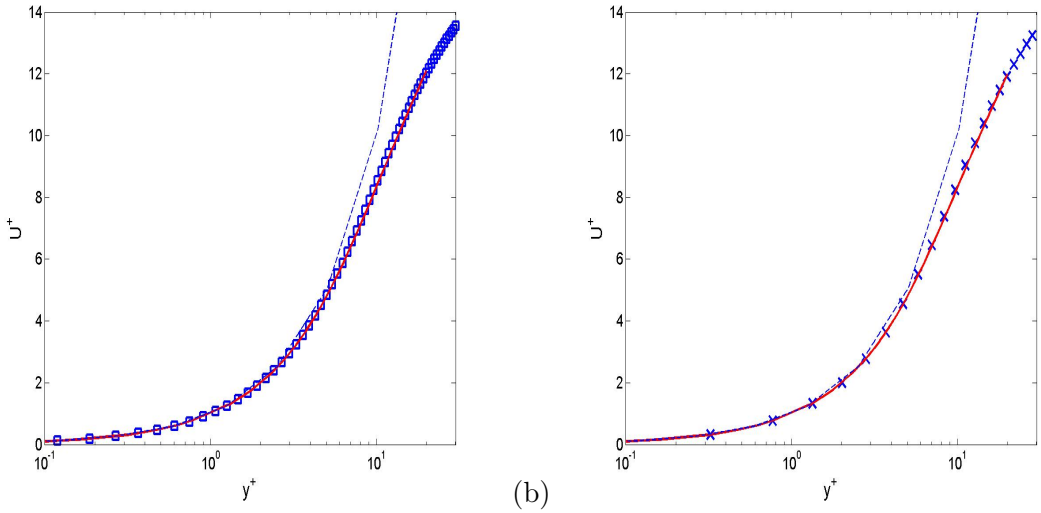


(a) (b)

FIGURE 6.2 – Mean streamwise velocity profiles $U^+(y^+)$ for $Re_\tau \geq 395$. Symbols, DNS data. Curves, Thin dashed line, $U^+ = y^+$. Red solid lines, solution of Eq. (6.2) with Eq. (6.10) ($A_l^+ = 26$, $A_k^+ = 8$) ; (a) $Re_\tau = 395$, squares [60], solid line ($C_\nu = 0.3$, $B = 0.132$) ; (b) $Re_\tau = 2003$, $\times$ [58], solid line ($C_\nu = 0.3$, $B = 0.158$).

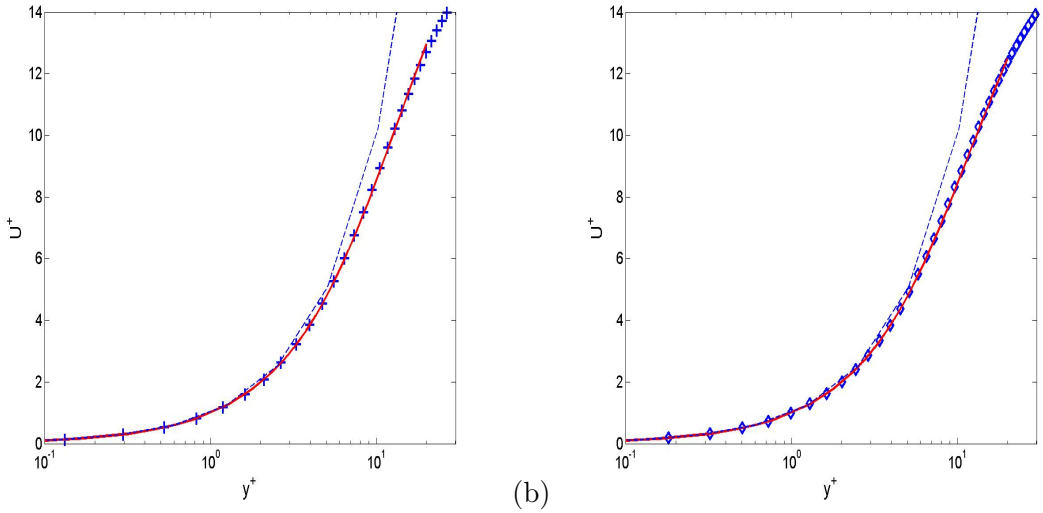


(a) (b)

FIGURE 6.3 – Mean streamwise velocity profiles $U^+(y^+)$ for $Re_\tau < 395$. Symbols, DNS data ; Curves, Thin dashed line, $U^+ = y^+$ ; Red solid lines, solution of Eq. (6.2) with Eq. (6.10) ($A_l^+ = 26$, $A_k^+ = 8$) ; (a) $Re_\tau = 109$, + [60], solid line ($C_\nu = 0.2$, $B = 0.11$) ; (b) $Re_\tau = 150$, diamonds [60], solid line ($C_\nu = 0.25$, $B = 0.116$) ;

In summary, mean streamwise velocity profiles $U^+$ was obtained by solving momentum equation with analytical eddy viscosity formulation based on a near-wall analytical solution for TKE and the van Driest mixing length equation. The parameters obtained from the calibration of $k^+$ was used for the computation of $U^+$. Comparisons with DNS data of fully-developed turbulent channel flows show good agreement. Our simulations show that for $Re_\tau \geq 395$, the coefficient of proportionality $C_\nu$ in the eddy viscosity equation is independent of $Re_\tau$ and equal to 0.3. However, for $Re_\tau < 395$, the coefficient $C_\nu$ is $Re_\tau$-dependent.

## 6.3 Eddy viscosity and velocity profiles in the outer layer

### 6.3.1 A roughness-dependent mixing length equation

The von Kármán's similarity hypothesis [113], which assumes that turbulent fluctuations are similar at all points of the field of flow (similarity rule), gives the mixing length in the form

$$l_m = -\kappa \left( \frac{\dfrac{\partial U}{\partial y}}{\dfrac{\partial^2 U}{\partial y^2}} \right) \tag{6.11}$$

For local equilibrium, an extension of von Kármán's similarity hypothesis allows to write

$$l_m = -\kappa \left( \frac{\dfrac{\sqrt{k}}{l_m}}{\dfrac{\partial}{\partial y}\left(\dfrac{\sqrt{k}}{l_m}\right)} \right) \tag{6.12}$$

We write Eq. (6.12) as [2]

$$l_m = \kappa \sqrt{k} \left( \int_{y_0}^{y} \frac{1}{\sqrt{k}} dy + \frac{y_0}{\sqrt{k_0}} \right) \tag{6.13}$$

where $k_0 = k(y_0)$. Equation (6.13) can be integrated using an algebraic equation for the turbulent kinetic energy.

Inserting Eq. (5.8) (or Eq. 5.20) into Eq. (6.13) and by integrating, we obtain a mixing length equation in the form [2]

$$l_m = \kappa \left( h_1 - (h_1 - y_0)\, e^{-\dfrac{y - y_0}{h_1}} \right) \tag{6.14}$$

where $h_1 = h/C_{k1} = 2A_1$ and $C_{k1}$ given by Eq. (5.22). For a smooth wall ($y_0 = 0$), Eq. (6.14) reverts to

$$\frac{l_m}{h_1} = \kappa \left( 1 - e^{-\dfrac{y}{h_1}} \right) \tag{6.15}$$

**Interest and limits of the proposed mixing length equation**

We analyzed the vertical profile of the proposed Eq. (6.14) [2]. The difference with the classical linear equation $l_m = \kappa\, y$ increases with $y$, but also with the roughness ($\xi_{1,0} = y_0/h_1$ is the relative roughness). We notice that from a same (imposed) value $\kappa\, y_0$ at $y_0$, our mixing length from Eq. (6.14) increases more slowly with $y$, the gradient $dl_m/dy$, which is equal to $\kappa(1-\xi_{1,0})exp(-(\xi_1-\xi_{1,0}))$, where $\xi_1 = y/h_1$, is everywhere (since $y > y_0$) smaller than $\kappa$. Moreover, the slope at the origin $y_0$, equal to $\kappa(1-\xi_{1,0})$, decreases with the roughness $y_0$ [2] ; this involves the introduction of an effective kappa $\kappa_*$ as $\kappa_* = \kappa(1-\xi_{1,0})$. The difference $\kappa_* \neq \kappa$ shows that even at the first order (linearization on the parameter $(\xi_1 - \xi_{1,0})$ which is assumed to be small, near the wall), our profile is different from the classical profile $l_m = \kappa\, y$. It is written as $l_m = \kappa_*\, y + \kappa\, y_0 \xi_{1,0}$. The two profiles are different even near the wall. They will be identical in the sole case of very small roughness (smooth wall). Only there, $\kappa_* = \kappa$ and $l_m \approx \kappa\, y$. We can conclude that the classical profile is able to describe the vertical profile of mixing length near the wall and only for smooth walls.

As a part of student's Ph.D. thesis [23], Eq. (6.14) was evaluated by a finite element CFD code. The validation of the profile (6.14) was made from a set of reference examples. The first example concerns the erosion of a bottom of sand in a uniform flow, and the second concerns the filling of an extraction pit (test from European project SANDPIT) [23].

### 6.3.2 An eddy viscosity formulation

In the equilibrium region $y^+ > 50$, the turbulent kinetic energy (TKE) is given by $\sqrt{k} \approx u_\tau\, exp(-y/h_1)$ (Eq. 5.8) [80]. Since in the inner region the streamwise velocity profile is given by the log-law, it is possible to write a mixing length as $l_m = \kappa\, y\, exp(-y/h_1)$ and therefore Eq. (6.7) for eddy viscosity. In fact, the assumption of local equilibrium in the log-law layer, which allows to write $dU/dy \approx \sqrt{k}/l_m = u_\tau/(\kappa\, y)$, provides a mixing length as $l_m = \kappa\, y\, exp(-y/h_1)$. The eddy viscosity is therefore given by $\nu_t \approx \kappa\, y\, u_\tau\, exp(-2\, y/h_1)$ which provids a shape similar to Eq. (6.7). In the equilibrium region $y^+ > 50$, TKE profile of Eq. (5.8) is therefore in agreement with eddy viscosity of Eq. (6.7) and log-law profile.

Taking into account this particular interest, we analysed Eq. (6.7) by DNS data. Figure (6.4) shows that, for the available DNS for $Re_\tau \leq 2000$, Eq. (6.7) is able to fit (white dashed lines) very satisfactory DNS data (Symbols = blue bold lines) for $50 < y^+ < 0.8\, Re_\tau$.

In order to allow a calibration, we write the eddy viscosity as [12]

$$\nu_t^+ = y^+\, e^{-\dfrac{y^+ + a_{\nu_t}^+}{A_{\nu_t}^+}} \tag{6.16}$$

where $A^+_{\nu_t} = \delta\, u_\tau/(C_1\, \nu)$ and $a^+_{\nu_t} = -A^+_{\nu_t}\, ln(\kappa\, \alpha_1)$ are two $Re_\tau$-dependent coefficients. Calibration by DNS data allows to find linear equations as : $A^+_{\nu_t} = 0.46\, Re_\tau - 5.98$ and $a^+_{\nu_t} = 0.34\, Re_\tau - 11.5$ [12].

Eddy viscosity profiles (Fig. 6.4) obtained from Eq. (6.16) allows a good description of DNS data [12].

### 6.3.3 Mean streamwise velocity profiles

Figures (6.6), (6.5) and (6.7) show predicted velocity $U^+(y^+)$ profiles for different $Re_\tau$ compared to DNS data [60] [58].

These figures show that the logarithmic profile (dash-dotted lines) provides accurate description of $U^+(y^+)$ in the log-law layer ($30 < y^+ < 0.2 Re_\tau$). However, it fails on the one hand in viscous and buffer layers and on the other hand in the outer layer.

Our study improves predicted mean streamwise velocity $U^+(y^+)$ profiles, which are obtained [9] :

— In the outer layer ($y^+ > 0.2\, Re_\tau$, solid lines) by Eq. (6.2) and Eq. (6.16) with a boundary condition for $U^+$ taken as the value of the log-law profile at $y^+ = 0.2\, Re_\tau$

— In inner and buffer layers (dashed lines) by Eq. (6.2) and Eq. (6.10)

Predicted $U^+(y^+)$ profiles with the proposed method (red solid and dashed lines) show good agreement with DNS data.

Semi-logarithmic plots of $U^+$ versus $y^+$ are more appropriate for the inner region. Figure (6.7) presents profiles plotted as $\kappa(U^+ - 5)$ versus $ln(y^+)$ according to $\kappa(U^+ - 5) = ln(y^+)$. The theoretical logarithmic mean velocity profile is a straight line passing by the origin and having a slope of 45° [9].

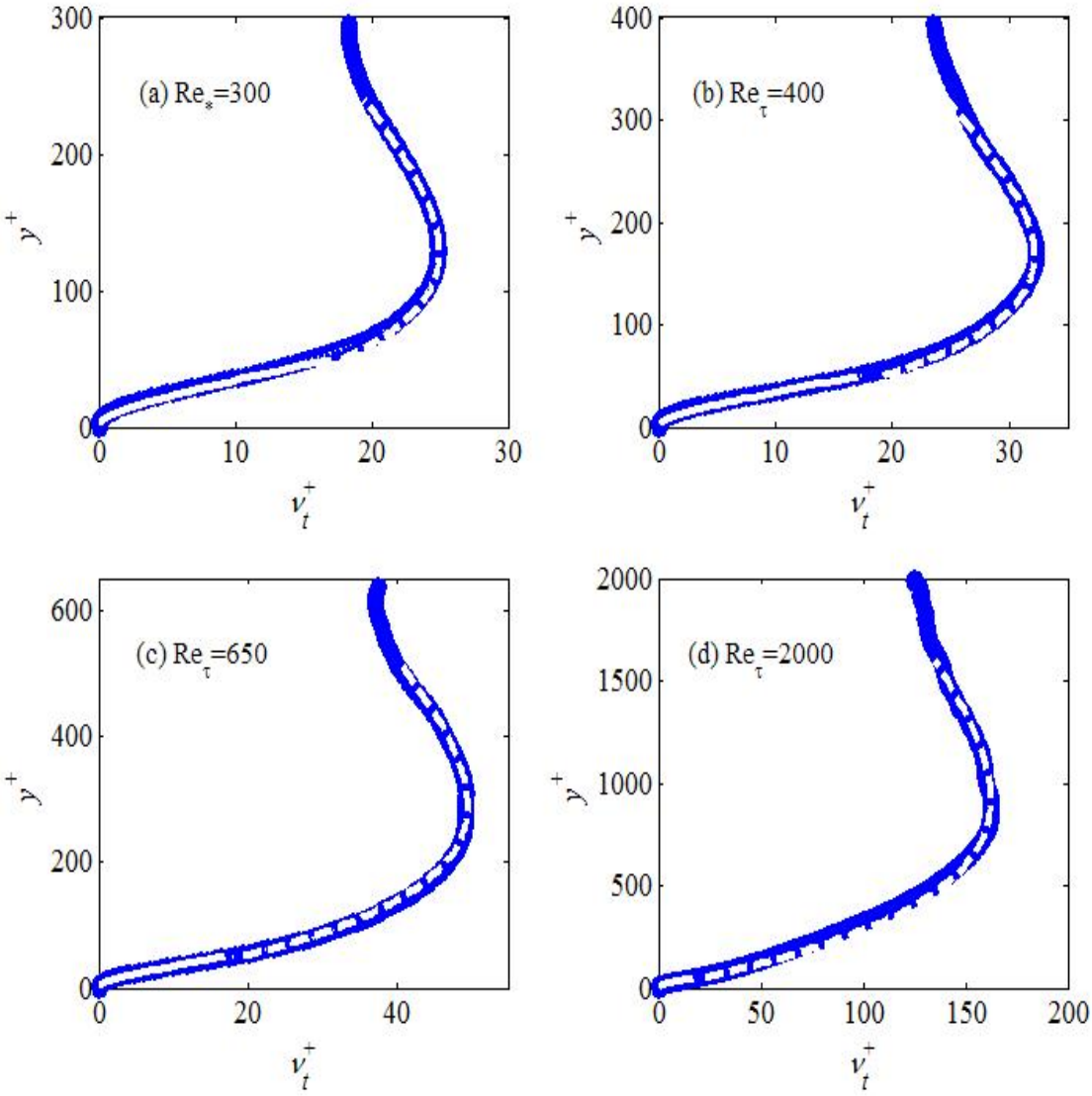


FIGURE 6.4 – Eddy viscosity profiles for different Reynolds numbers $Re_\tau$. Symbols (bold blue lines) : DNS data ; white dashed lines : Eq. (6.16) ; white solid lines : Eq. (6.8).

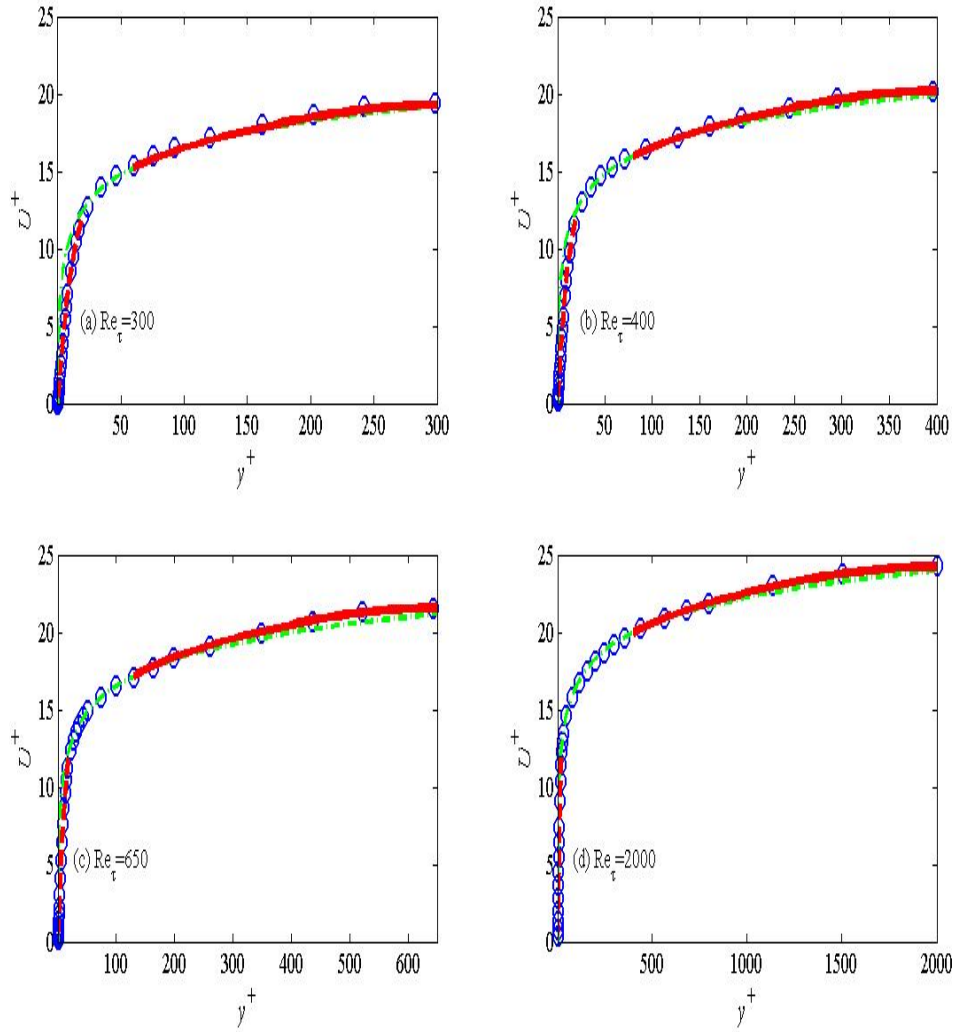


FIGURE 6.5 – Mean streamwise velocity profiles in linear scale. Symbols : DNS data ; green dash-doted lines : log-law ; red solid and dashed lines : present study.

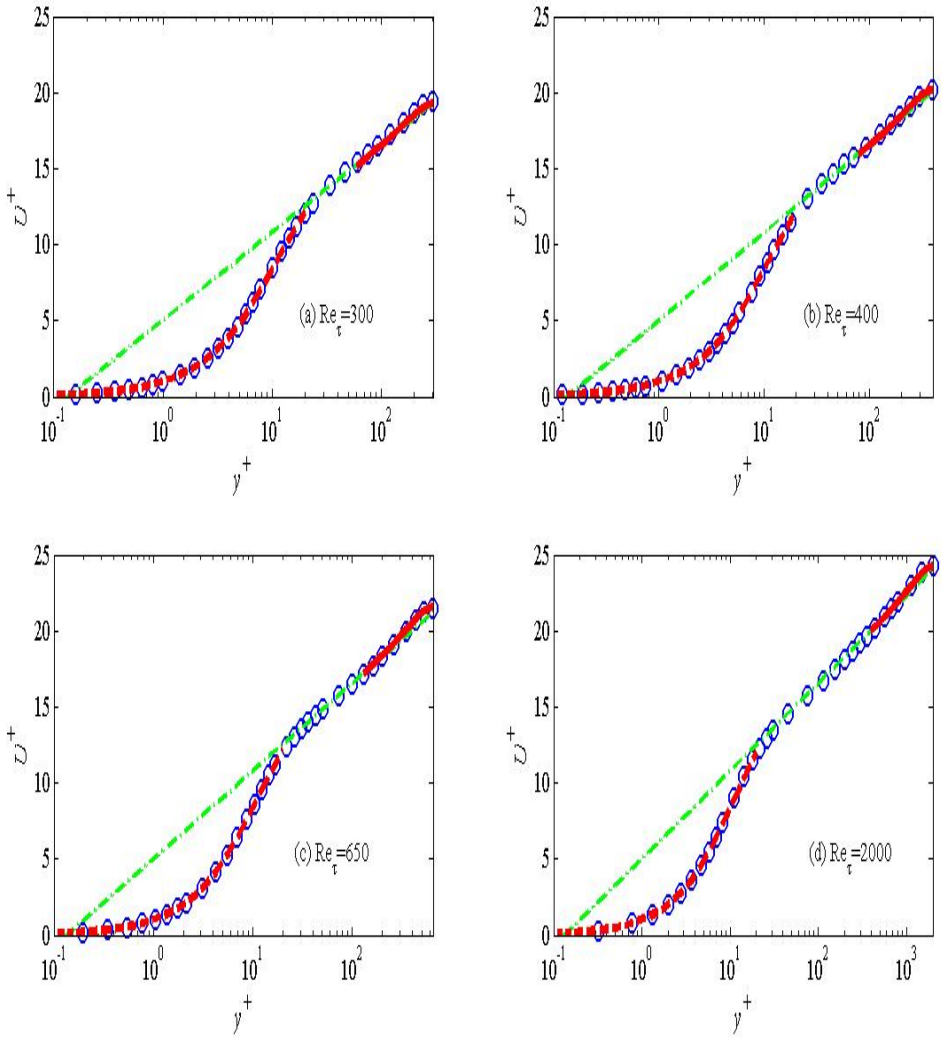


FIGURE 6.6 – Mean streamwise velocity profiles in log scale. Symbols : DNS data ; green dash-doted lines : log-law ; red solid and dashed lines : present study.

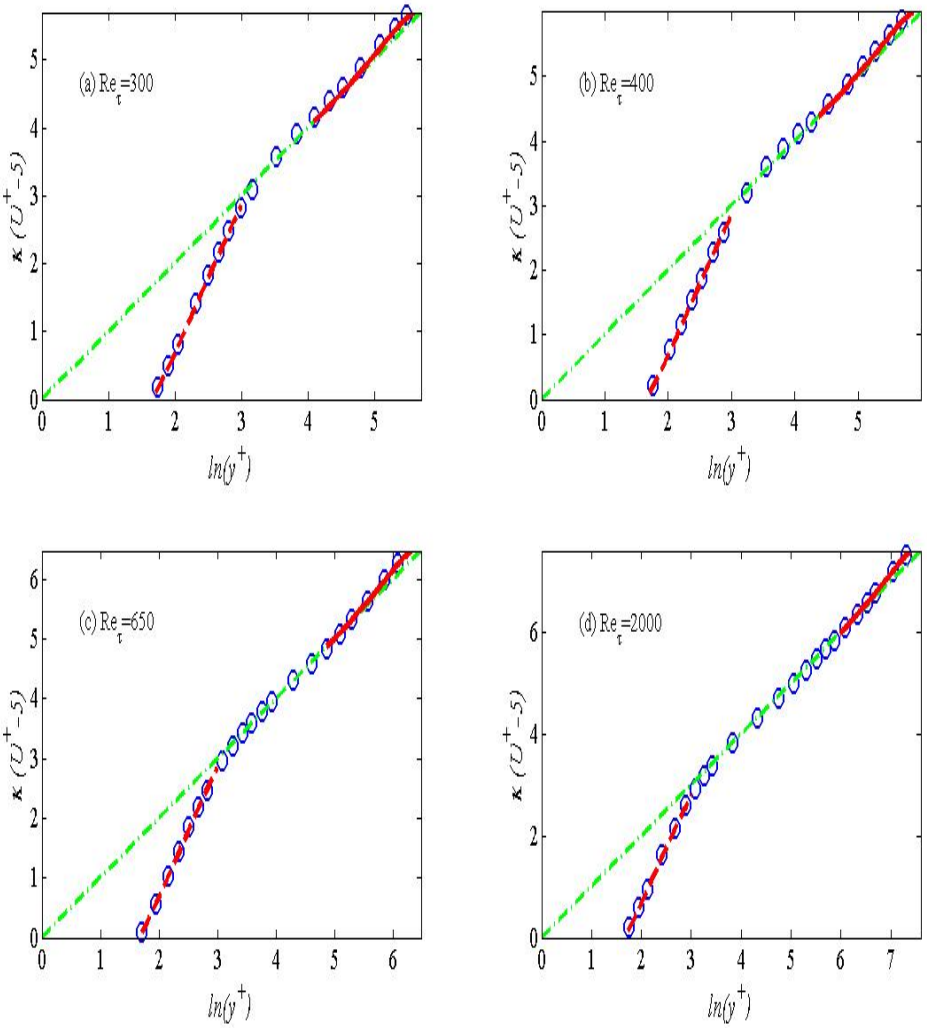


FIGURE 6.7 – Mean streamwise velocity profiles in log scale. Symbols : DNS data ; green dash-doted lines : log-law ; red solid and dashed lines : present study.

## 6.4 Velocity distribution and dip-phenomenon in open channel flows

Due to its practical applications, velocity distribution in open-channel flows has raised up investigations of many engineers and researchers for many years. The vertical velocity profile is well described by the classical log law in the inner region ($\xi < 0.2$), where $\xi$ is the ratio of the distance from the bed $y$ to the water depth $h$ [81] [20] [80] [70]. However, in most cases the log law deviates from experimental data in the outer region ($\xi > 0.2$). This deviation is accounted for by adding the Coles' wake function [25] [55]. In 2D open-channel flows, the log-wake law appears to be the most reasonable extension of the log law [80]. However, in narrow open-channels (i.e. aspect ratio $A_r$ smaller than about 5, where $A_r$ is the ratio of the channel width $b$ to the water depth $h$, Fig. 6.8.a) and near the side walls (i.e. in corner zones) even for wide open-channels [108], the maximum velocity appears below the free surface (i.e. the velocity-dip-phenomenon) involving deviation from the log-wake law. This phenomenon, which was reported more than a century ago [42] [100], was observed both in open-channels and rivers. It is related to secondary currents which appear in 3D open-channel flows [115]. Coles' wake function is unable to represent this behavior since it predicts a velocity which increases with distance from the bed.

The standard two-equation $k - \varepsilon$ model is unable to predict secondary currents and the related velocity-dip-phenomenon since it assumes isotropic turbulence. Accurate predictions of velocity-dip-phenomenon require therefore more sophisticated RANS-based anisotropic turbulence models such as Reynolds stress model (RSM) [61]. Large eddy simulation (LES) and direct numerical simulation (DNS) allows predicting secondary currents in a narrow open-channels [53]. Instead of these turbulence models, analytical and/or empirical relations were proposed to predict the velocity-dip-phenomenon for engineering applications. Sarma *et al.* [96] proposed a generalized version of the binary velocity distribution law, which combines the logarithmic law for the inner region with the parabolic law for the outer region. Guo and Julien [48] [49] proposed a modified-log-wake law (MLW-law) which fits velocity profiles with dip-phenomenon. However, this law could not be used for predictive applications since it requires to fit the near free surface velocities to the parabolic law in order to obtain dip position and maximum velocity [49]. As indicated in [49], the MLW-law could be used only in flow measurements since it requires sampled velocities. Yang *et al.* [118] proposed a dip-modified-log law (DML-law) based on the analysis of the Reynolds-averaged Navier-Stokes (RANS) equations. This law, which consists of two logarithmic distances one from the bed (i.e. the log law) and the other from the free surface, presents the advantage that it contains only one parameter of dip-correction $\alpha$. The dip-modified-log law (DML-law) reverts the classical log law for $\alpha = 0$.

Even if the dip-modified-log law [118] predicts dip-phenomenon for smooth uniform open channel flows, it presents important difference with experimental data in the rough wall flow regime [7]. In most cases, it is not possible to improve ve-

locity profiles by adjusting the parameter $\alpha$. The aim is to improve the prediction of velocity distribution with dip phenomenon in open channel flows. We will first present model equations, which are based on the Reynolds-averaged Navier-Stokes (RANS) equations, and the related assumptions. A simple dip-modified-log-wake law (sDMLW-law), which reverts to log-wake law for large values of $A_r$, will be presented. Finaly, we will present an ordinary differential equation (ODE) for velocity distribution in open channel flows obtained using a log-wake modified eddy viscosity distribution. Numercial and semi-analytical solutions (full dip-modified-log-wake law, fDMLW-law) of the proposed ODE will be validated by experimental data of measured velocities in open-channels.

### 6.4.1 Model equations

For steady uniform open-channel flows, using the continuity equation, the Reynolds-averaged Navier-Stokes (RANS) momentum equation becomes in the streamwise direction $x$ (Fig. 6.8)

$$\frac{\partial\, U\, V}{\partial\, y} + \frac{\partial\, U\, W}{\partial\, z} = \nu\frac{\partial^2 U}{\partial\, y^2} + \nu\frac{\partial^2 U}{\partial\, z^2} + \frac{\partial - \overline{u\, v}}{\partial\, y} + \frac{\partial - \overline{u\, w}}{\partial\, z} + g\, sin\theta \tag{6.17}$$

where $x$, $y$ and $z$ are respectively the streamwise, vertical and lateral directions and $U$, $V$ and $W$ the three corresponding mean velocities ($u$, $v$ and $w$ are the turbulent fluctuations), $\nu$ the fluid kinematic viscosity, $g$ the gravitational acceleration, and $\theta$ is the angle of the channel bed to the horizontal axis (Fig. 6.8.b). We write Eq. (6.17) as

$$\frac{\partial\left(U\, V - \left[\nu\frac{\partial\, U}{\partial\, y} - \overline{u\, v}\right]\right)}{\partial\, y} + \frac{\partial\left(U\, W - \left[\nu\frac{\partial\, U}{\partial\, z} - \overline{u\, w}\right]\right)}{\partial\, z} = g\, S \tag{6.18}$$

where $S = sin\theta$ is the channel slope.

In the central zone of the channel (Fig. 6.8.a), we assume that the vertical gradients ($\partial/\partial y$) are dominating, we neglect therefore the horizontal gradients ($\partial/\partial z$) [118]. For large values of $y$, the viscous part ($\nu\, dU/dy$) of the shear stress $\tau/\rho = (\nu\,\partial U/\partial\, y) - \overline{u\, v}$ ($\rho$ is the fluid density) is small compared with the turbulent part $-\overline{uv}$ [4], Eq. (6.18) becomes

$$\frac{\partial\, U\, V}{\partial\, y} + \frac{\partial\overline{uv}}{\partial\, y} = g\, S \tag{6.19}$$

Integration of Eq. (6.19) gives

$$\frac{-\overline{uv}}{u_\tau^2} = \left(1 - \frac{y}{h}\right) - \alpha_1\,\frac{y}{h} + \frac{U\, V}{u_\tau^2} \tag{6.20}$$

where $u_\tau$ is the friction velocity, $h$ the water depth and $\alpha_1 = (g\, S\, h/u_\tau^2) - 1$. By assuming [118]

$$\frac{U\, V}{u_\tau^2} \approx -\alpha_2\frac{y}{h} \tag{6.21}$$

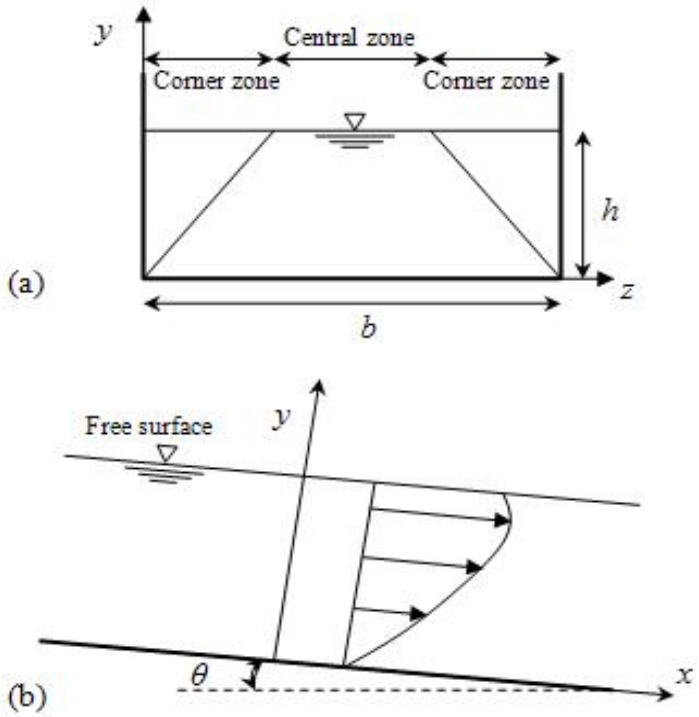


FIGURE 6.8 – Definition sketch for steady uniform open-channel flow.

where $\alpha_2$ is a positive coefficient, Eq. (6.20) becomes

$$\frac{-\overline{uv}}{u_\tau^2} = \left(1 - \frac{y}{h}\right) - \alpha \frac{y}{h} \tag{6.22}$$

where $\alpha = \alpha_1 + \alpha_2$.
With the Boussinesq assumption

$$-\overline{uv} = \nu_t \frac{dU}{dy} \tag{6.23}$$

Eq. (6.22) gives

$$\frac{d\,U}{d\,y} = \frac{u_\tau^2}{\nu_t}\left[\left(1 - \frac{y}{h}\right) - \alpha \frac{y}{h}\right] \tag{6.24}$$

Eq. (6.24) contains two unknowns namely $(d\,U/d\,y)$ and $\nu_t$. Since the aim of our study is to predict velocity profiles in open-channel flows, we need therefore the eddy viscosity.

### 6.4.2 Dip-modified laws

With an eddy viscosity profile $\nu_t(y)$, integration of Eq. (6.24) will provide the velocity distribution.

#### 6.4.2.1 Dip-modified log law

Yang *et al.* [118] obtained a dip-modified-log law (DML-law) based on Eq. (6.24) and the parabolic eddy viscosity Eq. (6.5), which allows to write Eq. (6.24) as

$$\frac{d\,U}{d\,y} = \frac{u_\tau}{\kappa\,y}\left(1 - \alpha\,\frac{\frac{y}{h}}{1-\frac{y}{h}}\right) \tag{6.25}$$

Integration of Eq. (6.24) gives [118]

$$\frac{U}{u_\tau} = \frac{1}{\kappa}\left[ln\left(\frac{y}{y_0}\right) + \alpha\,ln\left(\frac{1-\frac{y}{h}}{1-\frac{y_0}{h}}\right)\right] \tag{6.26}$$

where $y_0$ is the distance at which the velocity is hypothetically equal to zero. Since $y_0/h << 1$ and with $U_a = U/u_\tau$, $\xi = y/h$ and $\xi_0 = y_0/h$, Eq. (6.26) can be simplified as

$$U_a = \frac{1}{\kappa}\left[ln\left(\frac{\xi}{\xi_0}\right) + \alpha\,ln\,(1-\xi)\right] \tag{6.27}$$

The dip-modified log law (Eq. 6.27) is able to predict the velocity-dip-phenomenon thanks to the second term of the right-hand-side of Eq. (6.27) which is linearly proportional to $ln(1-y/h)$ the logarithmic distance from the free surface. The factor of proportionality $\alpha$ is the dip-correction parameter [118]. This law presents the advantage that it contains only this unique parameter and reverts to the classical log law for $\alpha = 0$.

Yang *et al.* [118] proposed for $\alpha$ an empirical formula $\alpha(z) = 1.3\,exp\,(-z/h)$, where $z$ is the lateral distance from the side wall $z$. On the channel centerline (at $z = b/2$ and therefore $z/h = A_r/2$, this equation becomes $\alpha(A_r) = 1.3\,exp\,(-A_r/2)$. In order to use a single general formula, we write $\alpha$ as

$$\alpha = C_1\,exp\,(-C_2\,A_r\,Z) \tag{6.28}$$

where $Z$ is the dimensionless (by the half channel width) lateral distance from the side wall $= z/(b/2) = (2z)/b$, $C_1$ and $C_2$ are two coefficients. From calibration of Yang *et al.* [118] $C_1 = 1.3$ and $C_2 = 0.5$. For wide open-channels (large value of $A_r$, > than about 5), $\alpha$ becomes equal to zero (Eq. 6.28) and DML-law (Eq. 6.27) reverts to log-law. However, log-law is valid only in the inner region ($\xi = y/h < 0.2$).

#### 6.4.2.2 Simple dip-modified-log-wake law

In the outer region ($\xi > 0.2$), log-law deviates from experimental data. In two-dimensional (2D) open-channel flows, this deviation is accounted for by adding the Coles [25] wake function $(2\,\Pi/\kappa)\,sin^2\,(\pi\,y/2\,h)$ as [55]

$$\frac{U}{u_\tau} = \frac{1}{\kappa}\left[ln\left(\frac{y}{y_0}\right) + 2\,\Pi\,sin^2\left(\frac{\pi\,y}{2\,h}\right)\right] \tag{6.29}$$

In 2D open-channel flows, the log-wake law (Eq. 6.29) appears to be the most reasonable extension of the log-law. However, the value of $\Pi$ seems to be not universal. Cebeci and Smith [21] found experimentally that $\Pi$ increased with the Reynolds number $Re$ in zero-pressure-gradient boundary layers, attaining an asymptotic value of $\Pi = 0.55$ at high $Re$. Laser Doppler Anemometry (LDA) velocity measurements in 2D fully developed open-channel flow over smooth beds [81] showed that $\Pi$ increases from zero with the friction Reynolds number $Re_\tau$ and becomes nearly constant $\Pi \cong 0.2$, for $Re_\tau > 2000$ (Reynolds number $Re > 10^5$). Cardoso *et al.* [20] observed, for uniform flow in a smooth open channel, in the core of the outer region ($0.2 < y/h < 0.7$) a wake of a relatively small strength ($\Pi \cong 0.08$), followed in the near-surface-zone ($0.7 < y/d < 1$) by a retarding flow which was associated to weak secondary currents. Velocity measurements by Kirkgoz [63], in a fully developed rectangular subcritical open channel flow on smooth bed, show Cole's parameter equal to 0.1. Measurements of Li *et al.* [70]), for Froude number $Fr > 1$ and $Re > 10^5$, show wake strength equal to 0.3.

In 3D open-channel flows with secondary currents, the log-wake law is unable to predict velocity-dip-phenomenon. A suitable simple law seems possible by adding, to the log law, both Coles' wake function (Eq. 6.29) and the term linearly proportional to the logarithmic distance from the free surface (Eq. 6.27) as [7]

$$U_a = \underbrace{\frac{1}{\kappa}\, ln\left(\frac{\xi}{\xi_0}\right)}_{Term\ I} + \underbrace{\frac{2\,\Pi}{\kappa}\, sin^2\left(\frac{\pi}{2}\,\xi\right)}_{Term\ II} + \underbrace{\frac{\alpha}{\kappa}\, ln\,(1-\xi)}_{Term\ III} \tag{6.30}$$

Eq. (6.30) is referred as the simple dip-modified-log-wake law (sDMLW-law).

This law presents the advantage that, in 2D open-channel flows, it reverts to log-wake law ($\alpha = 0$).

### 6.4.3 Proposed ordinary differential equation for velocity distribution and dip phenomenon

#### 6.4.3.1 Ordinary differential equation

Instead of the parabolic profile for the eddy viscosity (Eq. 6.5), we can use a more appropriate approximation in accordance to log-wake law (Eq. 6.6) [81].

By inserting Eq. (6.6) into Eq. (6.24), we obtain an ordinary differential equation (ODE) for velocity distribution

$$\frac{d\,U}{d\,y} = \frac{u_\tau}{\kappa\,h}\left(1 - \alpha\,\frac{\dfrac{y}{h}}{1-\dfrac{y}{h}}\right)\left[\frac{h}{y} + \pi\,\Pi\, sin\left(\frac{\pi\,y}{h}\right)\right] \tag{6.31}$$

For $\alpha = 0$, Eq. (6.31) gives the log-wake law. We write Eq. (6.31) as

$$\frac{d\,U}{d\,y} = \frac{u_\tau}{\kappa\,y}\left(1 - \alpha\,\frac{\dfrac{y}{h}}{1-\dfrac{y}{h}}\right)\left[1 + \pi\,\Pi\,\frac{y}{h}\, sin\left(\frac{\pi\,y}{h}\right)\right] \tag{6.32}$$

For $\Pi = 0$, Eq. (6.32) reverts to Eq. (6.25) which provide the dip-modified-log law (Eq. 6.27).

Or with dimensionless variables [7]

$$\frac{d\,U_a}{d\,\xi} = \frac{1}{\kappa}\left(1 - \alpha\,\frac{\xi}{1-\xi}\right)\left[\frac{1}{\xi} + \pi\,\Pi\,sin\,(\pi\,\xi)\right] \tag{6.33}$$

For $\alpha = 0$ and $\Pi = 0$, integration of Eq. (6.33) gives the log law. Eq. (6.33) provides the dip distance $\xi_{dip}$ or the dimensionless distance (from the bed) of the maximum velocity $U_{a\,max} = U_a(\xi = \xi_{dip})$. Since $d\,U_a/d\,\xi = 0$ at $\xi = \xi_{dip}$, $\alpha$ is given therefore from Eq. (6.33) by

$$\alpha = \frac{1}{\xi_{dip}} - 1 \tag{6.34}$$

The maximum velocity occurs therefore at $\xi_{dip} = 1/(\alpha + 1)$.

#### 6.4.3.2 Full dip-modified-log-wake law

Integration of Eq. (6.33), with $\xi_0 << 1$, gives [7]

$$U_a = \underbrace{\underbrace{\frac{1}{\kappa}\,ln\left(\frac{\xi}{\xi_0}\right)}_{Term\ I} + \underbrace{\frac{2\,\Pi}{\kappa}\,sin^2\left(\frac{\pi}{2}\,\xi\right)}_{Term\ II} + \underbrace{\frac{\alpha}{\kappa}\,ln\,(1-\xi)}_{Term\ III}}_{sDMLW-law} - \underbrace{\frac{\alpha\,\pi\,\Pi}{\kappa}\int_{\xi_0}^{\xi}\frac{\xi}{1-\xi}sin\,(\pi\,\xi)\;d\xi}_{additional\ term\ IV} \tag{6.35}$$

Eq. (6.35) is referred as the full dip-modified-log-wake law (fDMLW-law). This equation (fDMLW-law) differs from the simple dip-modified-log-wake law (sDMLW-law, Eq. 6.30) only by the additional term $(IV)$ (Eq. 6.35).

In order to evaluate the difference between fDMLW-law (Eq. 6.35) and sDMLW-law (Eq. 6.30), we need to integrate $(\xi\,sin(\pi\,\xi))/(1-\xi)$ in the additional term $(IV)$ which is possible by the trapezoidal rule for numerical integration.

For wide open-channels ($A_r > 0.5$), $\alpha$ becomes equal to zero, and proposed full dip-modified-log-wake law (fDMLW-law) reverts to log-wake law since terms III and IV vanish for $\alpha = 0$.

### 6.4.4 Results and discussion

In Fig. (6.9), we use values of $\alpha$ obtained from estimated dip positions (Eq. 6.34) while the value of $\Pi$ remains equal to 0.45. In addition to log-law (thin solid lines), log-wake-law (Eq. 6.29, dashed lines), simple dip-modified-log-wake law (sDMLW-law, (Eq. 6.30, dash-dotted lines) and full dip-modified-log-wake law (fDMLW-law, Eq. 6.35, bold solid lines), figures (6.9.a.1, 6.9.b.1 and 6.9.c.1) present numerical solutions (bold dots) of ODE (6.33). The fDMLW-law and numerical solutions of ODE provide very accurate velocity profiles. Figure (6.9) shows that there is no difference between full dip-modified-log-wake law (fDMLW-law) profiles (bold solid lines) and numerical solutions of ODE (6.33) (bold dots). These comparisons, with numerical solutions of EDO, show the accuracy of the full dip-modified-log-wake law (fDMLW-law).

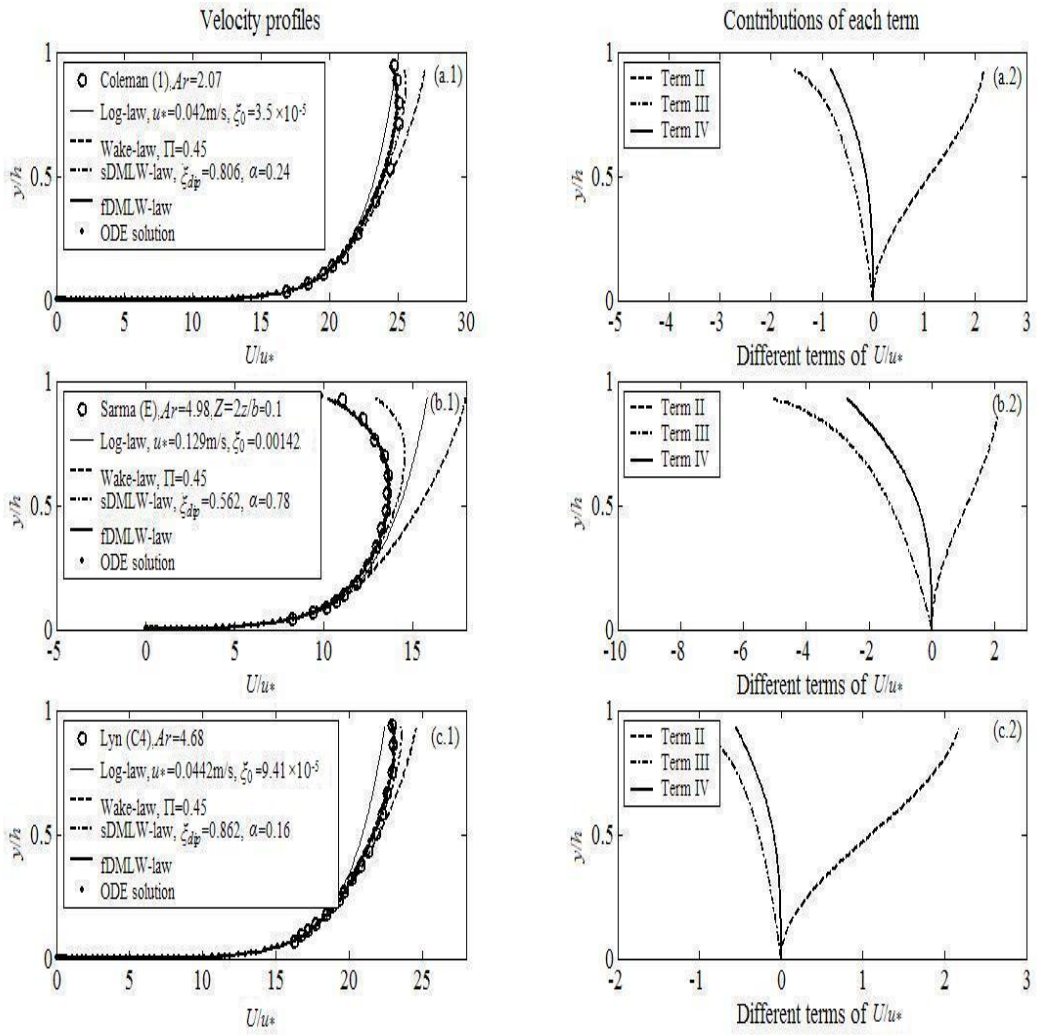


FIGURE 6.9 – Velocity profiles with $\Pi = 0.45$ and $\alpha$ obtained from estimated dip positions (Eq. 6.34). Comparison between log-law, log-wake-law (Eq. 6.29), simple dip-modified-log-wake law (sDMLW-law, (Eq. 6.30), full dip-modified-log-wake law (fDMLW-law, Eq. 6.35), numerical solutions of ODE (6.33) and experimental data of Coleman [24], Sarma *et al.* [96] and Lyn [73]. Figures (a.2), (b.2) and (c.2) : effect of each term in sDMLW-law and fDMLW-law.

Chapitre 7

# Turbulent diffusion of suspended particles

$p@@p@12$



## 7.1 The turbulent Schmidt number

For mass transfer applications, CFD codes need turbulent Schmidt number $Sc_t$. Two formulations of $Sc_t$ are introduced based on a kinetic model for turbulent two-phase flows [30] [119] [44] [8] and a finite-mixing-length theory [85].

### 7.1.1 Introduction

The coefficient of turbulent diffusion of suspended particles $\varepsilon_s$ is related to the eddy viscosity $\nu_t$ by the parameter $\beta$ (i.e., the inverse of the turbulent Schmidt number $Sc_t$)

$$\varepsilon_s = \beta\,\nu_t = (1/Sc_t)\,\nu_t \tag{7.1}$$

In this equation, $\beta = 1/Sc_t$ describes the difference between diffusivity of momentum (diffusion of a fluid "particle") and diffusivity of solid particles (for example sediments). It is possible to write Eq. (7.1) as $\varepsilon_s = (1 + a\,Ri)^b\,(1/Sc_t)\,\nu_t$, where $Ri$ is the Richardson number and $a$ and $b$ empirical coefficients.

The value of $\beta$ has been the subject of much research for suspended sediment transport in open-channels. Researchers found that $\beta$ approaches unity for fine sediments and deviates for coarse ones [33] [46]. In suspension flows over movable beds,

experiments show that depth-averaged $\beta$-values are smaller than unity ($\beta < 1$) for flows without bed forms while they are larger than unity ($\beta > 1$) for flows with bed forms [46].

Elghobashi [38] has classified fluid-solid two phase flows on the basis of the volumetric particle concentration and Stokes number $St = \tau_p/\tau_t$, where : $\tau_p$ is the particle timescale and $\tau_t$ the integral turbulence timescale or turnover time of large eddy. A large value of $St$ corresponds to a weak sedimentation process and therefore to a more uniform concentration profile. At the opposite, a small value of $St$ corresponds to a strong concentration gradient. Rogers and Faton [93] defined the particle response time as

$$\tau_p = \frac{\omega_s}{\left(1 - \frac{\rho_f}{\rho_s}\right) g} \tag{7.2}$$

where $\omega_s$ is the settling velocity of particles, $\rho_f$ fluid density, $\rho_s$ solid density and $g$ the gravitational acceleration. This timescale is the ratio of particles settling velocity to their vertical acceleration (vertical force - gravity minus buoyancy - per unit mass). The integral turbulence timescale (mixing time by the large eddies) is given by $\tau_t \approx l_m/u_{rms} \approx l_m/\sqrt{k}$ or by $\tau_t = \alpha\, k/\varepsilon$ [107], where $k$ is the turbulent kinetic energy (TKE), $\varepsilon$ the dissipation of TKE and $\alpha$ a coefficient. In our study, the eddy turnover time is defined as

$$\tau_t \approx \frac{\nu_t}{k} = \alpha_0 \frac{\nu_t}{k} \tag{7.3}$$

For a two-equation $k$-$\varepsilon$ model the eddy viscosity is $\nu_t = C_\mu k^2/\varepsilon$ and therefore $\alpha_0 = \alpha/C_\mu$.

Different analytical formulations for $Sc_t$ are considered based on basic conservation equations for sediment-water mixtures in turbulent open-channel flows based on a kinetic model and finite-mixing-length model.

### 7.1.2 Kinetic model

Kinetic models for turbulent two-phase flows [30] [119] [44] accounts for both particle-turbulence interactions and particle-particle collisions. In turbulent solid-liquid flows, the Lagrangian equations of particle dynamics are

$$\frac{dr_{pi}}{dt} = v_{pi} \quad and \quad \frac{v_{pi}}{dt} = \frac{u_i - v_{pi}}{\tau_p} + F_i + W_i \tag{7.4}$$

where the particle position in the phase space is ($r_{pi}$ ;$v_{pi}$) at time $t$, $u_i$ is the fluid velocity, $F_i$ is the sum of external forces (including gravity and interphase forces) and $W_i$ is the sum of forces due to interparticle collisions which comes from Boltzmann equations [82]. The kinetic model deals with passing from Lagrangian equation to

the Eulerian ones though a stochastic description. The method of moments is used in order to simplify the equations [30] [119] [82] [44]. Fu *et al.* [44] used kinetic model based on three stochastic motions over position $x_k$ at time $t$ : 1/ the particle velocity $v_k$, 2/ the fluid velocity $u_i$, and 3/ the forces $W_i$. Derevich *et al.* [30] assume that Furutsu-Novikov equations prove that all those random variables in $x_k$ at time $t$ are Gaussian. The phase space (position and velocity) is a space of dimensions 6 (3 position coordinates and 3 velocity components). In this phase space, we define a probability density distribution function (PDF) $f$ as the probability of presence of a solid particle per unit volume of this space ($dx\,dy\,dz\,dv_x\,dv_y\,dv_z$). This function f is equal to 1 in the presence of a solid particle (Dirac or Delta function equal to 1), and 0 elsewhere (Delta function equal to 0). The average <> over an ensemble of turbulent realisations gives

$$f = \langle \delta\left(x_k - r_{pi}\right) \delta\left(v_k - v_{pi}\right) \rangle \tag{7.5}$$

Integrated over the velocity components, f provides the concentration of solid particles per unit space volume in position

$$c = \int f dv_k \tag{7.6}$$

Fu *et al.* [44] obtained a general conservation equation of mass/impulsion/energy, in the space phase. The first moment is obtained with $\overline{cv_i} = \int v_i f dv_k$. For the case of two-dimensional fully developed steady open-channel flow it is possible to write [44] [8]

$$\varepsilon_s = \left( \frac{1}{1+St} + St \frac{\overline{v_y'^2}}{\overline{u_y'^2}} \right) \nu_t \tag{7.7}$$

where $\overline{u_y'^2}$ and $\overline{v_y'^2}$ are turbulence intensities respectively of fluid phase and solid phase. It is possible to write a relationship between $\overline{u_y'^2}$ and $\overline{v_y'^2}$ as $\overline{u_y'^2} \cong \left(1 - \frac{\rho_f}{\rho_s}\right) \overline{v_y'^2}$, or as a function of eddy viscosity [98]

$$\overline{v_y'^2} \cong \frac{\nu_t}{\tau_t \left(1 - \frac{\rho_f}{\rho_s}\right)} \tag{7.8}$$

The hypothesis of Eq. (7.8) with $\nu_t \approx \tau_t \, \overline{u_y'^2}$ allow writing [12]

$$Sc_t = \left( \frac{St}{1 - \frac{\rho_f}{\rho_s}} + \frac{1}{1+St} \right)^{-1} \tag{7.9}$$

With Stokes number given from Eqs. (7.2) and (7.3) by

$$St = \frac{\omega_s}{\left(1 - \frac{\rho_f}{\rho_s}\right) g} \frac{k}{\alpha_0 \, \nu_t} \tag{7.10}$$

Kinetic model provides $Sc_t$ that are dependent on characteristics of solid particles (settling velocity) and turbulent flow (TKE and eddy viscosity). Eq. (7.9) was analysed and compared to analytical formulation from a two-fluid description [12].

### 7.1.3 Finite-mixing-length model

For the case of sediments, concentrations depend on the interaction between suspended sediments and the flow's turbulence. The feedback between sediment and turbulence has an important effect on sediment transport [27]. It is possible to write that concentrations of suspended sediment result from the balance between an upward mixing flux $\vec{q_m}$ and a downward settling flux $\vec{q_s} = c(y)\vec{\omega_s}$ as

$$q_m - c(y)\omega_s = 0 \tag{7.11}$$

#### 7.1.3.1 Classical gradient diffusion model

The gradient or Fickian diffusion model assumes that the mixing flux is proportional to the concentration gradient

$$q_m = -\varepsilon_s \frac{d\,c}{d\,y} \tag{7.12}$$

where $\varepsilon_s$ is the sediment diffusivity. Equations (7.11) and (7.12) allow to write the classical diffusion equation

$$\frac{d\,c}{d\,y} = -\frac{\omega_s}{\varepsilon_s}\, c \tag{7.13}$$

Equation (7.13) needs the sediment diffusivity $\varepsilon_s$.

#### 7.1.3.2 Finite-mixing-length model

In the finite-mixing-length model [85] the swapping of fluid parcels (including suspended sediment) between different levels generates a net vertical flux of momentum and suspended sediment. The sediment concentrations in a lower parcel and in an upper parcel are respectively $c(y - l_m/2)$ and $c(y + l_m/2)$. If the parcels travel vertically with equal and opposite velocities $\pm v_m$, the resulting flux is

$$q_m = v_m \; [c\,(y - l_m/2) - c\,(y + l_m/2)] \tag{7.14}$$

where $v_m$ is the mixing velocity and $l_m$ the mixing length. The Taylor expansion of $c\,(y - l_m/2)$ and $c\,(y + l_m/2)$ gives

$$q_m = -v_m l_m \left[ \frac{d\,c}{d\,y} + \frac{l_m^2 d^3\,c}{24 d\,y^3} + ... \right] \tag{7.15}$$

Inserting Eq. (7.15) into (7.11) and by including only the first two terms of the Taylor expansion in the brackets [85], gives a third order ordinary differential equation (for more details see [85])

$$\frac{l_m^2}{24}\,\frac{d^3\,c}{d\,y^3} + \frac{d\,c}{d\,y} + \frac{\omega_s}{v_m l_m} c(y) = 0 \tag{7.16}$$

Equations (7.12) and (7.15) give

$$\varepsilon_s = v_m l_m \left[ 1 + \frac{l_m^2}{24}\,\frac{\dfrac{d^3\,c}{d\,y^3}}{\dfrac{d\,c}{d\,y}} + ... \right] \tag{7.17}$$

#### 7.1.3.3 A $\beta(y)$ profile

If the eddy viscosity $v_t$ is given by a similar expression to (7.17) with $c$ replaced by $u$, the parameter $\beta$ is determined by the ratio between the function in the brackets for each quantity or with $L_c^{-2} \approx (d^3 c/dy^3)/(dc/dy)$ and $L_u^{-2} \approx (d^3 u/dy^3)/(du/dy)$ as [85]

$$\beta = \frac{\varepsilon_s}{\nu_t} = \frac{1 + \dfrac{l_m^2}{24} L_c^{-2} + ...}{1 + \dfrac{l_m^2}{24} L_u^{-2} + ...} = 1 + \frac{l_m^2}{24}\,\left( L_c^{-2} - L_u^{-2} \right) + ... \tag{7.18}$$

It is possible to obtain a theroretical $\beta(y)$ profile, based on finite-mixing-length model, from Eq. (7.18) since $l_m$ is $y$-dependent. With a linear mixing length $l_m = \lambda y$, Eq. (7.18) gives [6]

$$\beta = 1 + C_{\beta 2}\, y^2 \tag{7.19}$$

where $C_{\beta 2}$ is a coefficient $C_{\beta 2} = (\lambda^2/24)\,\left( L_c^{-2} - L_u^{-2} \right)$.
It is possible to fit Eq. (7.19) by the following $\beta(y)$-function

$$\beta = \beta_b\, f_\beta(y) \tag{7.20}$$

where $\beta_b$ is the value of $\beta$ close to a bed.

In order to obtain an increasing or decreasing $\beta(y)$-function and therefore an increasing/decreasing $\varepsilon_s$, we suggest [6]

$$f_\beta(y) = e^{C_\beta \frac{y}{\delta}} \tag{7.21}$$

where $C_\beta$ is a coefficient which should depend on sand grain size. The $\beta(y)$ profile obtained by Eqs. (7.20) and (7.21) increases with $y$ for $C_\beta > 0$ and decreases for $C_\beta < 0$. As we will see in the next section, the $\beta(y)$ profile given by Eq. (7.20) and (7.21) will be particularly useful for the analytical study of suspended sediments over wave ripples.

## 7.2 Suspended sediments over wave ripples

When considering suspended sediment in oscillatory flows, it is necessary to distinguish between the sheet flow regime (Shields numbers $> 0.8$) and the ripple regime at lower shear stresses. If the ripples are relatively steep ($\eta_r/\lambda_r \geq 0.12$, where $\eta_r$ is the ripple height and $\lambda_r$ is the ripple wavelength), the mixing close to the bed is dominated by coherent, periodic vortex structures [78] [17] [84] [105]. Above rippled beds, the mixing in the near-bed layer is dominated by the mechanism of vortex shedding which entrains sediments near flow reversal during each wave half cycle to several ripple heights [109].

Examination of concentration profiles for different sand sizes suspended in the same flow over wave ripples provides information about the involved mechanisms. Field and laboratory measurements of suspended sediments over wave ripples show a contrast between an upward convex concentration profiles, time-averaged in semi-log plots, for fine sand and an upward concave profiles for coarse sand [76] [84]. The classical gradient (Fickian) diffusion model allows a good description of fine sediment concentrations but fails to describe concentration profiles for coarse sand [85]. The finite-mixing-length model [85], which is of similar generality to the Lagrangian Taylor's model, contains gradient (Fickian) diffusion model as a limiting case for $l_m/L \to 0$, where $l_m$ is the mixing length and $L$ the scale of the distribution under consideration. Even if the finite-mixing-length model improves the concentration profile $c(y)$ for coarse sand (where $y$ is the distance from the bed), a difference with experimental data remains. However, it is possible to improve this profile by a suitable turbulent mixing which is able to increase the upward concavity of $c(y)$ [1]. This is possible with a turbulent diffusivity $\varepsilon_s$ which takes into account the effect of grain size. The diffusivity of sediments $\varepsilon_s$ is related to the diffusivity of momentum, the eddy viscosity $\nu_t$, by a coefficient $\beta = \varepsilon_s/\nu_t$ (i.e., the inverse of the turbulent Schmidt number). In order to include the effect of sand grain size on $\varepsilon_s$, it is important to consider a realistic function for $\beta$ which is dependent on grain size and concentrations and therefore on the distance from the bed $y$.

In oscillatory flows, it is known that cycle-mean sediment diffusivity above ripples is significantly greater than the cycle-mean eddy viscosity, i.e. $\beta > 1$ [84] [105]. This

difference has not yet been clearly explained, but seems rest on the spatial-temporal correlation between suspended concentrations and vertical velocities in the flow field [105]. For 1-DV models, the value of $\beta$ was suggested empirically a constant equal to about 4 for rippled beds [84] [105]. However, $\beta$ should depend on grain size and concentrations and should be therefore $y$-dependent.

Careful examination of measured concentrations for coarse sand shows a near-bed upward convex profile beneath the main upward concave profile. This near-bed profile was related to particles settling velocity which decreases near the bottom for high concentrations. Experiments have demonstrated that particle settling velocities are lower at higher concentrations. This behavior is described by the well known Richardson and Zaki [91] equation which depends on an empirically determined exponent. This equation was adapted for natural marine sands by Baldock *et al.* [14].

The aim is to : 1) improve the prediction of concentration profiles by the gradient (Fickian) diffusion model ; 2) provide an analytical interpretation of the main upward concave concentration profile and the near-bed upward convex profile for coarse sand. This interpretation requires a relation between sediment diffusivity, particles settling velocity and sediment concentrations. The following Section presents gradient (Fickian) diffusion and finite-mixing-length modeling of suspended sediment concentrations. The effect of sand grain size on sediment diffusivity and concentration profiles will be considered. Finaly, we will present possible effects of settling velocity or convective sediment entrainment process on the near-bed upward convex profile for coarse sand.

### 7.2.1 Eddy viscosity in oscillatory boundary layers

#### 7.2.1.1 Practical eddy viscosity formulation for wave boundary layers

Nielsen and Teakle [85] used an eddy viscosity formulation, similar to Eq. (6.7), given by

$$\nu_t = \lambda\, y\, v_{m0}\, e^{\left[-\dfrac{(y-y_0)}{L_v}\right]} \tag{7.22}$$

where $v_{m0} = v_m(y = y_0)$ is the mixing velocity at level $y_0$ ; $\lambda$ and $L_v$ are two parameters. This model is based on a linearly increasing mixing length and an exponentially decreasing mixing velocity given respectively by

$$l_m = \lambda\, y \qquad and \qquad v_m = v_{m0}\, e^{\left[-\dfrac{(y-y_0)}{L_v}\right]} \tag{7.23}$$

Eq. (6.7) was used in oscillatory boundary layers over rough flat beds [56] and over wave ripples [85]. Predicted velocity profiles in oscillatory boundary layers showed very good agreement with experimental data [56].

The exponentially decreasing mixing velocity $v_m$ was chosen in agreement with turbulence measurements of du Toit and Sleath [32] who observed that the turbulence intensity decayed exponentially upwards from a level $y_0$ very close to the ripple crest. Eq. (7.22) reverts to Eq. (6.7) with $\alpha_1\,\kappa\,u_* = \lambda\,v_{m0}\,e^{\left[\frac{y_0}{L_v}\right]}$ and $L_v = \dfrac{\delta}{C_1}$ [1].

#### 7.2.1.2 Analysis by a two-equation model

Eq. (6.7) for eddy viscosity was validated in the last chapter for the case of steady plane channel flow. However for use in wave boundary layers, we need to assess this equation for the case of oscillatory flows. Eq. (6.7) is therefore analyzed by the baseline (BSL) $k$-$\omega$ model. This model allows accurate prediction of velocity profiles in oscillatory boundary layers [102].

Figure (7.1) presents temporal and spatial variation of dimensionless eddy viscosity for a sinusoidal wave. Figure (7.1.b) shows comparison between period-averaged eddy viscosity obtained by BSL $k$-$\omega$ model (symbols) and analytical profile of Eq. (6.7) (dashed line). Even if the eddy viscosity is highly time-dependent (figure 7.1.a), the period-averaged dimensionless eddy viscosity (Figure 7.1.b) has a shape which is well described by the analytical profile given by Eq. (6.7) for $y/h < 0.6$ (figure 7.1.b) where $h$ is the water depth or the distance from the wall to the axis of symmetry or free surface [10].

Figure (7.2) presents temporal and spatial variation of dimensionless eddy viscosity for asymmetric waves. Figure (7.2.b) shows comparison between period-averaged eddy viscosity obtained by BSL $k$-$\omega$ model (symbols) and analytical profile of Eq. (6.7) (dashed line). Even for the case of asymmetric wave, the period-averaged dimensionless eddy viscosity has a shape which is well described by Eq. (6.7) for $y/h < 0.5$ (figure 7.2.b) [10].

Figures (7.1.b) and (7.2.b) shows that the period-averaged eddy viscosity profile for sinusoidal wave is different from the profile for asymmetric wave. This indicates that the period-averaged eddy viscosity profile should depend on the wave non-linearity parameter given by $N_i = U_c/\hat{u}$, where $U_c$ is the velocity at wave crest and $\hat{u}$ is the total velocity amplitude. We need therefore a specific calibration for parameters of Eq. (6.7) using full-range equations of friction coefficient [103] and wave boundary layer thickness [95].

### 7.2.2 Gradient diffusion versus finite-mixing-length model

In order to analyze concentration profiles obtained by gradient (Fickian) diffusion and finite-mixing-length models, we use experimental data obtained by McFetridge and Nielsen [76].

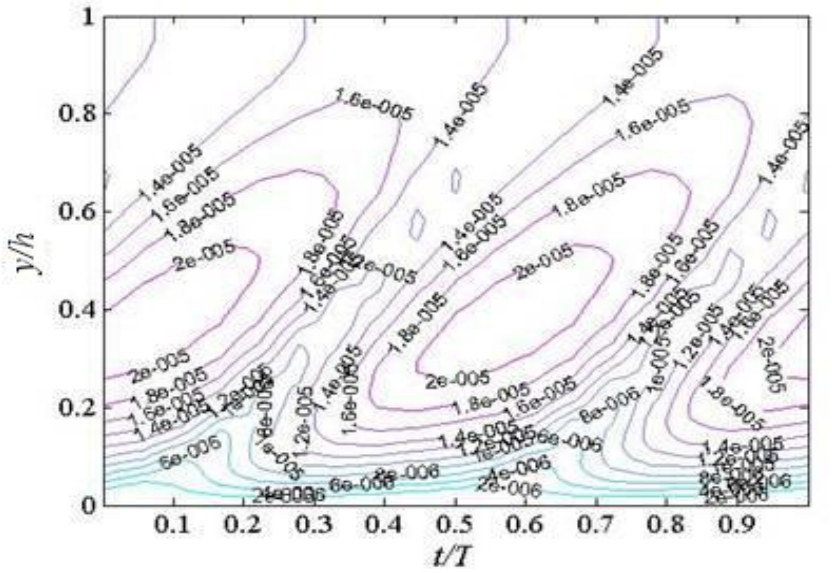


(a)

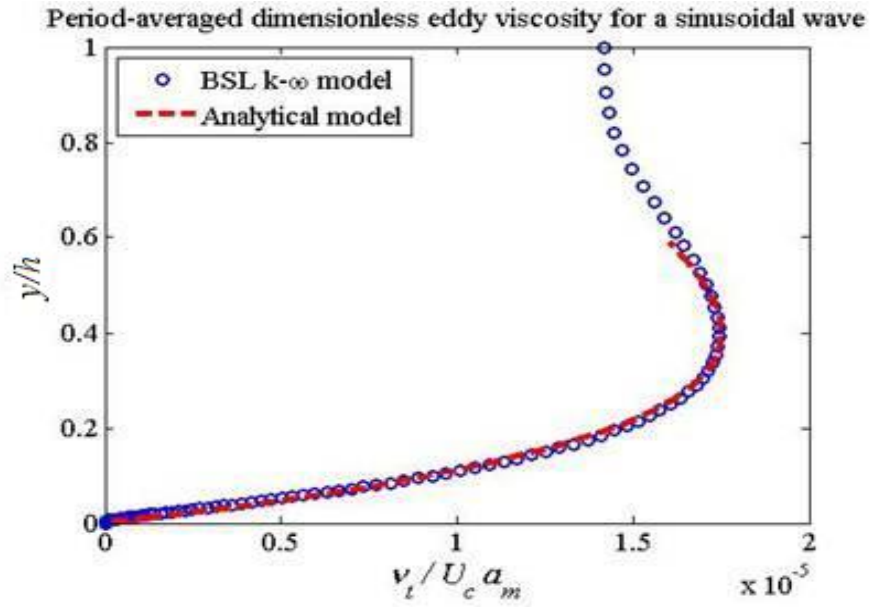


(b)

FIGURE 7.1 – Dimensionless eddy viscosity ; (a) : Temporal and Spatial Variation ; (b) : Period-averaged dimensionless eddy viscosity ; for a sinusoidal wave [10].

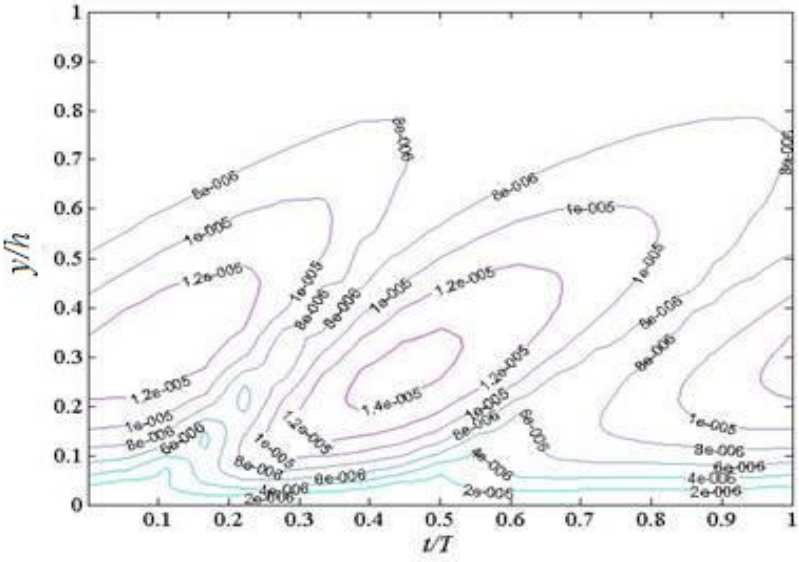


(a)

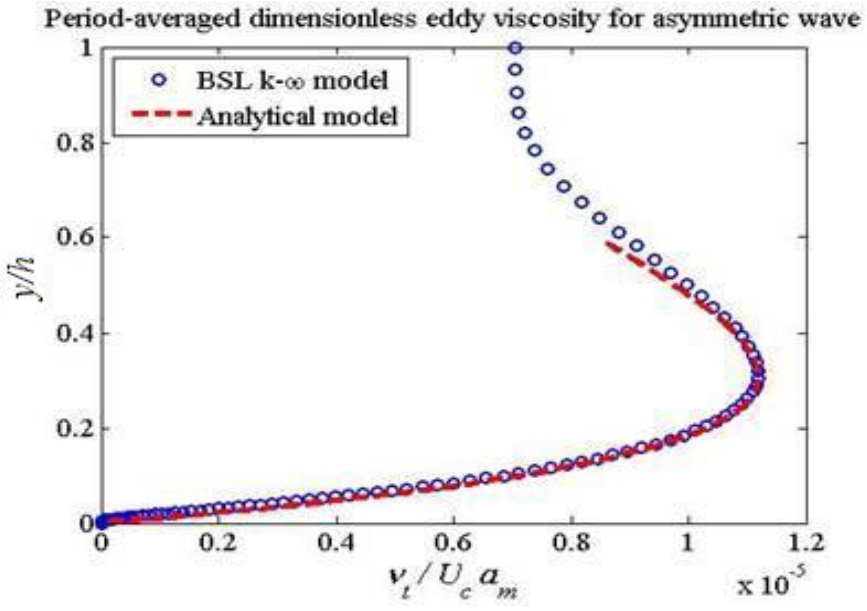


(b)

FIGURE 7.2 – Dimensionless eddy viscosity ; (a) : Temporal and Spatial Variation ; (b) : Period-averaged dimensionless eddy viscosity ; for an asymmetric wave [10].

#### 7.2.2.1 Experiments of McFetridge and Nielsen

In these experiments [76], suspended sediments are due to non-breaking waves over rippled beds. In order to establish reliable time-averaged concentration profiles, an extensive series of trials under a single set of wave conditions was chosen rather than a limited number of trials under a variety of wave conditions. Natural beach sand was used, wave maker piston amplitude, period, and water depth were adjusted to maximize near bed velocities and therefore suspended sediment concentrations. The flow parameters are : wave period $T = 1.51\ seconds$, mean wave height $H = 13\ cm$, maximum near-bed flow velocity $U_{0m} = 27.8\ cm/s$, near-bed flow semi-excursion $a = 6.68\,cm$ and maximum return velocity at the bed $= 21.6\,cm/s$, mean depth of flow $h = 30\,cm$. The ripples which were produced were highly uniform and regular with a mean ripple height of $1.1\ cm$, a mean ripple length of $7.8\ cm$ and therefore a mean ripple steepness of 0.14. Measured concentrations were obtained by sieving suction samples from different elevations above ripple crest [76].

#### 7.2.2.2 Time-averaged concentration profiles

Fig. (7.3) shows a comparison between time-averaged concentration profiles, $ln(c)$ versus linear $y$ plots, obtained with gradient (Fickian) diffusion and finite-mixing-length models and measurements [76] for fine ($d = 0.06 - 0.11\ mm$) and coarse sediments ($d = 0.42 - 0.60\,mm$), where $d$ is grain diameter. Settling velocities are respectively $\omega_s = 0.65\,cm/s$ for fine and $\omega_s = 6.1\,cm/s$ for coarse sediments [85].

Predicted concentration profiles were obtained by solving differential equations (7.13) and (7.16) with respectively (7.22) and (7.23). We use the parameters proposed by Nielsen and Teakle [85], namely $\lambda = 1$, $y_0 = 0.005\ m$, $v_{m0} = 0.025\ m/s$, $L_v = 0.022\ m$. Concentration profiles (Fig. 7.3) are the same as profiles of figure (6 of [85]). Even if the upward convex profile for fine sand versus upward concave for coarse sand is reproduced with the finite-mixing-length model, it remains a difference with experimental data for coarse sand at the top of Fig. (1) ($y$ between 0.04 and $0.09\ m$) which seems to become more important for $y > 0.09\ m$. Since the aim of the study is to predict observed differences between concentration profiles for fine versus coarse sand suspended in the same flow, the turbulent flow's parameters were the same for fine and coarse sand (Fig. 7.3).

### 7.2.3 Effect of sediment diffusivity on concentration profiles

In order to investigate the effect of sediment diffusivity on concentration profiles, we consider in this section a settling velocity constant over the boundary layer thickness, equal to $\omega_{st}$ the terminal settling velocity in an infinite fluid. In our study we will consider that $\beta$ approaches unity for fine sediments and deviates for coarse ones.

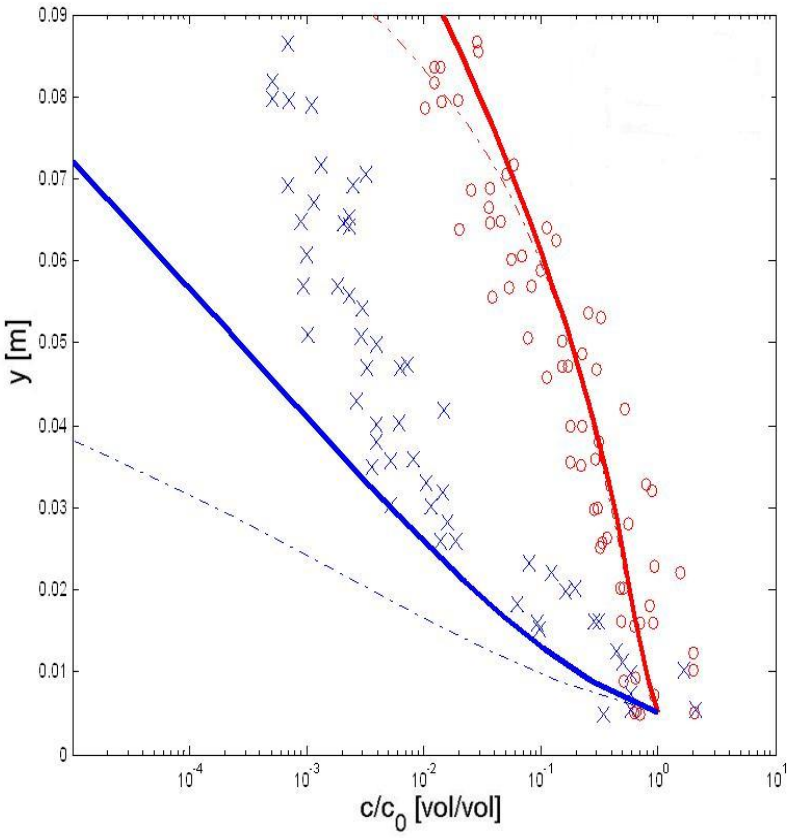


FIGURE 7.3 – Time-averaged concentration profiles over wave ripples : gradient (Fickian) diffusion model versus finite-mixing-length model. symbols, measurements [76], o, Fine sand ($\omega_s = 0.65\, cm/s$) ; $\times$, coarse sand ($\omega_s = 6.1\, cm/s$). Dash-dotted lines are solutions of gradient (Fickian) diffusion model (Eq. 7.13) while solid lines are solutions of finite-mixing-length model (Eq. 7.16), $\lambda = 1$, $y_0 = 0.005\, m$, $v_{m0} = 0.025\, m/s$, $L_v = 0.022\, m$.

#### 7.2.3.1 Concentration profile for fine sediments

The assumption $\beta \approx 1$ for fine sediments allows us to write

$$\varepsilon_s \approx \nu_t = \alpha_1 \, \kappa \, u_* \, y \, e^{-C_1 \, \frac{y}{\delta}} \tag{7.24}$$

Careful examination of time-averaged concentration profile (Fig. 7.3) for fine sand ($\omega_s = 0.65 \; cm/s$) shows a small near-bed upward concave profile followed by the main upward convex profile. These profiles are associated to a sediment diffusivity $\varepsilon_s$ profile which increases then decreases [6]. The decreasing sediment diffusivity $\varepsilon_s$ allows an upward convex concentration $c(y)$ profile while an increasing sediment diffusivity $\varepsilon_s$ allows an upward concave $c(y)$ profile.

Upward concavity/convexity of concentration profiles is, on $ln(c)$ versus linear $y$ plots, related to $\dfrac{d^2 \, ln \, c}{d \, y^2}$, while increasing/decreasing of $\varepsilon_s$ is related to $\dfrac{d \, \varepsilon_s}{d \, y}$. In order to understund this link, we need therefore a relation between $\dfrac{d^2 \, ln \, c}{d \, y^2}$ and $\dfrac{d \, \varepsilon_s}{d \, y}$.

We are able to write

$$\frac{d \, ln \, c}{d \, y} = \frac{1}{c} \left( \frac{d \, c}{d \, y} \right) \tag{7.25}$$

and with Eq. (7.13)

$$\frac{d \, ln \, c}{d \, y} = -\frac{\omega_s}{\varepsilon_s} \tag{7.26}$$

The derivative of Eq. (7.13) and Eq. (7.26) are respectively

$$\frac{d^2 \, c}{d \, y^2} = \frac{\omega_s \, c}{\varepsilon_s^2} \left( \frac{d \, \varepsilon_s}{d \, y} + \omega_s \right) \tag{7.27}$$

and

$$\frac{d^2 \, ln \, c}{d \, y^2} = \frac{1}{c} \left[ \frac{d^2 \, c}{d \, y^2} \right] - \frac{1}{c^2} \left[ \frac{d \, c}{d \, y} \right]^2 \tag{7.28}$$

Inserting Eq. (7.13) and Eq. (7.27) into Eq. (7.28), we obtain

$$\frac{d^2 \, ln \, c}{d \, y^2} = \frac{1}{c} \left[ \frac{\omega_s \, c}{\varepsilon_s^2} \left( \frac{d \, \varepsilon_s}{d \, y} + \omega_s \right) \right] - \frac{1}{c^2} \left[ -\frac{\omega_s}{\varepsilon_s} \, c \right]^2 \tag{7.29}$$

After simplifying Eq. (7.29), we obtain

$$\frac{d^2 \, ln \, c}{d \, y^2} = \frac{\omega_s}{\varepsilon_s^2} \, \frac{d \, \varepsilon_s}{d \, y} \tag{7.30}$$

Eq. (7.30) provides a link between $\frac{d^2\, ln\, c}{d\, y^2}$ and $\frac{d\, \varepsilon_s}{d\, y}$, and therefore between upward concavity/convexity of concentration profiles and increasing/decreasing of sediment diffusivity profiles. Since $\frac{\omega_s}{\varepsilon_s^2}$ is always $> 0$, $\frac{d^2\, ln\, c}{d\, y^2}$ and $\frac{d\, \varepsilon_s}{d\, y}$ have the same sign and therefore increasing sediment diffusivity allows upward concave concentration profile, while decreasing sediment diffusivity allows an upward convex concentration profile [6].

#### 7.2.3.2 Concentration profile for coarse sediments

Due to grain size of coarse sediments, $\varepsilon_s$ becomes different from $\nu_t$. The difference in the shape of concentration profiles of fine and coarse sediments seems to be related to sand grain size which impacts sediment diffusivity through the parameter $\beta$.

The analysis presented in the last section suggests that an increasing sediment diffusivity is needed to predict the upward concave concentration profile for coarse sand.

No experimental data of $\beta(y)$ above wave orbital ripples are available, we use therefore $\beta(y)$-function given by Eq. (7.21). With the eddy viscosity (Eq. 6.7), the sediment diffusivity is therefore given by

$$\varepsilon_s = (\beta_b\, \alpha_1\, \kappa\, u_*)\, y\, e^{-(C_1 - C_\beta)\frac{y}{\delta}} = \alpha_s\, y\, e^{-\frac{y}{\delta_s}} \tag{7.31}$$

where $\alpha_s = \beta_b\, \alpha_1\, \kappa\, u_*$ and $\delta_s = \frac{\delta}{(C_1 - C_\beta)}$ are the two parameters of sediment diffusivity.

Results of time-averaged concentration profiles over wave ripples are presented in Fig. (7.4) for fine ($\omega_s = 0.65 cm/s$) and coarse ($\omega_s = 6.1 cm/s$) sand. Comparisons with experimental data [76] show good agreement. The upward convex profile for fine sand versus upward concave for the coarse sand is reproduced with the gradient (Fickian) diffusion model. The imperfection which was observed in figure (7.3) for coarse sand ($y$ between 0.04 and 0.09 m) is improved.

Our results show that the decreasing sediment diffusivity $\varepsilon_s$ for fine sand allows an upward convex concentration $c(y)$ profile while an increasing sediment diffusivity $\varepsilon_s$ for coarse sand allows an upward concave $c(y)$ profile (Fig. 7.4).

### 7.2.4 The near-bed upward convex profile for coarse sand

Careful examination of measured concentrations for coarse sand, in semi-log plots, shows a small near-bed upward convex concentration profile beneath the main upward concave profile. Examination of other experimental data [33] confirms the presence of near-bed upward convex profiles.

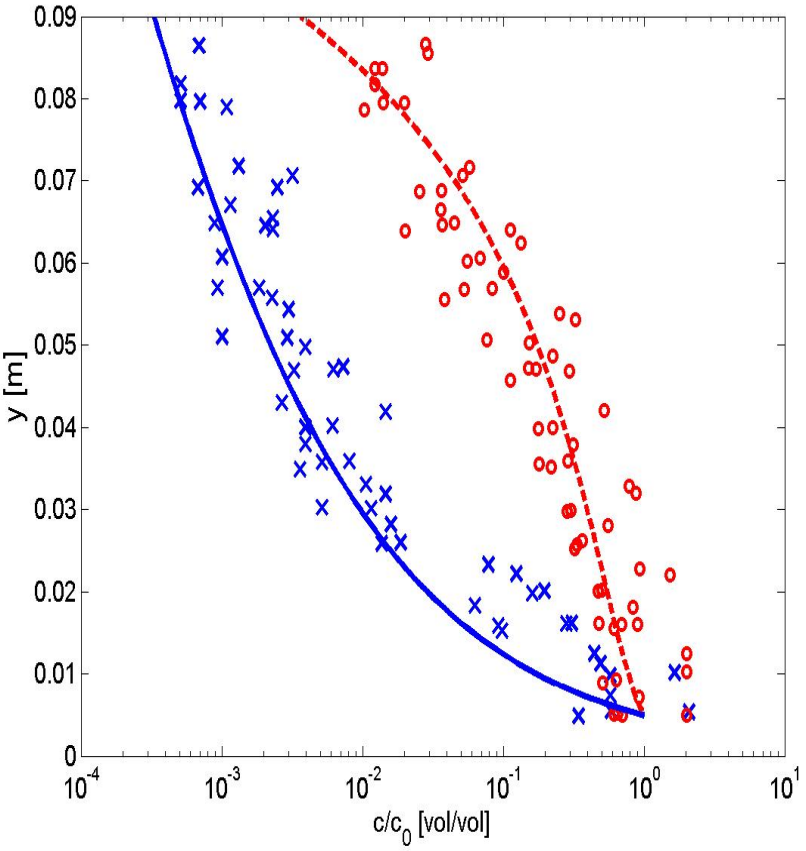


FIGURE 7.4 – Time-averaged concentration profiles over wave ripples : gradient (Fickian) diffusion model with proposed $\beta(y)$-function. symbols, measurements [76], o, Fine sand ($\omega_s = 0.65\,cm/s$) ; $\times$, coarse sand ($\omega_s = 6.1\,cm/s$). Curves, model with $\alpha_s = 0.025\,m/s$ ; dashed line (fine sand) $\delta_s = L_v = \dfrac{\delta}{C_1} = 0.022\,m$ ; solid line (coarse sand) $\delta_s = \dfrac{\delta}{(C_1 - C_\beta)} = 0.24\,m$.

The 1-DV gradient diffusion model predicts the main upward concave profile for coarse sediments thanks to an adequate $\beta(y)$-function. The resulting sediment diffusivity $\varepsilon_s$ with a constant settling velocity ($\omega_s = \omega_{st}$) is unable to predict the near-bed upward convex profile. In order to predict this profile, we need an additional parameter. The sediment diffusivity should be modulated by an $y$-dependent parameter $\alpha$ which depends on sand grain size and decreases with $y$. If we consider a constant settling velocity ($\omega_s = \omega_{st}$), we write equation (7.13) as

$$\frac{d\,c}{d\,y} = -\frac{\omega_s}{\alpha(y)\,\varepsilon_s(y)}\,c \tag{7.32}$$

Eq. (7.30) becomes therefore

$$\frac{d^2\,ln\,c}{d\,y^2} = \frac{\omega_s}{(\alpha\,\varepsilon_s)^2}\,\frac{d\,(\alpha\,\varepsilon_s)}{d\,y} \tag{7.33}$$

As in the analysis presented in the last section, Eq. (7.33) provides a link between upward concavity/convexity of concentration profiles and increasing/decreasing of $\alpha\,\varepsilon_s$. Increasing $\alpha\,\varepsilon_s$ allows upward concave concentration profile, while decreasing $\alpha\,\varepsilon_s$ allows an upward convex concentration profile. Since $\varepsilon_s$ increases with $y$ for coarse sand, the near-bed upward convex concentration profile needs a decreasing $\alpha$.

#### 7.2.4.1 Possible effect of settling velocity

The near-bed upward convex profile could be related to settling velocity which decreases for high concentrations. Experiments have demonstrated that particle settling velocities are lower at higher concentrations. This behavior is given by the well known semi-empirical Richardson and Zaki [91] equation. We write Richardson and Zaki's equation as

$$\frac{\omega_s}{\omega_{st}} = \left(1 - \frac{c}{c_0}\right)^n \tag{7.34}$$

where $c_0 = c(y = y_0)$ and $n$ is an empirically determined exponent dependent on the particle Reynolds number $R_t$ at $\omega_{st}$ and is constant for a particular particle. This exponent was determined experimentally as between 4.65 and 2.4 for increasing $R_t$. A review of empirical expressions for $n$ is given by Di Felice [31]. These empirical values describing the variation of $n$ with $R_t$ were derived from fluidization and sedimentation experiments with spheres. Cheng [22] proposed expressions for $n$ which are functions of both Reynolds number and concentration. A method of determining $n$ for natural sands was proposed by Baldock *et al.* [14] and was verified against laboratory fluidization data for marine sands. Settling velocity could be therefore not a constant on the vertical, and could depend on sediment grain size and concentrations and therefore on $y$. We write an $y$-dependent settling velocity, required by our analytical study, as

$$\omega_s(y) = \omega_{st}\ f_s(y) \tag{7.35}$$

where $f_s(y)$ is a function which is equal to 1 far from the bed where concentrations are small ($c \approx 0$) and decreases near the bottom for high concentrations. In the last Section, we assumed that $\omega_s = \omega_{st} = constant$ and therefore $f_s = 1$. However, if this approximation is valid only far from the bed where concentrations are very small, the observed near-bed upward convex concentration profile for coarse sand could be related to $f_s(y)$. We need a suitable function for $f_s(y)$ in order to evaluate the effect on concentration profiles.

### $y$-dependent functions for settling velocity

We propose two $y$-dependent functions for $\omega_s$. The first is based on a simple concentration profile given by

$$\frac{c(y)}{c_0} = exp\left(-\frac{y - y_0}{L_c}\right) \tag{7.36}$$

Inserting equation (7.36) into equation (7.34), we obtain an $y$-dependent function for settling velocity

$$f_s(y) = \frac{\omega_s(y)}{\omega_{st}} = \left(1 - exp\left(-\frac{y - y_0}{L_c}\right)\right)^n \tag{7.37}$$

The second is an empirical function given by

$$f_s(y) = \frac{\omega_s(y)}{\omega_{st}} = \frac{1}{1 + exp(-\frac{y - y_s}{h_s})} \tag{7.38}$$

where $y_s$ and $h_s$ are two parameters which should depend on concentrations and particles size. In order to validate these functions, data of settling velocity $w_s$ were derived from measured concentrations for coarse sand and Richardson and Zaki's equation. Data of $f_s(y)$ are therefore obtained from equation (7.34) and measured $c/c_0$ values, as

$$f_s(y)_{exp} = \left(\frac{\omega_s(y)}{\omega_{st}}\right)_{exp} = \left(1 - \left(\frac{c(y)}{c_0}\right)_{exp}\right)^n \tag{7.39}$$

Comparisons show that the second function is more accurate.

### Effect on concentration profiles

In the last Section, $f_s$ was taken to be equal to 1 and concentration profiles depend only on $\varepsilon_s$. Here, $f_s$ is equal to 1 only far from the bottom where the concentration is small.

Taking into account (Eq. 7.35), equation (7.13) becomes

$$\frac{d\,c}{d\,y} = -\frac{\omega_s(y)}{\varepsilon_s(y)}\,c = -\frac{\omega_{st}\ f_s(y)}{\varepsilon_s(y)}\,c = -\frac{\omega_{st}}{\frac{\varepsilon_s(y)}{f_s(y)}}\,c \tag{7.40}$$

In Eq. (7.40), $\alpha = 1/f_s$. Concentration profiles depend therefore on the ratio between sediment diffusivity and dimensionless settling velocity $\frac{\varepsilon_s(y)}{f_s(y)}$ and not on the sediment diffusivity $\varepsilon_s(y)$ alone.

Eq. (7.30) becomes therefore [6]

$$\frac{d^2\, ln\, c}{d\, y^2} = \frac{\omega_{st}}{\left(\frac{\varepsilon_s}{f_s}\right)^2} \frac{d\left(\frac{\varepsilon_s}{f_s}\right)}{d\, y} \tag{7.41}$$

We are able to generalize the previous result : upward concavity/convexity of concentration profiles is, on $ln(c)$ versus linear $y$ plots, related to increasing/decreasing of $\frac{\varepsilon_s(y)}{f_s(y)}$. Eq. (7.41) provides a link between $\frac{d^2\, ln\, c}{d\, y^2}$ and $\frac{d\, \frac{\varepsilon_s(y)}{f_s(y)}}{d\, y}$, and therefore between upward concavity/convexity of concentration profiles and increasing/decreasing of $\frac{\varepsilon_s(y)}{f_s(y)}$. Since $\frac{\omega_{st}}{\left(\frac{\varepsilon_s}{f_s}\right)^2}$ is always $> 0$, $\frac{d^2\, ln\, c}{d\, y^2}$ and $\frac{d\, \frac{\varepsilon_s(y)}{f_s(y)}}{d\, y}$ have the same sign and therefore increasing $\frac{\varepsilon_s(y)}{f_s(y)}$ allows upward concave concentration profile, while decreasing $\frac{\varepsilon_s(y)}{f_s(y)}$ allows an upward convex concentration profile.

Data of settling velocity $w_s$ were derived from measured concentrations for coarse sand and Richardson and Zaki's equation. The empirical function $f_s$ obtained from these data allows predicting the near-bed upward convex profile. However, the dimensionless settling velocity function $f_s$ decreases from $y = 4\, cm$ and at $y = 2\, cm$ the decreasing in settling velocity is of 50%. This seems to be quite larger than would be expected and therefore seems to be outside the range of observed hindered settling.

#### 7.2.4.2 Possible effect of convective sediment entrainment process

The process of vortex formation and shedding at flow reversal above ripples is a relatively coherent phenomenon. The associated convective sediment entrainment process may also be characterized as coherent, instead of a pure disorganized "diffusive" process represented in the classical gradient diffusion model [105]. Above ripples, in a ripple-averaged sense, the convective term can dominate the upward sediment flux in the bottom part of the wave boundary layer [106]. Nielsen [84] indicated that both convective and diffusive mechanisms are involved in the entrainment processes. In the combined convection-diffusion formulation of Nielsen [84], the steady state advection-diffusion equation is given by

$$\omega_s\, c + \varepsilon_s(y)\, \frac{d\, c}{d\, y} - \omega_s\, c_0\, F(y) = 0 \tag{7.42}$$

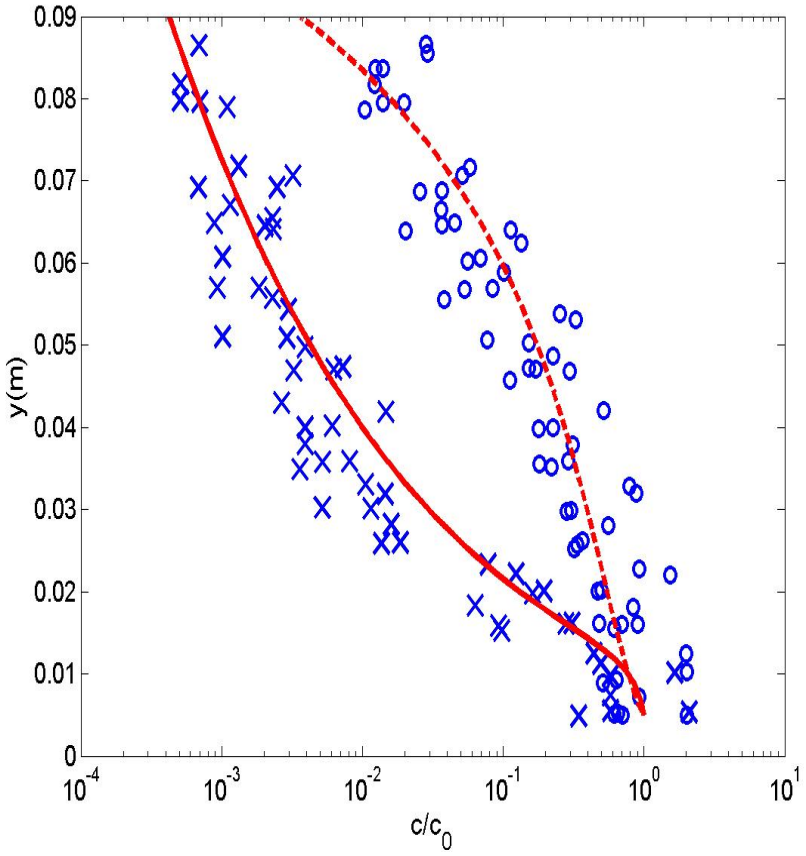


FIGURE 7.5 – Time-averaged concentration profiles over wave ripples. Symbols, measurements (McFetridge and Nielsen, 1985), ($o$) fine sand ; ($x$) coarse sand. Curves are solutions of gradient diffusion model with proposed $\beta(y)$ and $\alpha(y)$ $(= 1/f_s(y))$ functions.

where $F(y)$ is a function describing the probability of a particle reaching height $y$ above the bed. The respective terms in Eq. (7.42) represent downward settling, upward diffusion, and upward convection [84] [69] [105]. Eq. (7.42) reverts to Eq. (7.32) with

$$\alpha(y) = \frac{1}{1 - (c_0/c)\ F(y)} \tag{7.43}$$

In this equation, $\alpha$ represents the effect of upward convection. The near-bed upward convex profile of fig. (7.6) could be predicted by using a parameter $\alpha(y) = 1/f_s(y)$ based on (Eq. 7.38), $\alpha$ is given therefore by

$$\alpha(y) = 1 + exp(-\frac{y - y_s}{h_s}) \tag{7.44}$$

### 7.2.5 Engineering modeling of sediment transport over ripples

The description of sediment transport in the coastal zone is of crucial importance for accurate predictions of coast line evolution and sea-bed changes. The modelling of coastal sediment transport needs a compromise between two types of models : the detailed mathematical formulations and engineering approaches. This compromise is imposed by on the one hand the accuracy of predictions and on the other hand the usability in practical applications. In coastal engineering, we need practical accurate engineering models which take into account the more important involved physics. The focus point of our study is the mixing of suspended sediments due to the presence of ripples. The aim is to improve the wave-related suspended transport component in engineering modelling of coastal sediment transport.

The net (averaged over the wave period) total sediment transport is obtained as the sum of the net bed load and net suspended load transport rates. For suspended load, the net sand transport is defined as the sum of the net current-related and the net wave-related transport components. The wave-related suspended sediment transport is defined as the transport of sediments by the high-frequency oscillatory flow or short waves (low-frequency transport is neglected).

In our study, special attention is given to the wave-related suspended transport component which is modeled [57] [111] [112] as

$$q_{s,w} = \gamma \frac{U_{on}^4 - U_{off}^4}{U_{on}^3 + U_{off}^3} \int c\, dy \tag{7.45}$$

where : $U_{on}$ is the near-bed peak orbital velocity in onshore direction (in wave direction) and $U_{off}$ the near-bed peak orbital velocity in offshore direction (against wave direction) and $\gamma$ a phase lag parameter = 0.44 [47] or between 0.1 and 0.2 for field conditions. Eq. (7.45) requires computation of the time-averaged sand concentration profile and integration of the time-averaged sand concentration profile in vertical direction.

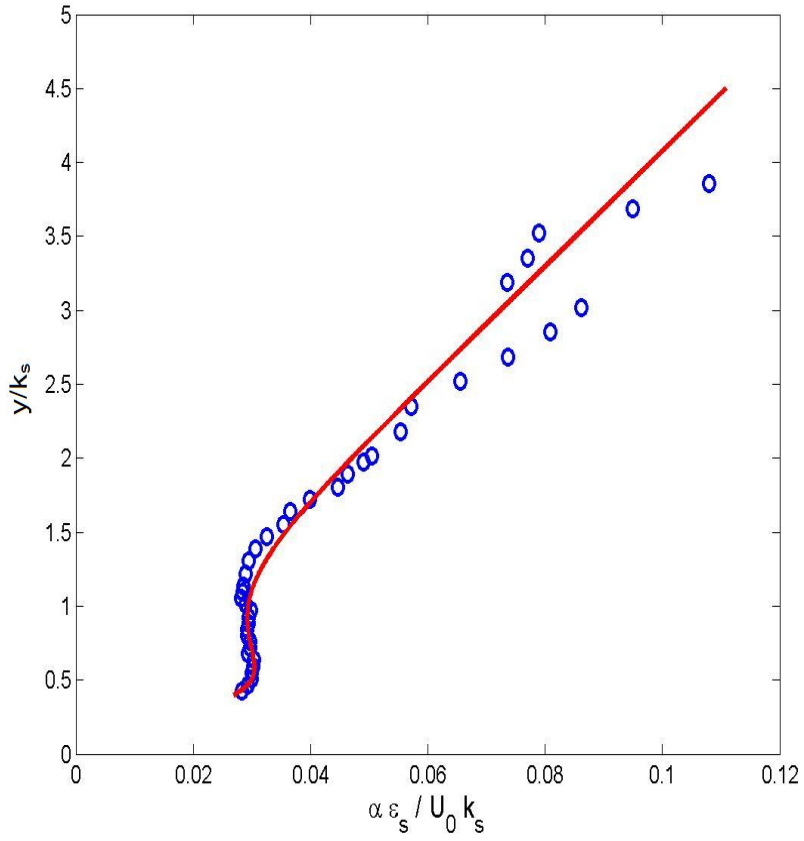


FIGURE 7.6 – Comparison of the mean measured normalized $\alpha\,\varepsilon_s$ (symbols) over medium sand bed [106], with calculations from proposed equations (curve).

Time-averaged concentrations could be obtained by Eq. (7.32). In this equation, $\alpha$ is a parameter related to convective sediment entrainment process associated to the process of vortex shedding above ripples which is a coherent phenomenon. Sediment diffusivity $\varepsilon_s$ describes the disorganized "diffusive" process. The classical 1-DV gradient diffusion model (Eq. 7.13) is therefore unable to predict the process of vortex formation and shedding above ripples.

The previous test case shows fine and coarse sediments over wave ripples in the same flow (figure 1) while the second test case (figure 2) shows comparison of measured ($\alpha\,\varepsilon_s$) and calculation (curve) from proposed equations. The shape (figure 2) confirms the profile used by [111] [112].

Troisième partie

# Participation to other activities

Chapitre 8

# Innovative methods in pedagogy : Interest of atypical experiments in teaching fluid mechanics

Fluid mechanics at EBI was considered by students as difficult who seemed somewhat unmotivated. In order to motivate them, we applied a new play-based pedagogy. Students were asked to draw inspiration from everyday life situations to find applications of fluid mechanics and to do experiments to verify and validate some theoretical results obtained in course. In this study, we present an innovative teaching/learning pedagogy which includes the concept of learning through play and its implications in fluid mechanics for engineering. Examples of atypical experiments in fluid mechanics made by students are presented. Based on teaching evaluation by students, it is possible to know how students feel the course. The effectiveness of this approach to motivate students is presented through an analysis of students' teaching assessment. Learning through play proved a great success in fluid mechanics where course evaluations increased substantially. Fluid mechanics has been progressively perceived as interesting, useful, pleasant and easy to assimilate. It is shown that this pedagogy which includes educational gaming presents benefits for students. These experiments seem therefore to be a very effective tool for improving teaching/learning activities in higher education.

## 8.1 Introduction

Teaching science and technology has been often related to experiments conducted to confirm or disprove a theory. If the path travelled by the scientists is marked by different experiments, the fact is that the idea of experience is rooted in our educational practices to become one of the top concerns of those seeking to understand or to solve a problem. Universities, institutes and education in general today are based on technical education that prepares students for the expected responsibilities. EBI, which provides education for engineers in applied industrial biology, listed its efforts in this process that commits teachers and students by giving everyone a role to play.

EBI provides a 5 years MSc Diploma course to train students to work as engineers in the field of pharmaceutics, cosmetics, food engineering, environment, and others. In the undergraduate cycle, students learn mathematics, physics, biology and chemistry. Among the courses of physics, "fluid mechanics" in 2nd year was


FIGURE 8.1 – Example of atypical experiments in fluid mechanics : emptying jerry cans, preparation of experiments.

considered by students as difficult and they seemed somewhat unmotivated. In order to encourage them to show more interest to this course, a new pedagogy based on atypical experiments was tested on students of year "P17". Students were asked to draw inspiration from everyday life situations to find applications of course and to do atypical experiments to verify and validate some theoretical results.

To assess the relevance of this new pedagogy, we will analyze course evaluations by students of "P17" and we will compare them with those of three other years (two before the new pedagogy and one after). The following study focuses on students of four years : "P15" (2005/2006), "P16" (2006/2007), "P17" (2007/2008) and "P18" (2008/2009).

## 8.2 Methodology

Our methodology is based on the goals of our institute which aims to provide industry with practical engineers. The education is based on the abilities of the

teacher to put into practice the program and give students the opportunity to become more involved. The relationship between teacher and learners determine the learning process to a large part. By empowering the student to enable him to become the cornerstone of the act of learning, the teacher performs half the way of the learning process. Our methodology is therefore based on the idea of motivating students with a play-based pedagogy through atypical experiments to verify and validate some theoretical results found in course by referring to daily life situations [11].

### 8.2.1 Example of atypical experiments in fluid mechanics

As examples of atypical experiments in fluid mechanics made by students of "P17", we present experiments of emptying jerry cans. These experiments of emptying jerry cans were made by three students : Lucie Clavel, Maëla Drouin, and Laure-Anne Gillon. Their work was presented in a report with : Goal of experiments, Material and Method, Experiments and Results, and Conclusions.

#### Presentation of the experiments

The students began by identifying the required material for these experiments, namely : two plastic jerry cans one blue non-transparent of 35 liters and a second white transparent of 20 liters, two plugs of 1 cm diameter, a stopwatch, a meter, a scales of 100g precision and a spirit level (figure 8.1). They chose to work with water for a practical purpose : its accessibility and physical properties as density.

They made holes of 1cm diameter in the jerry cans to allow a slow flow, easy to measure with a stopwatch, hence a more accurate measured emptying time. The holes were placed in the bottom part of jerry cans in order to allow an adequate visualization of the flow (figure 8.1). They were also made to obtain a contraction coefficient $C_c$ equal to 0.61. When discharging, the jerry cans were placed on a coffee table, which horizontality was controlled with a spirit level. Thus, the height of water level measured in the jerry cans is uniform. Before beginning the experiments, the jerry cans filled with water were weighed to determine the mass of water passed by subtracting the mass of the jerry can at the end of the drain.

The students found that the theoretical emptying time is lower than the experimental one. Since the result found in course was for a perfect or ideal fluid ($\mu = 0$), they explained the difference between theoretical and experimental results by the fact that they neglected the viscosity $\mu$ of water in the theoretical time (assumed equal to 0). They concluded that the viscosity of water ($\mu \neq 0$) will increase the value of the theoretical emptying time and will allow therefore a more accurate value.

### 8.2.2 Teaching evaluation by students

The impact of our new pedagogy could be assessed from teaching or course evaluation. These evaluations could be considered as a useful tool in order to improve

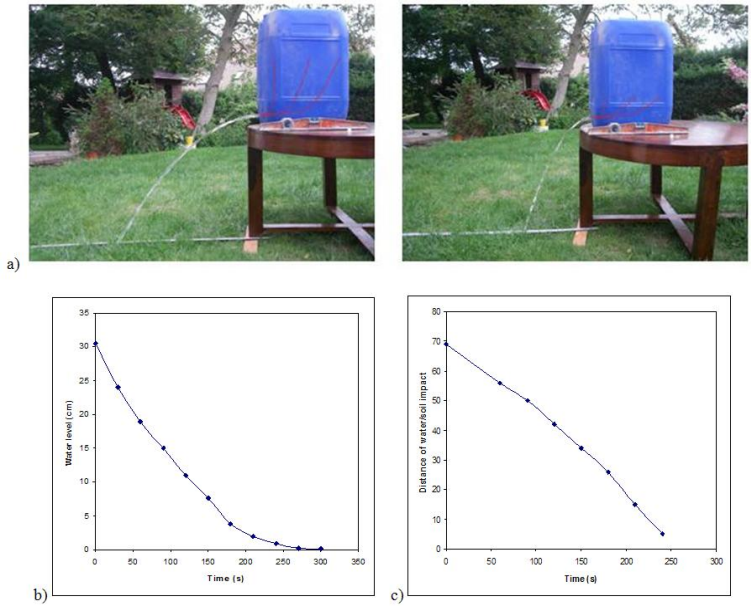


FIGURE 8.2 – Example of atypical experiments in fluid mechanics : Emptying of a 35 liters plastic jerry can. (a) Experiments. Evolution of water level (b) and distance of water/soil impact (c) vs time.

the exchange between teacher and students. Different studies have been conducted on the effectiveness of this tool and its relevance or not [26] [74] [75] [99]. Course evaluations by students are performed at EBI on the website of studies.

Process of teaching evaluations by students : In order to start the online teaching evaluations, students need first to select the course and the year. The evaluation includes two parts (figure 8.3) : - The first consists on evaluating on a scale of 4 : (1) average, (2) satisfactory, (3) good, (4) very good ; the following criteria : organization, required work, clarity of explanations, pedagogy used, interactivity, implication of students, controls. - The second consists on answering two questions related to principal forces and issues to be improved. It is also possible to write additional comments and observations.

## 8.3 Main results and assessment of experience impact on student's learning

### 8.3.1 Analysis of teaching evaluation

Figure (8.4) presents an example of teaching evaluation for fluid mechanics by students of year "P17". This figure presents the total number of students 122, the number of students who participated in the teaching evaluation 58 and the percentage of participation 47.54%. The different criteria are evaluated on a scale of 4, the average of each criterion is indicated : organization (3.29/4), required work (3.09/4),

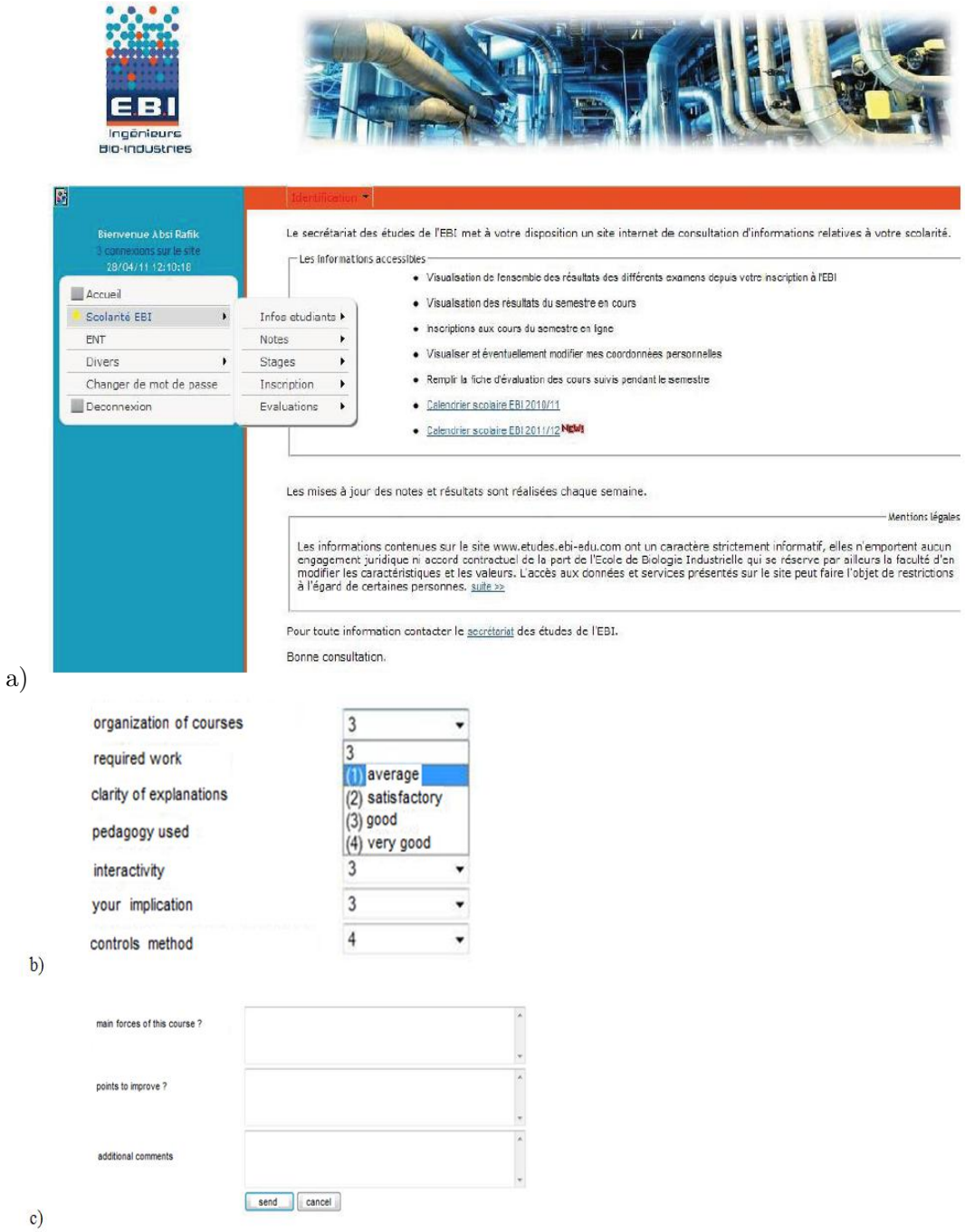


FIGURE 8.3 – Online course evaluations by students : (a) EBI studies web site, (b) evaluation by "'(1) average, (2) satisfactory, (3) good or (4) very good" of each criteria, (c) second part of evaluation : two questions and additional comments.

| | |
|---|---|
| course | PHY215P- fluid mechanics |
| year | 2008-02-01 session n° 16 |
| teacher | ABSI Rafik |
| total number of student | 122 |
| number of student who participated in the evaluation | 58 |
| percentage of participation | 47.54 |
| excellence index (% of very good) | 40.15 |
| performance index (% of very good + good) | 87.44 |
| satisfaction index (% of very good + good + satifactory) | 98.77 |
| organization | 3.29 |
| required work | 3.09 |
| clarity of explanations | 3.47 |
| used pedagogy | 3.41 |
| interactivity | 3.28 |
| implication of student | 2.97 |
| controls | 3.34 |
| global average | 3.26 |

FIGURE 8.4 – Sample of teaching evaluation of fluid mechanics course by P17 students.

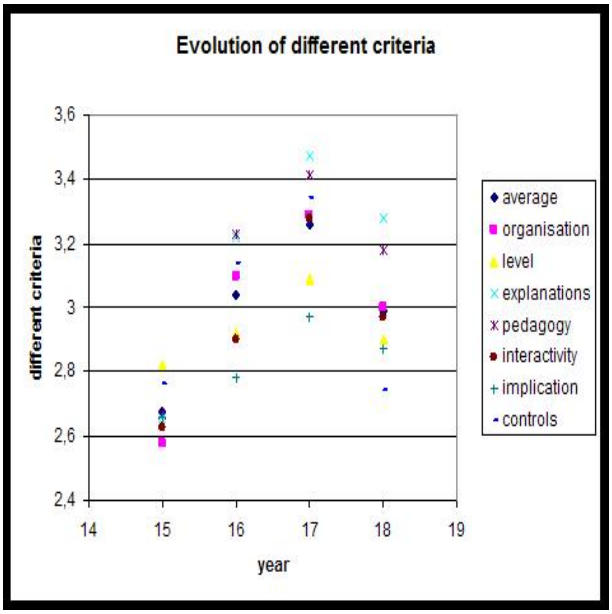


FIGURE 8.5 – Evolution of different criteria for each year (from P15 to P18).

clarity of explanations (3.47/4), used pedagogy (3.41/4), interactivity (3.28/4), implication of students (2.97/4), controls (3.34/4). The global average of the evaluation is indicated at the bottom 3.26. It shows also three indices respectively : excellence index (40.15%), performance index (87.44%) and satisfaction index (98.77%). The satisfaction index indicates the percentage of students who evaluated all the criteria at least 2/4. The performance index indicates the percentage of students who evaluated all the criteria at least 3/4. The excellence index indicates the percentage of students who evaluated all the criteria 4/4 [11].

Figure (8.5) presents the average of the different criteria for students of four years (P15 to P18). This figure allows observing a peak for students of year P17 who were concerned by the new pedagogy based on atypical experiments. This peak indicates that all criteria have maximum values and therefore that the teaching was considered as the best on the basis of the evaluation of the different criteria namely : organization, required work, clarity of explanations, pedagogy used, interactivity, implication of students and controls.

It is important to note that the number of students who participated in the teaching evaluation has decreased from year P15 to P18 (figure 8.6). This should have a significant effect on the evaluation results and their analysis.

### 8.3.2 Semantic analysis of comments and observations

The students' comments were analyzed. We identified the different "words" hereafter called "quotations", which were written by students in their comments and observations. These quotations have been grouped by semantic fields and groups [11]. The occurrence which is the number of quotations "n" associated to each field

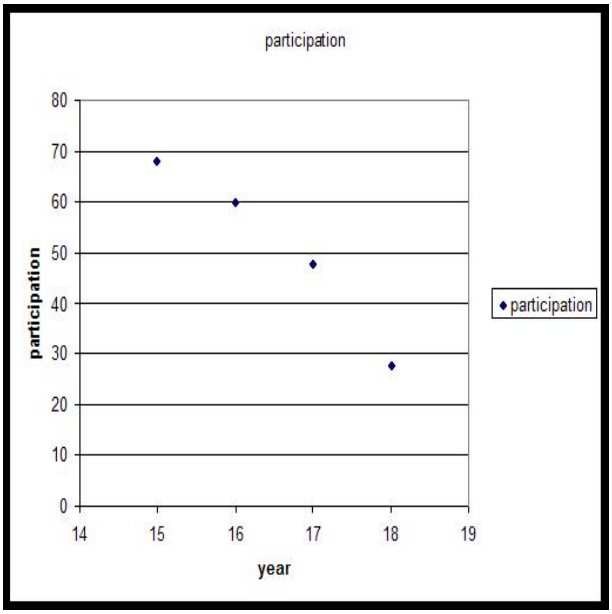


FIGURE 8.6 – Percentage of students' participation to teaching evaluation (from P15 to P18).

by year was presented. In order to take into account the effect of the number of students who participate in the course evaluation "N", we divided "n" by "N" [11].

Figure (8.7.a) presents the number of quotations "n" related to each field by year. Figure (8.7.b) shows the effect of number of responses or number of students who participate in the teaching evaluation "N". The parameter "n/N" for year P17 (solid line) is above the other lines (three other years) for criteria "experience", "clarity" and "interactivity". However, we notice that the criteria "concrete" decreases for P17, while atypical experiments should raise this criterion. We can explain this by the fact that students are not obliged to write comments and therefore some students found enough to rate each specified criterion (on scale of 4). There is some redundancy between the quantitative evaluations related to the specified criteria and free comments.

### 8.3.3 Impact on students' learning

Students participation in improving teaching through atypical experiments and course assessment gives teaching a new dimension. By this free participation in these experiments, the student discovers the value of effort and no longer hesitates to ask questions or seek solutions to encountered problems. Thus learning is no longer a mere reproduction of abstract knowledge or non-practical applications but an anchorage in the environment.

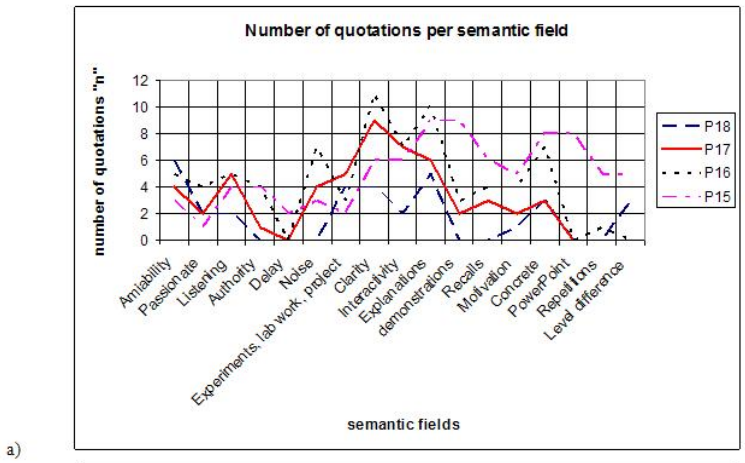


a)

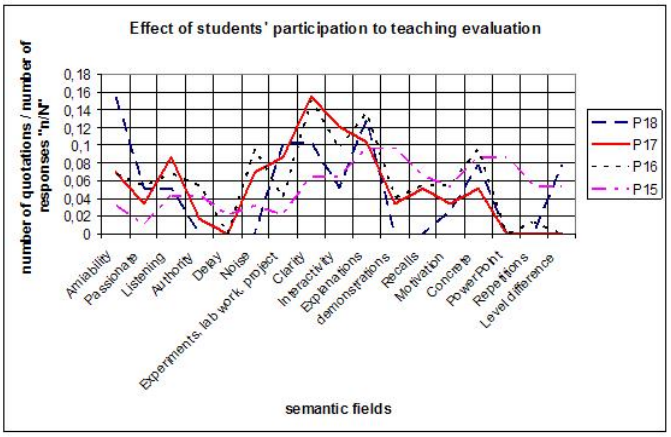


b)

FIGURE 8.7 – (a) Number of quotations "n" related to each semantic field by year. (b) Effect of the number of students who participated in the teaching evaluation "N", n/N VS semantic fields.

## 8.4 Conclusions

We presented an innovative teaching/learning pedagogy based on the concept of atypical experiments and its implications in teaching fluid mechanics. This new pedagogy was tested at EBI on students of year “P17”. Students of "P17" were asked to draw inspiration from everyday life situations to find applications of course and to do experiments to verify and validate some theoretical results. The experiment of emptying of jerry cans is presented as an example of these atypical experiments. The impact of this innovative pedagogy has been evaluated from online teaching assessment made by students. We analyzed the course evaluations by students of “P17” and we compared them with those of three other years (two before the application of the new pedagogy and one after). The teaching evaluation concerns : (1) a first part which consists on assessing on a scale of 4 the criteria : organization, required work, clarity of explanations, pedagogy used, interactivity, implication of students and controls ; (2) a second part which consists on two questions related to main forces and issues to be improved and free comments and observations.

The analysis of teaching assessment shows for part 1 (assessment of criteria on a scale of 4 for years P15 to P18) a peak in all criteria for students of year P17, which was concerned by the application of the new pedagogy based on atypical experiments. This result is very interesting and shows the efficiency of this approach to motivate students. In addition to the quantitative analysis, we analyzed comments and observations of students (part 2 in the teaching assessment). We identified first the main “words” called “quotations” which were grouped into semantic field and groups. We compared first the occurrence which is the number of quotations “n” related to each field for a given year. However, in order to account for “N” the number of students who took part in the teaching assessment, we introduced the parameter “n/N”. The parameter “n/N” for year P17 is above the three other years for criteria “experience”, “clarity” and “interactivity”.

Learning through play proved a great success in fluid mechanics which has been progressively perceived as interesting, useful, pleasant and easy to assimilate. We showed that this pedagogy which includes educational gaming presents benefits for students. These experiments seem therefore to be an effective tool for improving teaching/learning activities in higher education.

We can deduce from this study that trust acquires in the cooperation and learning is based on both knowledge and students involvement. In this exchange, the teacher learns as much as student, because in teaching him to remain curious, it reinforces his skills to seek solutions to encountered problems.

Chapitre 9

# National and international research collaborations

## 9.1 Research at St. Anthony Falls Laboratory, University of Minnesota

I visited the St. Anthony Falls Laboratory (SAFL) of the University of Minnesota from January 19 till February 15, 2009. During that period, I led several research activities and worked closely with Prof. F. Porté-Agel and graduate students in the Environmental Fluid Mechanics research group. In addition, I was very active establishing contacts with representatives from several Departments at the University of Minnesota in order to explore potential exchange opportunities for undergraduate and graduate students. We made important progress during relatively short time, in the following two lines of research :

### 9.1.1 Large-eddy simulation (LES)

Large-eddy simulation (LES) was conducted with a new-generation of subgrid-scale models [88] [89]. I have modified the LES code developed by the research group to include sediment transport equations. I have performed unsteady three-dimensional simulations using computer resources from the Minnesota Supercomputing Institute. This research has led to an extended abstract for the 6th International Symposium on Turbulence, Heat and Mass Transfer (Rome, Italy, September, 2009).

### 9.1.2 Wind tunnel experiments

Wind tunnel experiments was conducted to study the distribution of turbulence kinetic energy (TKE) and temperature variance in turbulent boundary layers. In particular, cross-wire anemometry was used to obtain high-frequency measurements of the three components of velocity and temperature (Fig. 9.1, 9.2). We are currently using those measurements to test and improve analytical models for the distribution of TKE and scalar variance in turbulent boundary layers.

The visit has made possible to establish strong research collaborations in a relatively short time. We expect to continue this collaboration in the coming months/years.

(a)

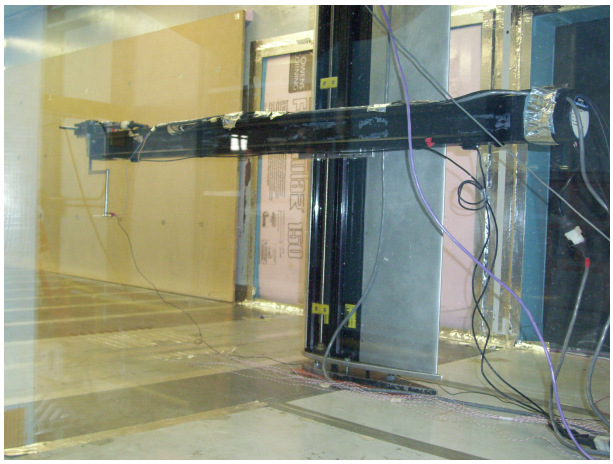

(b)

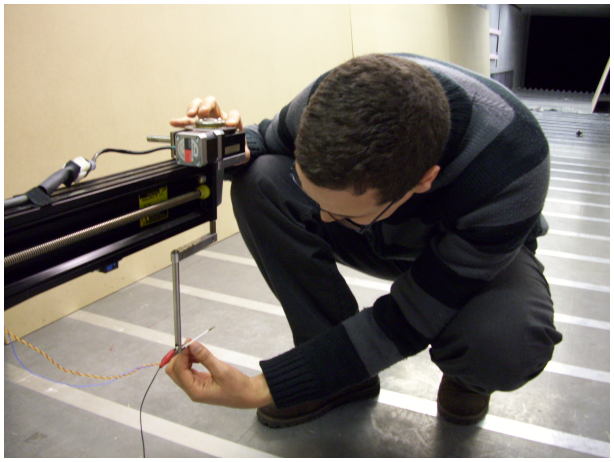

FIGURE 9.1 – (a) wind tunnel ; (b) cross-wire anemometry.

(a)

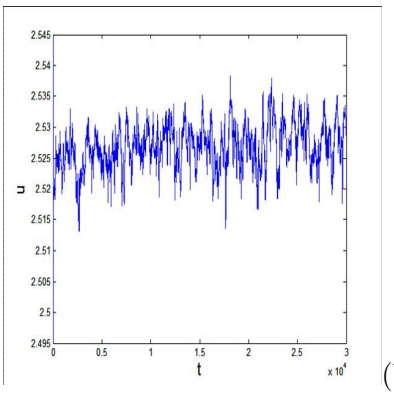


(b)

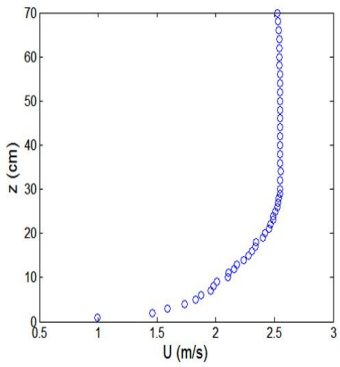


FIGURE 9.2 – (a) Sample of velocity measurement ; (b) experimental mean streamwise velocity profile.

## 9.2 Collaboration with Tohoku University, Japan

Part of the Proposal for 7th EC Framework Programme Integrating Activity : Hydralab IV : Alongshore variation of the depth of closure near coastal structures : Experimental investigation through a short access period to the wave basin of DHI.

### 9.2.1 Alongshore variation of the depth of closure near coastal structures

*Scientific context of the study*

Depth of closure "DoC" is a useful concept in coastal morphology. It is involved in prediction of shoreline position (one-line assumption). Most models, using one-line theory of shoreline change, don't make any small assumption with respect to the incident wave angle and the shoreline direction. Available equations such as Hallermeir's equation [51] don't allow alongshore variation of DoC around structures. However, DoC should depend on the alongshore distance [71] [54] [83] [114] [94] especially near structures. Our analysis of field data shows that this dependency is related to different parameters. Wave transformation theory was applied to analyze wave height in term of refraction, shoaling and reflection phenomenon. The angle between wave direction and coastal structure (port) seems play an important role.

*Interest of wave basin experiments*

The state-of-the-art show that most measurements of DoC carried out in the past were in field conditions and laboratory wave flumes. On the one hand, our former study based on in situ data shows that the phenomenon is very complex in field conditions. In order to allow simpler situations which allow better analysis wave basin experiments are required. On the other hand, wave flume experiments don't allow experimental tests with different angles between waves and coastal structures. In order to allow different wave directions we need wave basin experiments. Wave basin seems to be the more adequate facility which allows simplification of the complex real behaviour but takes into account the more important involved physics. We will consider ideal conditions, a straight beach with a port perpendicular to the shore and various wave conditions and different wave angles. After each experiment, we will measure cross sections bathymetry (cross shore profiles for different shoreline distances), shoreline position, wave height and alongshore current.

*Objectives of our study*

— Measurements of DoC for different wave directions by using variation of cross shore profiles and shoreline position. Bathymetry data of cross shore profiles will be analyzed to determine DoC values. We expect to find deeper DoC around structures.

— Assessment of the effect of the angle between the wave and the coastal structure
— Assessment of the influence of coastal structure on wave transformation
— The aim is to provide a practical and reliable analytical equation for coastal engineering applications in shoreline change modelling systems and demonstrate its capabilities through experimental tests

### 9.2.2 Investigation from fiels measurements

In the former study conducted at Tohoku University, we used field data from the area of Sendai Bay Coast in Japan [92]. The analysis of bathymetry data of cross shore profiles (figures 2) has shown that DoC is deeper near coastal structures (figure 3). DoC variation in Yuriage Port is shallower than Sendai Port (figure 3). This seems to be related to less wave reflection in Yuriage Port which is due to the angle and length of the breakwater. To examine influence of coastal structures, wave transformation theory was applied to analyze wave height in term of refraction, shoaling and reflection phenomenon. The transformed wave was utilized to re-calculate DoC in Sendai Port and Yuriage Port using Hallermeir's equation.

### 9.2.3 Wave basin experiments

Figure (9.3) presents wave basin experiments conducted in the Coastal Engineering Laboratory of the University of Tokyo. Figure (9.3.b) shows measurement of shoreline position. In these experiments, the scales were : Space scale = 1/1000 ; Depth scale = 1/200 ; Slope = 1/10 and after 6 cm depth, slope = 1/20.

*Tentative presentation of wave basin experiments at DHI*

We will consider a straight beach with various coastal structures. We will consider first ideal conditions with a port perpendicular to the shore, various wave conditions and different wave directions (angle between the wave and the coastal structure). Duration of each experiment from 30 minutes to 3 hours Measurements after each experiment [13] :

— Measurements of cross sections bathymetry (cross shore profiles for different shoreline distances  15 cm)
— Shoreline position
— Wave height and alongshore current

(a)

(b)

FIGURE 9.3 – Wave basin experiments of 17 and 18 January 2011, Coastal Engineering Laboratory, the University of Tokyo ; (a) Propagation of southern waves near the port (b) Measurements of shoreline position.

## 9.3 Research at AFSSET (now ANSES)

In accordance with the quality procedure in force at AFSSET, based on the use of standard NF X 50-110 protocols relating to expert appraisal quality, the solicitation to evaluate the safety of adjuvants for artificial snow production was submitted to a dedicated working group of 10 experts. The final report was examined by the committee of specialised experts responsible for the assessment of risks linked to water and biological agents appointed by AFSSET.

In this study, I was involved in both working group (of 10 expert) and the committee of specialised experts. My work was related to the understanding of the process of artificial snow production.

The reduction in natural snow cover is becoming increasingly evident, in the Alps, where a rise in winter night-time temperatures is coupled with a decrease in precipitation. In this context, winter sports resorts are using more and more artificial snow to ensure good snow cover on their slopes. A technological advance in the past 20 years in the manufacture of artificial snow is the use of biological additives derived from a specific bacterium, an ice nucleation active strains of Pseudomonas syringae strain (here referred to as INAPSS), which has the capacity to optimise the freezing of water. Artificial snow production based on the use of such biological additives is now practiced worldwide and environmental concerns related to its use have been discussed for more than two decades. Used in France since 1992, from 2005, INAPSS derived products have been suspended, at the request of the French National Ski Lift Union, following doubts concerning its potential impact on human health and the environment. In this context, both the French Ministries for Health and for Ecology have requested that AFSSET assess the health risks linked to the use of INAPSS derived products to make artificial snow. All conclusions and related recommendations have been extensively detailed in a published report to the French authorities [66].

Most additive products presented by manufacturers as aiding the production of artificial snow are derived from a lyophilized biological preparation containing the inactivated bacterium P. syringae. This application exploits the ice-nucleating capabilities of the bacterium, promoted by an outer membrane-associated protein, INP. Our study shows that the chemical composition of manufactured INAPSS derived products does not indicate the presence of any chemical substances toxic to humans at the concentrations used. On a microbiological level, INAPSS derived products are only composed of inactivated strain 31a of P. syringae, an epiphytic bacterium, naturally present in the environment. The health hazards for humans of INAPSS derived products were studied on the basis of an assumption of infectious, toxicity and allergenic capacity. The scientific literature does not report any infectious capacity of P. syringae for humans. Also, it was considered that P. syringae and consequently, INAPSS derived products, do not present any pathogenic capacity for

humans. Considering that humans are currently exposed in their normal environment to P. syringae, and that repeated contact with high doses of antigens causes tolerance rather than hypersensitivity, the danger linked to allergy to INAPSS related products was considered to be minimal. However, the risk of possible allergy in some particularly sensitive individuals cannot be excluded. During the mixing and cleaning phases of INAPSS derived product preparation, snowmakers are the only category of people potentially exposed to a the product. The risk was estimated to be negligible to low if workers comply with safety precautions recommended, but it was estimated higher if snowmakers operated without PPE. Thus for snowmakers, the systematic wearing of PPE during the preparation phase was recommended. It was also considered that the use of a respiratory protection would be necessary, whereas this was not recommended by the manufacturer. Moreover, it is advised to avoid procedures that are different from the manufacturer's protocol, such as pre-mixing the product in a bucket of water. Concerning exposure to artificial snow from the plume of snow guns, the estimated risk was found negligible to low for snowmakers and nil to negligible for skiers (adults and children), slope managers, slope safety officers, instructors and rescue workers and nil for snow grooming machine drivers and ski lift operators. Concerning exposure to artificial snow on the ground, the estimated risk was nil to negligible for all the people concerned. The artificial snowmaking process generally uses natural water of variable quality, that includes microorganisms pathogenic to humans (staphylococci, viruses, etc.). It appeared that INAPSS derived products were a source of nutrients which can facilitate the development of such microorganisms. In addition, considering the susceptibility of aquifers and drinking water catchments in mountain areas to pollution, the thawing of artificial snow made from water of poor microbiological quality may have an impact on the sanitary quality of water intended for the production of water for human consumption. Without a specific regulation specifying the water quality to be used in snowmaking, we recommend the use of water of a quality that is fit for human consumption and advise keeping the mixture in the dilution tank for no more than 24 hours. Concerning the protection of drinking water catchments, it seems pertinent to take into account in the definition of protection perimeters, the ski resort practices in terms of artificial snow production with the use of additives and/or water of poor chemical and/or microbiological quality. In order to reduce the occurrence of dangers during the production of artificial snow, it was recommended, in view of the health risk assessment conclusions, to systematically wear protective equipment (goggles, gloves and mask) when preparing the snowmaking product solution, to use water with a good microbiological quality for the dilution of the product, and to store the mixture for no more than 24 hours. In addition, as part of a health monitoring approach, it would be pertinent to further consider the potential impacts linked to the use of additives other than INAPSS derived products, and in particular those used to maintain snow coverage, which could lead to impacts on the soil and the quality of water sources, through snow melt.

Quatrième partie

# Conclusion et Perspectives

Ce mémoire m'a permis de faire le point sur l'ensemble de mes activités dans les domaines de l'enseignement et de la recherche ainsi que mon implication dans la vie de l'établissement.

En matière de recherche, rappelons tout d'abord que le principal objectif consistait à proposer aux ingénieurs et expérimentateurs des outils analytiques pratiques, accessibles, faciles à utiliser et précis. Les principaux résultats obtenus dans ce domaine sont :

- Résolution analytique de l'équation de transport modélisée pour l'énergie cinétique turbulente (ECT) $k$ :
  - Révision de la solution semi-analytique de Nezu et Nakagawa pour les écoulements à surface libre
  - Généralisation de la solution et proposition d'une seconde solution au voisinage immédiat de la paroi ($y^+ < 20$) [3] : Solution validée par des données de simulation numérique directe (DNS) obtenues pour des écoulements en canal turbulent et évaluée par ma doctorante au niveau du code commercialisé Fluent [34] [37].
- Les solutions analytiques pour l'ECT, nous ont permis de :
  - Améliorer la description des vitesses en utilisant des viscosités turbulentes basées sur les solutions analytiques pour $k$ [5].
  - Proposer une relation analytique pour la longueur de mélange basée sur la première solution pour $k$ et l'hypothèse de similitude de von Karman [2]. Les profils de vitesses obtenus ont été comparés à des données de mesures. Cette relation analytique pour la longueur de mélange a été évaluée au niveau d'un code d'écoulements à surface libre (travail mené avec un doctorant [23], thèse soutenue en 2008).
- A partir d'une analyse des équations de Navier-Stokes moyennées au sens de Reynolds (RANS), nous avons obtenu une équation différentielle ordinaire (EDO) pour les vitesses ainsi que sa solution semi-analytique. Cette EDO permet de calculer des profils de vitesses avec un maximum au-dessous de la surface libre (phénomène de "dip") pour les écoulements dans des canaux étroits (rapport d'aspect $< 5$) [7].
- Ecriture d'une relation analytique pour le nombre de Schmidt turbulent $Sc_t$, basée sur le modèle cinétique [30] [119] [44], donné en fonction du nombre de Stokes [8] [12].
- Malgrès le caractére instationnaire des écoulements oscillants, la viscosité turbulente moyennée sur la période est bien décrite par le modèle analytique de viscosité turbulente présenté et validé par DNS pour les écoulements stationnaires. Ce résultat a été validé par comparaison avec le modèle à deux équations $k$-$\omega$.
- Analyse des profils de concentrations de sédiments en suspension sous l'effet d'un écoulement oscillant sur un fond de rides, importance du phénomène de détachement tourbillonnaire [6].

Dans le domaine de la pédagogie, j'ai cherché des méthodes pour faciliter

l'enseignement de la mécanique des fluides. L'analyse des fiches d'évaluations a montré que l'idée des expériences atypiques a été particulièrement concluante [11]. Nous continuons ce travail pédagogique au sein de la commission 'Pédagogie par compétences' de l'EBI, dont le but est de proposer et de mettre en oeuvre des solutions pédagogiques innovantes afin d'améliorer les enseignements.

L'identification de perspectives de recherche s'inscrit dans l'activité professionnelle de l'enseignant-chercheur. Ces perspectives évoluent en fonction des besoins industriels, environnementaux, de l'intérêt scientifique et des moyens disponibles. Pour ma part, je conçois ces perspectives de recherche sous deux paramètres :

1. les sujets porteurs (intéressants du point de vue scientifique et opérationnel)
2. l'exploitation des moyens matériels disponibles au niveau du Laboratoire de Recherche et Développement de l'EBI (Annexe A)

Dans le cadre de mes activités à l'EBI, je dois me consacrer au développement de l'activité de recherche "Modélisation d'écoulements Environnementaux, Biologiques et Industriels" (Annexe A) en rapport avec mes enseignements afin de renforcer les liens entre la théorie et la pratique. Voici la liste non exhaustive des sujets à traiter :

1. Ecoulements environnementaux
   — Transport sédimentaire :
   - Poursuite du travail de modélisation des concentrations de sédiments sous l'effet d'écoulements oscillants, suite à la mission de professeur visitant au Japon (Tohoku University) financée par JSPS [1] (Japan Society for the Promotion of Science) du 12 décembre 2010 au 7 février 2011.
   - Reprise du travail de calcul des concentrations de sédiments par simulation des grandes échelles (LES) initié pendant mon séjour au St. Anthony Falls Laboratory (SAFL) à l'Université du Minnesota, Minneapolis, USA, du 19 janvier au 15 février 2009.
   - Validation de l'équation pour $Sc_t$ [12], calcul des profils de concentration de sédiments en suspension et comparaison avec des données de mesures [39].
   - Modélisation diphasique du transport sédimentaire sous l'effet d'écoulements oscillants en collaboration avec Dr. H. Liu (the University of Tokyo).
   - Projet HYDRALAB en collaboration avec Prof. Hitoshi Tanaka (Tohoku University, Japan), Dr. François Sabatier (Université d'Aix Marseille, France) ; Prof. Peter D. Thorne (Liverpool University, United Kingdom) et Dr. Maarten G. Kleinhans (Universiteit Utrecht, The Netherlands).
   — Couche limite atmosphérique : Application des outils analytiques développés et comparaisons avec les résultats expérimentaux obtenus en soufflerie dans le cadre du séjour effectué au St. Anthony Falls Laboratory (SAFL) à l'Université du Minnesota (Minneapolis, USA).

1. http ://www.jsps.go.jp/english/

— Ecoulements à surface libre :
- Validation de la solution semi-analytique [7] et analyse du paramètre Π.
- Etude de l'écoulement à laval du point de commencement du phénomène d'entraînement d'air dans des canaux à forte pente [41] [50], collaboration avec l'Ecole Nationale Polytechnique (ENP, Algérie), application au canal en marches descaliers (accueil d'un enseignant-chercheur de l'ENP à l'EBI du 25 novembre au 10 décembre 2010).
- Investigation expérimentale de couches limites turbulentes en utilisant différentes techniques de mesures, collaboration avec Dr.-Ing. Katsuaki Shirai (Technische Universität Dresden, Germany).

2. Ecoulements biologiques
— Etude des écoulements pulsatiles intra-artériels : L'Athérosclérose (maladie de la paroi artérielle) est caractérisée par des dépôts d'athéromes au niveau des parois artérielles. Sous l'effet de l'action du coeur, l'écoulement dans les artères est fortement pulsatile. Les formes des ondes de l'écoulement et de la pression sont complexes [79]. L'écoulement est fortement instable et peut devenir turbulent même à des nombres de Reynolds relativement bas. La turbulence jouerait un rôle majeur dans la formation de ces dépôts ainsi que dans leur détachement. L'écoulement turbulent modifierai l'expression génétique des cellules endothéliales qui est à l'origine de proliférations cellulaires responsables ainsi d'altération du tissu vasculaire (endothélium), favorisant l'athérosclérose [28]. L'objectif serait d'étudier l'effet de l'écoulement intra artériel sur les cellules, le tissu et la pathologie.

3. Ecoulements industriels
— Projet de Brevet : Mise en place d'un procédé de nettoyage en place des conduites industrielles. *Ce procédé est particulièrement utile dans l'élimination de dépôts et résidus susceptibles d'apparaître dans les conduites industrielles, mais aussi dans l'élimination de micro-organismes et de biofilms. Le procédé selon l'invention représente une alternative avantageuse aux techniques exploitant des écoulements pulsatiles du fait de l'augmentation des frottements, ce qui augmente l'efficacité du nettoyage*[2].
— Etude du transfert de chaleur dans les chaudières, application à la chaudière de récupération élément de base des centrales solaires à cycle combiné. Collaboration avec le Centre de Développement des Énergies Renouvelables, Division Energie Solaire Thermique et Géothermie, et l'Université des Sciences et Technologies (USTHB) Algérie.

— Un autre sujet intéressant qui touche à la fois à l'environnement et aux procédés industriels concerne la pollution des mers et océans par les déchets plastiques ainsi que les procédés de fabrication de produits bioplastiques aux caractéristiques équivalentes aux plastics traditionnels mais

2. Compte-rendu d'étude de brevetabilité, Cabinet PLASSERAUD, Réf. AVB100099 AAY

Biodégradables et Compostables.

# Bibliographie


[1] Absi R. (2005) Comment on 'Turbulent diffusion of momentum and suspended particles : A finite-mixing-length-theory', *Physics of Fluids*, American Institute of Physics, **17**(7), 079101. 2, 27, 28, 64, 66

[2] Absi R. (2006) A roughness and time dependent mixing length equation, *Journal of JSCE*, Japan Society of Civil Engineers, Division B : *Doboku Gakkai Ronbunshuu B*, **62**(4), 437-446. 2, 40, 44, 45, 103

[3] Absi R. (2008a) Analytical solutions for the modeled k-equation, *Journal of Applied Mechanics*, Transactions of the ASME, American Society of Mechanical Engineers, **75**(4), 044501. 1, 21, 25, 32, 33, 34, 41, 103

[4] Absi R. (2008b) Comments on 'Turbulent velocity profile in fully-developed open channel flows', *Environmental Fluid Mechanics*, Springer, **8**(4), 389-394. 2, 52

[5] Absi R. (2009) A simple eddy viscosity formulation for turbulent boundary layers near smooth walls, *Comptes Rendus Mecanique*, Académie des Sciences, Elsevier, **337**, 158-165. 2, 34, 39, 41, 103

[6] Absi R. (2010) Concentration profiles for fine and coarse sediments suspended by waves over ripples : An analytical study with the 1-DV gradient diffusion model, *Advances in Water Resources*, Elsevier, **33**(4), 411-418. 2, 63, 64, 71, 72, 76, 103

[7] Absi R. (2011) An ordinary differential equation for velocity distribution and dip phenomenon in open-channel flows, *Journal of Hydraulic Research*, IAHR, Taylor & Francis, **49**, 82-89. 2, 51, 55, 56, 103, 105

[8] Absi R. (2011) Discussion of 'Vertical mixing in the fully developed turbulent layer of sediment-laden open-channel flow', *Journal of Hydraulic Engineering*, ASCE, American Society of Civil Engineers, **137**(9), in press. 2, 22, 59, 61, 103

[9] Absi R., Analytical modeling of eddy viscosity and velocity profiles in turbulent channel flows, submitted. 30, 46

[10] Absi R., Tanaka H. (2011) Toward improving prediction of sediment transport over wave-induced ripples, *Tohoku Journal of Natural Disaster Science*, Japan, Vol. **47**, pp 213-218. 66, 67, 68

[11] Absi R., Nalpas C., Dufour F., *et al.* (2011) Teaching fluid mechanics for undergraduate students in applied industrial biology : from theory to atypical experiments, *International Journal of Engineering Education* (IJEE), **27**(3), **27**(3), 550-558. 85, 89, 90, 104

[12] Absi R., Marchandon S., Lavarde M. (2011) Turbulent diffusion of suspended particles : analysis of the turbulent Schmidt number, *Defect and Diffusion Forum*, Trans Tech Publications, Vols. **312-315**, pp 794-799. 2, 28, 45, 46, 61, 62, 103, 104

[13] Absi R., Tanaka H., Sabatier F., Thorne P.D., Kleinhans M.G., Alongshore variation of the depth of closure near coastal structures : Experimental investigation through a short access period to the wave basin of DHI, *Proposal for 7th EC Framework Programme Integrating Activity : Hydralab IV*. 96

[14] Baldock T.E., Tomkins M.R., Nielsen P., Hughes M.G. (2004) Settling velocity of sediments at high concentrations. *Coast. Eng.*, **51**, 91-100. 65, 74

[15] Ben Hamed H., Bennacer R. 2008, Poiseuille Rayleigh-Bénard problem in a horizontal duct of finite length in streamwise direction : stability analysis, *Progress in Comput. Fluid Dynamics*, **8**(6), 342-350. 37

[16] Bernard C., Broyart B., Absi R., *et al.*, Prediction of Thermohydric-history of whey protein concentrate droplets during spray, Drying Technology, in revision.

[17] Blondeaux P., Vittori G. (1991) Vorticity dynamics in an oscillatory flow over a rippled bed, *J. Fluid. Mech.*, **266**, 257-289. 64

[18] Buffone C., Sefiane K., Christy J.R.E. (2005) Experimental investigation of self-induced thermocapillary convection for an evaporating meniscus in capillary tubes using micro-particle image velocimetry, *Phys. Fluids*, **17**(5), 052104. 37

[19] Businger J.A., Arya S.P.S. (1974) Heights of the mixed layer in the stable stratified planetary boundary layer, *Adv. Geophys.*, **18**A, 7392. 40

[20] Cardoso A.H., Graf W.H., Gust G. (1989) Uniform flow in a smooth open channel. *J. Hydraul. Res.*, **27**(5), 603616. 51, 55

[21] Cebeci T., Smith M.O. (1974) *Analysis of turbulent boundary layers*. Academic, San Diego. 55

[22] Cheng N.S. (1997) Effect of concentration on settling velocity of sediment particles. *J. Hydraul. Eng.*, ASCE, **123**(8), 728-731. 74

[23] Cherif E.A., Absi R., *et al.* (2008) Modélisation numérique des processus de transport des sédiments et de l'évolution des fonds, *European Journal of Environmental and Civil Engineering*, Lavoisier/Hermès, **12**(1-2), 87-104. 2, 45, 103

[24] Coleman N. (1986) Effects of Suspended Sediment on the Open-Channel Velocity Distribution, *Water Resour. Res.*, **22**(10), 1377-1384. 57

[25] Coles D. (1956) The law of the wake in turbulent boundary layer. *J. Fluid Mech.*, **1**, 191-226. 22, 51, 54

[26] Conle C. (1999) Moments of interpretation in the perception and evaluation of teaching, *Teaching and Teacher Education*, **15**(7), 801-814. 86

[27] Conley D.C., Falchetti S., Lohmann I.P., Brocchini M. (2008) The effects of flow stratification by non-cohesive sediment on transport in high-energy wave-driven flows. *J. Fluid. Mech.*, **610**, 43-67. 62

[28] Davies P.F., Shi C., Depaola N., Helmke BP., Polacek DC. (2001) Hemodynamics and the focal origin of atherosclerosis : a spatial approach to endothelial structure, gene expression, and function. *Ann. N. Y. Acad. Sci.*, **947**, 7-16. 105

[29] del Alamo J.C., Jimenez J., Zandonade P. and Moser R. D., (2004) Scaling of the energy spectra of turbulent channels, *J. Fluid Mech.* **500**, **135**, 135-144. 21

[30] Derevich I.V., Zaichick L.I., (1988) Particule deposition from a turbulent flow, *Fluid Dyn.*, **23**, 722-729. 2, 22, 59, 60, 61, 103

[31] Di Felice R. (2008) Hydrodynamics of liquid fluidisation. *Chem. Eng. Sci.*, **50**, 1213-1245. 74

[32] du Toit C.G., Sleath J.F.A. (1981) Velocity measurements close to rippled beds in oscillatory flow. *J. Fluid. Mech.*, **112**, 71-96. 66

[33] Dohmen-Janssen C.M., Hassan W.N., Ribberink J.S. (2001) Mobile-bed effects in oscillatory sheet flow. *J. Geophys. Res.*, **106**(C11), 27103-27115. 59, 72

[34] El Gharbi N., Absi R., Benzaoui A. Numerical simulations of heat transfer in plane channel flow, to appear in *Defect and Diffusion Forum*, Trans Tech Publications, **312-315**, pp 671-675. 2, 103

[35] El Gharbi N., Absi R., Benzaoui A., Numerical investigation toward improving heat transfer predictions in a turbulent channel flow, *International Journal of Thermal Science*, Elsevier, accepted, in press. 38

[36] El Gharbi N., Absi R., Benzaoui A., Amara E.-H. (2009) Effect of near-wall treatments on airflow simulations, *International Conference on Computational Methods for Energy Engineering and Environment*, 20-22 November 2009, Sousse, Tunisia, 185-189. 2, 26, 36, 37

[37] El Gharbi N., Absi R., Benzaoui A., Bennacer R. (2011) An improved near wall treatment for turbulent channel flows, *International Journal of Computational Fluid Dynamics*, Taylor & Francis, **25**(1), 41-46. 2, 26, 36, 37, 103

[38] Elghobashi S.E. (1994) On predicting particle laden turbulent flows. *Appl. Sci. Res.*, **52**, 309-329. 60

[39] Einstein H.A., Chien N., Effects of heavy sediment concentration near the beds on velocity and sediment distribution, Eng. Div. MRD-8, 1955. 104

[40] Ferrari G., Meerdink G., Walstra P. (1989) Drying kinetics for a single droplet of skim-milk. *Journal of Food Engineering*, **10**, 215-230.

[41] Falvey, H.T. (1990). Cavitation in chutes and spillways. Water Resources Technical Publication, Engineering monograph 42, U.S. Dept. of Interior, U.S. Printing Office, Denver CO. 105

[42] Francis J.B. (1878). On the cause of the maximum velocity of water flowing in open channels being below the surface. *Trans. ASCE.* 51

[43] Fluent, 2005, Fluent 6.2 user's guide. 36

[44] Fu X., Wang G., Shao X. (2005) Effect of concentration on settling velocity of sediment particles. J. Hydraul. Eng., ASCE, **131**(10), 877-888. 2, 22, 59, 60, 61, 103

[45] Graf W.H. (1984) *Hydraulics of Sediment Transport*, Water Resources Publications, Littleton, CO, USA. 40

[46] Graf W.H., Cellino M. (2002) Suspension flows in open channels : experimental study. *J. Hydraul. Res.*, **40**(4), 435-447. 59, 60

[47] Grasmeijer B.T., Chung D.H., Van Rijn L.C. (1999) Depth-integrated sediment transport in the surf zone. *Proc. Coastal Sediments 1999*, New York, ASCE, 325-340. 78

[48] Guo J., Julien P.Y. (2003) Modified log-wake law for turbulent flows in smooth pipes. *J. Hydraul. Res.*, **41**(5), 493-501. 51

[49] Guo J., Julien P. Y. (2008). Application of the modified log-wake law in open-channels. *J. Appl. Fluid Mech.* **1**(2), 17-23. 51

[50] Hager, W.H., Blaser, F. (1998). Drawdown curve and incipient aeration for chute flow. *Can. J. Civil Engng.* **25**(3), 467473. 105

[51] Hallermeier, R. J. (1981). A profile zonation for seasonal sand beaches from wave climate, *Coastal Engineering*, **4**, 253-277. 95

[52] Hanjalić K., and Launder B.E., (1976) Contribution towards a Reynolds-stress Closure for low-Reynolds-number turbulence, *J. Fluid Mech.*, **74**, pp 593-610. 21, 25, 34

[53] Hayashi S., Ohmoto T., Honda I. (2006). Direct numerical simulation of secondary currents and vortex structures in an open-channel flow, *Doboku Gakkai Ronbunshuu B, JSCE*, **62**(1), 80-99 (in Japanese). 51

[54] Hinton, C. and R.J. Nicholls (1998). Spatial and temporal behaviour of depth of closure along the Holland coast. *Proc. 26th Int. Conf. Coast. Eng.*, ASCE, 2913-2925. 95

[55] Hinze J. O. (1975). *Turbulence*. McGraw-Hill, New York. 22, 51, 54

[56] Hsu T.W., Jan C.D. (1998) Calibration of BusingerArya type of eddy viscosity models parameters. *J. Waterw. Port Coastal. Ocean. Eng.*, ASCE, **124**(5), 281-284. 40, 65

[57] Houwman K.T., Ruessink B.G. (1996) Sediment transport in the vicinity of the shoreface nourishment of Terschelling. Dep. of Physical Geography. University of Utrecht, The Netherlands. 78

[58] Hoyas S. and Jiménez J., (2006) Scaling of velocity fluctuations in turbulent channels up to $Re_\tau = 2003$, *Phys. Fluids*, **18**, 011702. 21, 34, 43, 46

[59] Iwamoto K., (2002) Database of fully developed channel flow, THTLAB Inernal Report No. ILR-0201, Dept. Mech. Eng., Univ. Tokyo. 28

[60] Iwamoto K., Suzuki Y. and Kasagi N., (2002) Reynolds number effect on wall turbulence : toward effective feedback control, *Int. J. Heat and Fluid Flow*, **23**, 678. 21, 28, 29, 34, 41, 42, 43, 46

[61] Kang H., Choi S.-U. (2006). Reynolds stress modelling of rectangular open-channel flow, *Int. J. Numer. Meth. Fluids*, **51**(11), 1319-1334. 51

[62] Kim J., Moin P. and Moser R. D., (1987) Turbulent statistics in fully developed channel flow at low Reynolds number, *J. Fluid Mech.*, **177**, 133, 133-166. 21

[63] Kirkgoz, M.S. (1989). The turbulent velocity profiles for smooth and rough channel flow. *J. Hydraul. Eng.*, ASCE, **115**(11), 1543-1561. 55

[64] Krogstad P.-A. and Antonia R. A., (1999) Surface roughness effects in turbulent boundary layers, *Exp. Fluids*, **27**, 450-460. 32

[65] Laadhari F. (2002) On the evolution of maximum turbulent kinetic energy production in a channel, *Phys. Fluids*, **14**(10), L65-L68. 39

[66] Lagriffoul A., Boudenne J.L., Absi R., *et al.* (2010) Bacterial-based additives for the production of artificial snow : What are the risks to human health ?, *Science of the Total Environment*, Elsevier, **408**(7), 1659-1666. 13, 98

[67] Langrish T. A. G., Kockel T. K. (2001) The assessment of a characteristic drying curve for milk powder for use in computational

fluid dynamics modelling. *Chemical Engineering Journal*, **84**, 69-74.

[68] Launder B.E. (1984) Low-Reynolds-number turbulence near walls, Rept. TFD/86/4, Dept. of Mechanical Engineering, Univ. of Manchester Inst. of Science and Technology, Manchester, England, UK. 21, 25, 34

[69] Lee T.H., Hanes D.M. (1996) Comparison of field observations of the vertical distribution of suspended sand and its prediction by models, *J. Geophys. Res.*, **101**, 35613572. 78

[70] Li X., Dong Z., Chen C. (1995). Turbulent flows in smooth-wall open channels with different slope *J. Hydraul. Res.*, **33**(3), 333-347. 51, 55

[71] List, J.H. et al., 1997. Bathymetric comparisons adjacents to the Louisiana barrier island : processes of large-scale change. *Journal of Coastal Research*, **13**(3), 670-678. 95

[72] L'vov V.S., Pomyalov A., Tiberkevich V., (2005) Simple analytical model for entire turbulent boundary layer over flat plane : from viscous and mixing layers to turbulent logarithmic region, *Env. Fluid Mech.*, **5**(4), 373-386. 21, 26

[73] Lyn D.A. (1986). Turbulence and Turbulent Transport in Sediment-Laden Open-Channel Flows. Rep KH-R-49, W. M. Keck Laboratory of Hydraulics and Water Resources, California Institute of Technology, Pasadena, CA. 57

[74] Marsh H.W. (1984) Students' evaluations of university teaching : Dimensionality, reliability, validity, potential baises, and utility, *Journal of Educational Psychology*, **76**(5), 707-754. 86

[75] Marsh H.W., Overall J.U. (1980) Validity of students' evaluations of teaching effectiveness : Cognitive and affective criteria, *Journal of Educational Psychology*, **72**(4), 468-475. 86

[76] McFetridge W.F., Nielsen P. (1985) Sediment suspension by non-breaking waves over rippled beds. Technical Report No UFL/COEL-85/005, Coast Oc Eng Dept, University of Florida. 64, 66, 69, 70, 72, 73

[77] Moser R.D., Kim J., Mansour N.N., (1999) Direct numerical simulation of turbulent channel flow up to $Re_\tau = 590$, *Phys. Fluids*, **11**, 943, 943-945. 21, 36, 41

[78] Nakato T., Locher F.A., Glover J.R., Kennedy J.F. (1977) Wave entrainment of sediment from rippled beds. *J. Waterway. Port. Coastal Ocean Div.*, **103**, 83-99. 64

[79] Nerem R.M. (1993) Hemodynamics and the Vascular Endothelium. *ASME Journal of Biomechanical Engineering*, **115**, 510-514. 105

[80] Nezu I., Nakagawa H. (1993). *Turbulence in open-channel flows.* AA Balkema (ed.), Rotterdam, The Netherlands. 1, 21, 22, 25, 26, 30, 37, 40, 45, 51

[81] Nezu I., Rodi W. (1986). Open-channel measurements with a laser Doppler anemometer. *J. Hydraul. Eng. ASCE* **112**(5), 335-355. 40, 51, 55

[82] Ni J.R., Wang G.Q., Borthwick A.G.L., (2000) Kinetic theory for particles in dilute and dense solid-liquid flows, *J. Hydraul. Eng.*, **126**, 893-903. 60, 61

[83] Nicholls, R. J., W. A Birkemeier, and G. Lee (1998). Evaluation of depth of closure using data from Duck, NC, USA, *International Journal of Marine Geology, Geochemistry and Geophysics*, **148**, 179 - 201. 95

[84] Nielsen P. 1992. *Coastal bottom boundary layers and sediment transport*, World Sci., 324 p. 64, 65, 76, 78

[85] Nielsen P., Teakle I.A.L. (2004) Turbulent diffusion of momentum and suspended particles : A finite-mixing-length-theory. *Phys. Fluids*, **16**(7), 2342-2348. 22, 59, 62, 63, 64, 65, 69

[86] Patel V.C., Rodi W. and Scheuerer G., (1985) Turbulence models for near-wall and low Reynolds numbers flows : A review, *AIAA J.*, **23**, 1308-1319. 26

[87] Pope, S.B. (2000) *Turbulent Flows*, University Press, Cambridge. 21, 25, 39

[88] Porté-Agel F, Meneveau C, Parlange MB, A scale-dependent dynamic model for large-eddy simulation : application to a neutral atmospheric boundary layer, *J. Fluid Mech.*, **415**, 216-284, 2000. 93

[89] Porté-Agel F, A scale-dependent dynamic model for scalar transport in large-eddy simulations of the atmospheric boundary layer, *Boundary-Layer Meteorology*, **112**(1), 81-105, 2004. 93

[90] Rahman M.M., Siikonen T. (2000) An eddy viscosity model with near-wall modifications, *Int. J. Num. Meth. Fluids*, **49**(9), 975-997. 26, 34

[91] Richardson J.F., Zaki W.N. (1954) Sedimentation and fluidisation : part 1. *Trans. Inst. Chem. Eng.*, **32**, 35-53. 65, 74

[92] Ritphring, S., and H. Tanaka (2006). Analysis of bathymetric change around Sendai Port. Proceedings of the *15th Congress of APD-IAHR and International Symposium on Maritime Hydraulics*, 701-707. 96

[93] Rogers C.B., Eaton J.K. (1990) The behavior of solid particles in a vertical turbulent boundary layer in air. *Int. J. Multiphase Flow.*, **16**, 819834. 60

[94] Sabatier, F., M. J. F. Stive., and F. Pons (2004). Longshore variation of depth of closure on a micro-tidal wave-dominated coast, *Proc. 29th Int. Conf. Coast. Eng.*, 2327-2339. 95

[95] Sana A., Tanaka H. (2007) Full-range equation for wave boundary layer thickness, *Coastal Engineering*, **54**, 639-642. 66

[96] Sarma K.V.N., Prasad B.V.R., Sarma A.K. (2000). Detailed study of binary law for open channels. *J. Hydraul. Eng. ASCE* **126**(3), 210-214. 51, 57

[97] Schlichting H., Gersten K. (2000) *Boundary layer theory*, 8th Revisited and Enlarged Edition, Springer. 39, 40

[98] Simonin O. (1990) Eulerain formulation for particle dispersion in turbulent twophase flows. *Proc. 5th Workshop on Twophase Flow Predictions*, Erlangen, FRG, 156-166. 61

[99] Sproule R. (2002) The underdetermination of instructor performance by data from the student evaluation of teaching, *Economics of Education Review*, **21**(3), 287-294. 86

[100] Stearns F.P. (1883). On the current meter, together with a reason why the maximum velocity of water flowing in open channel is below the surface. *Trans. ASCE*, **7**, 331-338. 51

[101] Sukhodolov A., Thiele M. and Bungartz H., (1998) Turbulence structure in a river reach with sand bed, *Water Resour. Res.*, **34**, 1317-1334. 30, 31, 32, 40

[102] Suntoyo, and Tanaka H. (2009) Effect of bed roughness on turbulent boundary layer and net sediment transport under asymmetric waves, *Coastal Engineering*, **56**(9), 960-969. 66

[103] Tanaka H., Thu A. (1994) Full-range equation of friction coefficient and phase difference in a wave-current boundary layer, *Coastal Engineering*, **22**, 237-254. 66

[104] Tennekes H., Lumley J.L. (1972) *A First Course in Turbulence*, MIT Press. 21

[105] Thorne P.D., Williams J.J., Davies A.G. (2002) Suspended sediments under waves measured in a large-scale flume facility, *J. Geophys. Res.*, **107**(C8), 3178. 64, 65, 76, 78

[106] Thorne P.D., Davies A.G., Bell P.S. (2009) Observations and analysis of sediment diffusivity profiles over sandy rippled beds under waves, *J. Geophys. Res.*, **114**, C02023. 76, 79

[107] Toorman E.A. (2008) Vertical mixing in the fully developed turbulent layer of sediment-laden open-channel flow, *J. Hydraul. Eng.*, **134**, 1225. 60

[108] Vanoni V.A. (1941). Velocity distribution in open channels. *Civ. Engrg. ASCE*, **11**(6), 356-357. 51

[109] van der Werf J.J., Ribberink J.S., O'Donoghue T., Doucette J.S. (2006) Modelling and measurement of sand transport processes over full-scale ripples in oscillatory flow, *Coast. Eng.*, **53**(8), 657-673. 64

[110] van Driest E.R., (1956) On turbulent flow near a wall, *J. Aero. Sci.*, **23**, 1007, 1007-1011. 2, 40, 41

[111] van Rijn L.C. (2003) Sand transport by currents and waves : general approximation formulae. *Proc. Coastal Sediments*, Clearwater Beach, Florida, USA. 78, 79

[112] van Rijn L.C. (2007) Unified View of Sediment Transport by Currents and Waves. II : Suspended Transport, *J. Hydraul. Eng. ASCE*, **133**(6), 668-689. 78, 79

[113] von Kármán Th. (1930) Mechanische Ähnlichkeit und Turbulenz, Nach. Ges. Wiss. Gottingen, *Math.-Phys. Klasse*, **58**. 2, 44

[114] Wang, P. and R.A. Davies, (1999). Depth of closure and the equilibrium beach profile : a case study from Sand key, West-Central Florida. *Shore and Beach*, **67**, 33-42. 95

[115] Wang Z.Q. and Cheng N.S. (2005). Secondary flows over artificial bed strips. *Adv. Water. Resour.*, **28**(5), 441-50. 51

[116] Wei T. and Willmarth W.W., (1989) Reynolds-number effects on the structure of a turbulent channel flow, *J. Fluid Mech.*, **204**, 57, 57-95. 21

[117] Yalin M.S. (1977) *Mechanics of sediment transport.* Pergamon Press, Oxford. 40

[118] Yang S.Q., Tan S.K., Lim S.Y. (2004). Velocity distribution and dip-phenomenon in smooth uniform open channel flows. *J. Hydraul. Eng. ASCE*, **130**(12), 1179-1186. 40, 51, 52, 54

[119] Zaichik L.I., Pershukov V.A., Kozelev M.V., Vinberg A.A., (1997) Modeling of dynamics, heat transfer, and combustion in two-phase turbulent flows : 1. Isothermal flow, Exper. Thermal and Fluid Science, **15**, 291-310. 2, 22, 59, 60, 61, 103

Annexe A

# EBInnov, Laboratoire de Recherche et Développement de l'EBI

## A.1 Activité 9 : Modélisation d'écoulements Environnementaux, Biologiques et Industriels, M2EBI

Annexe B

# Tirés-à-part de quelques articles dans des revues internationales

---

— **Absi R.** (2011) An ordinary differential equation for velocity distribution and dip phenomenon in open-channel flows, ***Journal of Hydraulic Research***, IAHR, Taylor & Francis, **49**(1), 82-89.

— El Gharbi N., **Absi R.**, Benzaoui A., Bennacer R. (2011) An improved near wall treatment for turbulent channel flows, ***International Journal of Computational Fluid Dynamics***, Taylor & Francis, **25**(1), 41-46.

— **Absi R.** (2010) Concentration profiles for fine and coarse sediments suspended by waves over ripples : An analytical study with the 1-DV gradient diffusion model, ***Advances in Water Resources***, Elsevier, **33**(4), 411-418.

— Lagriffoul A., Boudenne J.L., **Absi R.**, *et al.* (2010) Bacterial-based additives for the production of artificial snow : What are the risks to human health ?, ***Science of the Total Environment***, Elsevier, **408**(7), 1659-1666.

— **Absi R.** (2009) A simple eddy viscosity formulation for turbulent boundary layers near smooth walls, ***Comptes Rendus Mecanique***, Académie des Sciences, Elsevier, **337**, 158-165.

— **Absi R.** (2008a) Analytical solutions for the modeled k-equation, ***Transactions of the ASME, Journal of Applied Mechanics***, American Society of Mechanical Engineers, **75**(4), 044501.

— **Absi R.** (2008b) Comments on 'Turbulent velocity profile in fully-developed open channel flows', ***Environmental Fluid Mechanics***, Springer, **8**(4), 389-394.

— **Absi R.** (2005) Comment on 'Turbulent diffusion of momentum and suspended particles : A finite-mixing-length-theory', ***Physics of Fluids***, American Institute of Physics, **17**(7), 079101.

**Absi R. (2011) An ordinary differential equation for velocity distribution and dip phenomenon in open-channel flows, *Journal of Hydraulic Research*, IAHR, Taylor & Francis, 49(1), 82-89.**

**El Gharbi N., Absi R., Benzaoui A., Bennacer R. (2011) An improved near wall treatment for turbulent channel flows, *International Journal of Computational Fluid Dynamics*, Taylor & Francis, 25(1), 41-46.**

**Absi R. (2010) Concentration profiles for fine and coarse sediments suspended by waves over ripples : An analytical study with the 1-DV gradient diffusion model, *Advances in Water Resources*, Elsevier, 33(4), 411-418.**

**Lagriffoul A., Boudenne J.L., Absi R., *et al.* (2010) Bacterial-based additives for the production of artificial snow : What are the risks to human health ?, *Science of the Total Environment*, Elsevier, 408(7), 1659-1666.**

**Absi R. (2009) A simple eddy viscosity formulation for turbulent boundary layers near smooth walls, *Comptes Rendus Mecanique*, Académie des Sciences, Elsevier, 337, 158-165.**

**Absi R. (2008a) Analytical solutions for the modeled k-equation, *Journal of Applied Mechanics*, Transactions of the ASME, American Society of Mechanical Engineers, 75(4), 044501.**

**Absi R. (2008b) Comments on 'Turbulent velocity profile in fully-developed open channel flows', *Environmental Fluid Mechanics*, Springer, 8(4), 389-394.**

**Absi R. (2005) Comment on 'Turbulent diffusion of momentum and suspended particles : A finite-mixing-length-theory', *Physics of Fluids*, American Institute of Physics, 17(7), 079101.**